

AD-A260 889



(2)

# NAVAL POSTGRADUATE SCHOOL

## Monterey, California



DTIC  
ELECTE  
MAR 1 1993  
S C D

# THESIS

AN ANALYSIS OF MESOSCALE CONVECTIVE  
SYSTEMS OBSERVED DURING  
THE 1992 TROPICAL CYCLONE MOTION FIELD  
EXPERIMENT

by

Eric J. McKinley

December 1992

Thesis Advisor

R.L. Elsberry

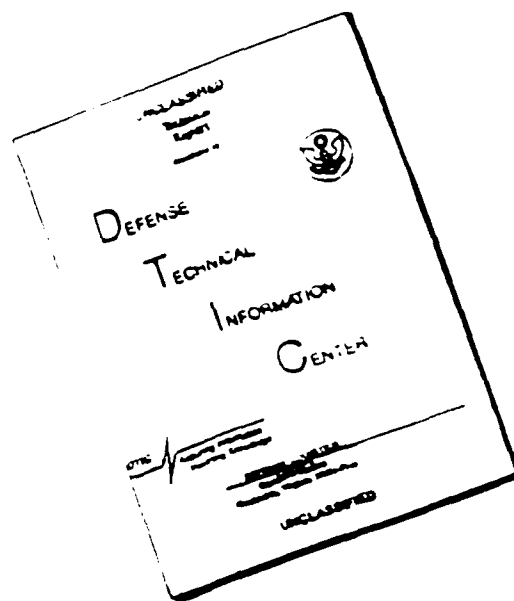
Approved for public release; distribution is unlimited.

98 2 26 037

93-04203



# DISCLAIMER NOTICE



THIS DOCUMENT IS BEST  
QUALITY AVAILABLE. THE COPY  
FURNISHED TO DTIC CONTAINED  
A SIGNIFICANT NUMBER OF  
PAGES WHICH DO NOT  
REPRODUCE LEGIBLY.

Unclassified

security classification of this page

## REPORT DOCUMENTATION PAGE

1a Report Security Classification <b>Unclassified</b>			1b Restrictive Markings		
2a Security Classification Authority			3 Distribution Availability of Report		
2b Declassification Downgrading Schedule			Approved for public release; distribution is unlimited.		
4 Performing Organization Report Number(s)			5 Monitoring Organization Report Number(s)		
6a Name of Performing Organization Naval Postgraduate School		6b Office Symbol (if applicable) 35	7a Name of Monitoring Organization Naval Postgraduate School		
6c Address (city, state, and ZIP code) Monterey, CA 93943-5000			7b Address (city, state, and ZIP code) Monterey, CA 93943-5000		
8a Name of Funding Sponsoring Organization		8b Office Symbol (if applicable)	9 Procurement Instrument Identification Number		
8c Address (city, state, and ZIP code)			10 Source of Funding Numbers		
			Program Element No	Project No	Task No
			Work Unit Accession No		
11 Title (include security classification) <b>AN ANALYSIS OF MESOSCALE CONVECTIVE SYSTEMS OBSERVED DURING THE 1992 TROPICAL CYCLONE MOTION FIELD EXPERIMENT</b>					
12 Personal Author(s) <b>Eric J. McKinley</b>					
13a Type of Report Master's Thesis		13b Time Covered From To		14 Date of Report (year, month, day) December 1992	
				15 Page Count 114	
16 Supplementary Notation The views expressed in this thesis are those of the author and do not reflect the official policy or position of the Department of Defense or the U.S. Government.					
17 Cosati Codes			18 Subject Terms (continue on reverse if necessary and identify by block number)		
Field	Group	Subgroup	Tropical Mesoscale Convective Systems, Tropical Cyclone		
19 Abstract (continue on reverse if necessary and identify by block number)					
<p>An analysis of two tropical Mesoscale Convective Systems (MCS) observed during the Tropical Cyclone Motion - 92 (TCM-92) mini-field experiment is accomplished. A discussion of TCM-92, its primary and secondary missions, and the resulting data sets is provided. Primary data sets for the two cases include high-density (one minute) WC-130 aircraft data, 44 omega dropwindsondes and visual and infrared (IR) geostationary satellite imagery. The observed characteristics exhibited by the tropical MCSs of the two cases are related to the hypothesized characteristics of midlatitude MCSs as suggested by Frank and Chen (1991), Raymond and Jiang (1990), Hertenstein and Schubert (1991), Menard and Fritsch (1989) and others. Thus, the goal of the analyses is to document, for the first time, the horizontal and vertical scales in terms of the expected structure and evolution of the tropical MCS. The MCSs of the two cases were in the mature and decaying stages of the convective life cycle. Mid-level (500 mb) vortices that are apparently created in the stratiform rain regions of the MCSs are clearly discernable in the wind fields. In both cases, these vortices are seen to build upward to 300 mb or originate higher than the 500 mb surface. Downward translation of the vortex to 700 mb is evident in both aircraft and satellite data in one case. Convective signatures in the temperature and dewpoint fields are not as significant as the wind fields. Because signatures are observed in the synoptic scale, such as anticyclonic outflow in the MCS regions, these systems apparently were significant mesoscale features of sufficient intensity and duration to alter the large-scale regime for over 24 h.</p>					
20 Distribution Availability of Abstract			21 Abstract Security Classification		
<input checked="" type="checkbox"/> unclassified unlimited <input type="checkbox"/> same as report <input type="checkbox"/> DTIC users			Unclassified		
22a Name of Responsible Individual R.L. Elsberry			22b Telephone (include Area code) (408) 646-2373		22c Office Symbol MR. Es

Approved for public release; distribution is unlimited.

An Analysis of Mesoscale Convective  
Systems Observed During  
the 1992 Tropical Cyclone Motion Field  
Experiment

by

Eric J. McKinley  
Captain, United States Air Force  
B.S., Plymouth State College, 1984

Submitted in partial fulfillment of the  
requirements for the degree of

MASTER OF SCIENCE IN METEOROLOGY

from the

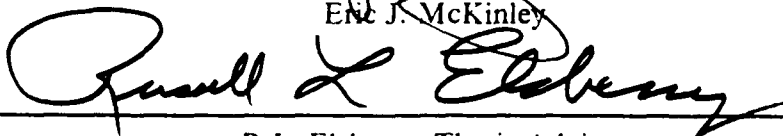
NAVAL POSTGRADUATE SCHOOL  
December 1992

Author:

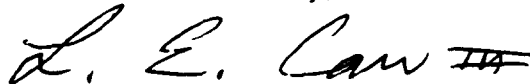


Eric J. McKinley

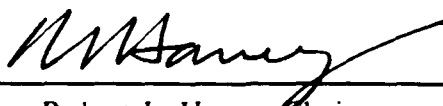
Approved by:



R.L. Elsberry, Thesis Advisor



L.E. Carr III, LCDR, USN, Second Reader



Robert L. Haney, Chairman,  
Department of Meteorology

## ABSTRACT

An analysis of two tropical Mesoscale Convective Systems (MCS) observed during the Tropical Cyclone Motion - 92 (TCM-92) mini-field experiment is accomplished. A discussion of TCM-92, its primary and secondary missions, and the resulting data sets is provided. Primary data sets for the two cases include high-density (one minute) WC-130 aircraft data, 44 omega dropwindsondes and visual and infrared (IR) geostationary satellite imagery. The observed characteristics exhibited by the tropical MCSs of the two cases are related to the hypothesized characteristics of midlatitude MCSs as suggested by Frank and Chen (1991), Raymond and Jiang (1990), Hertenstein and Schubert (1991), Menard and Fritsch (1989) and others. Thus, the goal of the analyses is to document, for the first time, the horizontal and vertical scales in terms of the expected structure and evolution of the tropical MCS. The MCSs of the two cases were in the mature and decaying stages of the convective life cycle. Mid-level (500 mb) vortices that are apparently created in the stratiform rain regions of the MCSs are clearly discernable in the wind fields. In both cases, these vortices are seen to build upward to 300 mb or originate higher than the 500 mb surface. Downward translation of the vortex to 700 mb is evident in both aircraft and satellite data in one case. Convective signatures in the temperature and dewpoint fields are not as significant as the wind fields. Because signatures are observed in the synoptic scale, such as anticyclonic outflow in the MCS regions, these systems apparently were significant mesoscale features of sufficient intensity and duration to alter the large-scale regime for over 24 h.

Accession For	
NTIS CRA&I	<input checked="" type="checkbox"/>
DTIC TAB	<input type="checkbox"/>
Unannounced	<input type="checkbox"/>
Justification	
By	
Distribution /	
Availability Codes	
Dist	Avail and/or Special
A-1	

## TABLE OF CONTENTS

I. INTRODUCTION .....	1
II. BACKGROUND .....	3
A. OVERVIEW OF TCM-92 .....	3
B. IMPORTANCE OF THE TROPICAL MESOSCALE CONVECTIVE SYSTEM .....	3
1. Track deviations due to asymmetric convection .....	4
2. Nonlinear interaction with adjacent mesoscale convective complex .....	5
3. Monsoon trough shear influences .....	7
C. PRIMARY MISSIONS OF TCM-92 .....	10
D. MCS CHARACTERISTICS .....	12
1. Formation .....	12
2. Maintenance .....	15
E. EXPECTED MCS STRUCTURES .....	23
1. The Western Pacific Region (WPR) MCS .....	23
2. Application to Tropical MCS .....	25
F. ALTERNATE MISSIONS OF TCM-92 .....	28
III. DATA SUMMARY .....	29
A. AIRCRAFT DATA .....	29
1. Improved Weather Reconnaissance System (IWRS) measurements .....	29
2. Flight-level data .....	30
3. Omega dropwindsonde data .....	32
B. SATELLITE DATA .....	34
1. MIDAS imagery .....	34
2. NSDS-G imagery .....	35
3. Special Sensor Microwave Imager (SSM/I) data .....	36
C. CONVENTIONAL DATA .....	36
IV. ANALYSIS .....	37
A. AIRCRAFT OBSERVATION PERIOD 7 OVERVIEW .....	37

B. AIRCRAFT OBSERVATION PERIOD 1 OVERVIEW .....	42
C. ANALYSIS OF WPAC .....	44
D. AOP ANALYSIS APPROACH .....	45
1. Satellite imagery .....	45
2. Hand analyses .....	46
E. STRUCTURE OF AOP 7 MCS .....	51
1. Horizontal structure .....	51
2. Vertical structure .....	56
F. STRUCTURE OF AOP 1 MCS .....	64
1. Horizontal structure .....	64
2. Vertical structure .....	69
V. SUMMARY .....	80
A. LOW- AND MID-LEVEL VORTICES .....	80
B. UPPER-LEVEL ANTICYCLONE .....	81
C. TEMPERATURE DISTRIBUTIONS .....	82
D. TD DEVELOPMENT .....	82
VI. CONCLUSIONS .....	84
APPENDIX A. GEOSTATIONARY SATELLITE IMAGERY .....	86
REFERENCES .....	97
INITIAL DISTRIBUTION LIST .....	100

## LIST OF TABLES

Table 1.	EXPECTED CHARACTERISTICS OF MCS STRUCTURE .....	38
Table 2.	OBSERVED CHARACTERISTICS OF MCS STRUCTURE DURING AOP 7 AND AOP 1 .....	80



## LIST OF FIGURES

Figure 1.	Vortex tracks each 3 h with (●) and without (dots) the inclusion of a fixed mass source-sink relative to the center of the vortex in the Willoughby (1992) barotropic model. . . . .	6
Figure 2.	Streamfunction after 18 h of the integration of the Willoughby (1992) barotropic model with the inclusion of a fixed mass source-sink and an environmental flow of 2 m/s as in Fig. 1. . . . .	7
Figure 3.	Mutual orbit and horizontal scales of MCC Alpha and Typhoon Sarah as depicted in geostationary satellite infrared imagery. . . . .	8
Figure 4.	Positions each 6 h of developing Typhoon Sarah, MCS Alpha and the centroid starting at 23 UTC 5 September 1989. . . . .	9
Figure 5.	Tracks of Typhoon Sarah and the superimposed mesoscale vortices from 18 h barotropic model experiments starting at 23 UTC on 7 September 1989. . . . .	
Figure 6.	Schematic of a curved band of the active monsoon trough cloudiness with the positions of tropical storm Caitlin and a MCS at two times. . . . .	11
Figure 7.	Schematic diagrams of the structure of an MCC and the associated mesovortex at (a) initial stage, (b) mesovortex genesis stage, and (c) mesovortex intensification stage (Frank and Chen 1991). . . . .	13
Figure 8.	Downward displacement of the relative vorticity maximum in the stratiform rain region at selected times during the numerical model integration of Frank and Chen (1991). . . . .	14
Figure 9.	Relative wind vectors in a coordinate system moving at the speed of the vortex and temperature (°C, dashed lines) at (a) 500 mb and (b) 200 mb. . . . .	15
Figure 10.	Upper-level analyses for: (a) 850 mb, (b) 700 mb, (c) 500 mb and (d) 200 mb, 1200 UTC 7 July 1982. . . . .	16
Figure 11.	Vertical profiles of relative vorticity . . . . .	17
Figure 12.	Sounding for Oklahoma City 0000 UTC 7 July 1982. . . . .	18
Figure 13.	Sketches of mechanisms by which lifting might occur in the presence of a potential vorticity anomaly in shear confined to below the anomaly on an east-west plane. . . . .	19
Figure 14.	Flow on horizontal sections at (a) $z = 3$ km and (b) $z = 10$ km. . . . .	20

Figure 15. Heating function (top), potential vorticity (middle), wind speeds and isotherms (lower) diagnosed in the Hertenstein and Schubert (1991) model. ....	22
Figure 16. Schematic of the sheared environmental wind profile and low-level trajectories of air parcels in a rear-inflow case deduced in an observational study by Fritsch (1992). ....	23
Figure 17. Comparison of MCS life cycles in U.S. and WPAC. ....	24
Figure 18. Geographical and monthly distributions of MCCs in the western Pacific region. ....	26
Figure 19. Schematic of early stage (top) and later stage (bottom) of multiple MCSs in an active monsoon trough region between enhanced monsoon westerlies and enhanced trade wind easterlies. ....	27
Figure 20. Location of primary Improved Weather Reconnaissance System (IWRS) components on a WC-130. ....	31
Figure 21. Modified Dvorak "BD" infrared enhancement curve for geostationary imagery. ....	35
Figure 22. 1200 UTC 14 August 1992 gradient-level analysis of WPAC. ....	39
Figure 23. 1200 UTC 14 August 1992 200 mb analysis for WPAC. ....	40
Figure 24. WC-130 flight track during AOP 7. ....	41
Figure 25. 1200 UTC 23 July 1992 gradient-level analysis for WPAC. ....	43
Figure 26. 1200 UTC 23 July 1992 200 mb analysis for WPAC. ....	44
Figure 27. WC-130 flight track during AOP 1. ....	45
Figure 28. AOP 7 nephanalysis for center time (2000 UTC 14 August 1992) with flight track overlaid. ....	47
Figure 29. AOP 1 nephanalysis for center time (0000 UTC 24 July 1992) with flight track overlaid. ....	48
Figure 30. Time sequence of -70 ° to -75 ° C cloud-top temperatures for AOP 7. .	49
Figure 31. As in Fig. 30 for AOP 1. ....	50
Figure 32. AOP 7 500 mb aircraft flight-level, dropwindsonde and 0000 UTC 15 August Guam rawindsonde winds (kt) (top), with streamline analysis (bottom). ....	52
Figure 33. AOP 7 300 mb winds and analysis as in Fig. 32. ....	53
Figure 34. AOP 7 700 mb streamline analysis of dropwindsonde and 0000 UTC 15 August Guam rawindsonde winds (kt). ....	54

Figure 35. AOP 7 850 mb streamline analysis of dropwindsonde and 0000 UTC 15 August Guam rawindsonde winds (kt). . . . .	54
Figure 36. AOP 7 gradient level (960 mb-surface) streamline analysis of dropwindsonde, 0000 UTC 15 August Guam rawindsonde. . . . .	55
Figure 37. AOP 7 Surface temperature and dewpoint depression analysis. . . . .	57
Figure 38. AOP 7 850 mb temperature and dewpoint depression analysis. . . . .	58
Figure 39. AOP 7 700 mb temperature and dewpoint depression analysis. . . . .	59
Figure 40. AOP 7 500 mb temperature and dewpoint depression analysis. . . . .	59
Figure 41. AOP 7 400 mb temperature and dewpoint depression analysis. . . . .	60
Figure 42. AOP 7 300 mb temperature and dewpoint depression analysis. . . . .	60
Figure 43. Ten AOP 7 dropwindsonde temperature and dewpoint profiles representing moist and cool conditions through all levels. . . . .	61
Figure 44. Eleven AOP 7 dropwindsonde temperature and dewpoint profiles that are warm and dry at low levels due to subsidence. . . . .	62
Figure 45. Four AOP 7 dropwindsonde temperature and dewpoint profiles with varying mid-level warm and dry layers due to subsidence. . . . .	62
Figure 46. Locations of AOP 7 dropwindsondes in relation to vertical profile: stars represent moist soundings; squares, dry low-levels; and triangles, dry mid-levels. . . . .	63
Figure 47. Skew T-ln p plot of 0000 UTC 15 August Guam rawindsonde. . . . .	63
Figure 48. AOP 1 500 mb aircraft flight-level and dropwindsonde winds (kt) (top), and 0000 UTC 24 July Guam, Yap and Belau (Koror) rawindsonde winds (kt) with streamline analysis (bottom). . . . .	65
Figure 49. AOP 1 300 mb winds and analysis as in Fig. 48. . . . .	66
Figure 50. AOP 1 700 mb streamline analysis of aircraft flight-level, dropwindsonde and 0000 UTC 24 July Guam, Yap and Belau (Koror) rawindsonde winds (kt). . . . .	67
Figure 51. AOP 1 850 mb streamline analysis of dropwindsonde and 0000 UTC 24 July Guam, Yap and Belau (Koror) rawindsonde winds (kt). . . . .	68
Figure 52. AOP 1 gradient level (960 mb-surface) streamline analysis of dropwindsonde and 0000 UTC 24 July Guam, Yap and Belau (Koror) rawindsonde. . . . .	69
Figure 53. AOP 1 Surface temperature and dewpoint depression analysis. . . . .	70
Figure 54. AOP 1 850 mb temperature and dewpoint depression analysis. . . . .	71
Figure 55. AOP 1 700 mb temperature and dewpoint depression analysis. . . . .	72

Figure 56. AOP 1 500 mb temperature and dewpoint depression analysis. . . . .	73
Figure 57. AOP 1 400 mb temperature and dewpoint depression analysis. . . . .	74
Figure 58. AOP 1 300 mb temperature and dewpoint depression analysis. . . . .	75
Figure 59. Nine AOP 1 dropwindsonde temperature and dewpoint profiles representing moist and cool conditions through all levels. . . . .	76
Figure 60. Four AOP 1 dropwindsonde temperature and dewpoint profiles that have weak mid-level warm and dry layers due to subsidence. . . . .	77
Figure 61. Four AOP 1 dropwindsonde temperature and dewpoint profiles that have weak low-level warm and dry layers due to subsidence. . . . .	78
Figure 62. Locations of AOP 1 dropwindsondes in relation to vertical profile: stars represent moist soundings; squares, dry low-levels; and triangles, dry mid-levels. . . . .	79
Figure A-1. 0930 UTC 14 August 1992 IR . . . . .	86
Figure A-2. (a) 1330 UTC IR and (b) 1730 UTC 14 August 1992 IR . . . . .	87
Figure A-3. (a) 1930 UTC IR and (b) 2330 UTC 14 August 1992 IR . . . . .	88
Figure A-4. (a) 0330 UTC 15 August IR and (b) 2130 UTC 14 August 1992 VIS . . . . .	89
Figure A-5. (a) 2330 UTC 14 August VIS and (b) 0130 UTC 15 August 1992 VIS . . . . .	90
Figure A-6. (a) 0330 UTC VIS and (b) 0630 UTC 15 August 1992 VIS . . . . .	91
Figure A-7. (a) 1630 UTC IR and (b) 1830 UTC 23 July 1992 IR . . . . .	92
Figure A-8. (a) 2230 UTC 23 July 1992 IR and (b) 0030 UTC 24 July 1992 IR . . . . .	93
Figure A-9. (a) 0230 UTC IR and (b) 0630 UTC 24 July 1992 IR . . . . .	94
Figure A-10. (a) 2230 UTC 23 July 1992 VIS and (b) 0230 UTC 24 July 1992 VIS . . . . .	95
Figure A-11. (a) 0430 UTC VIS and (b) 0630 UTC 24 July 1992 VIS . . . . .	96

## ACKNOWLEDGEMENT

Many people contributed significantly to this thesis, however a special thanks must first go to my advisor, Professor Russell Elsberry. He presented me with the truly unique opportunity to act as aircraft scientist during TCM-92, and provided me the challenge of participating in the planning and execution of the experiment. It is his technical expertise and guidance, as well as patience with my, shall we say intriguing, writing style that made this thesis possible in such a short period of time.

Those who participated in TCM-92, whether deployed to Guam or as members of the Joint Typhoon Warning Center (JTWC), must be acknowledged for making the experiment the success it was. The TCM-92 team of LCDR George Dunnavaan, Mark Boothe, Pat Harr, Liz Ritchie and John Knaff deserve a great deal of credit. Contributions from LCOL Chip Guard, Frank Wells and all the folks of JTWC were integral parts in the accomplishments of the TCM-92 experiment. In addition, my thanks go to Mark Lander for lending his knowledge as well as his analyses. Last, but without whom TCM-92 would not have occurred, are the personnel of the 815th Weather Squadron at Keesler AFB, MS. Many long days and nights were put in by these people in an effort to provide this one-of-a-kind data set and their efforts are gratefully acknowledged.

Further acknowledgement is given to the ONR Marine Meteorology program, the NPS Direct Research Fund and AFIT for providing funds necessary for my participation in TCM-92.

The task of assimilating the data set into the IDEA Lab became a difficult one in which many worked to rectify. The efforts by Pat Harr, Professor Wendell Nuss, LCDR Dave Titley, Jim Cowie, Mark Boothe and LCDR George Dunnavaan were critical in producing a usable TCM-92 data set. Their countless hours enduring my persistent requests for help are both accomplishments and appreciated. In the many hours spent working the analyses, I must thank LCDR Les Carr for providing his guidance and expertise. His inputs to the analyses and the thesis as second reader were significant and again, are sincerely appreciated.

Finally, I can think of no other person who enabled me more to press on and complete this work than my wife, Mandy. Her love for me, frequently expressed in letters to Guam, is unceasing. Her constant support and endurance of my long hours, and weeks, away from home can not be surpassed. To her, I dedicate this work and give my greatest thanks of all.

## I. INTRODUCTION

It is well known that forecasting the movement of tropical cyclones in the western Pacific Ocean (WPAC) is a difficult task. The primary agency for such forecasts in this region is the Joint Typhoon Warning Center (JTWC) located on Guam. Recent research (Elsberry and Abbey 1991) has centered on better understanding of how the motion of these cyclones is affected by adjacent synoptic features, such as the presence of a Tropical Upper Tropospheric Trough (TUTT) cell or another tropical cyclone. These adjacent features contribute to the large-scale environmental flow in which the cyclones are moving. On still smaller scales, mesoscale convective systems (MCS) within the tropical cyclone circulation region may interact with the cyclone. The long-term benefit of improved understanding of these interactions is an improvement in track forecasts made by agencies such as JTWC. By achieving better understanding of the physical processes involved, improved conceptual and numerical models for use in track forecasting should result. For example, the forecaster may benefit by having documented examples of how a MCS interacts with a tropical cyclone and the resultant change in the cyclone.

The focus of this paper is indeed on improved understanding of how a MCS is believed to have a direct effect on the motion of tropical cyclones. In addition to its role in track alteration, such systems have been hypothesized (Frank and Chen 1991; Ritchie and Holland 1992) to contribute to genesis, i.e., the formation of the Tropical Depression (TD). As no data sets exist to describe these mesoscale systems, which has hindered research involving the tropical MCS, the primary motivation is to obtain an *in situ* data set from multiple levels in the troposphere.

It was this motivation to observe several MCSs (Elsberry et al. 1992) that prompted the deployment of a USAF Reserve WC-130 weather reconnaissance aircraft to the western North Pacific from 21 July 1992 to 21 August 1992. The aircraft data collection was part of the Tropical Cyclone Motion-92 (TCM-92) mini-field experiment (Dunnavan et al. 1992). As a background, this thesis will first present a motivation for the TCM-92 experiment, which included validation of several hypotheses regarding MCS structure and development. A brief description will be given of the theories that form the basis of the TCM-92 hypotheses that are to be validated with the analyzed data sets. Brief summaries of the aircraft missions are then given to illustrate the potential of the

TCM-92 data set. A summary of the overall TCM-92 data set used in this analysis is then provided.

An analysis of two missions in which tropical MCSs were observed during TCM-92 will be presented. Specifically, an analysis is accomplished in terms of wind, temperature and dewpoint depression fields. Geostationary visual and infrared (IR) satellite imagery, with 2.7 n mi resolution, captured at the same time as the aircraft observations, plays a key role in documenting the structure and evolution of the TCM-92 MCSs.

The specific objective of the analyses is to test the various hypotheses that have been based on midlatitude MCS structures. These hypotheses are summarized in the form of specific characteristics expected to be present within the MCSs observed during TCM-92. For example, the expected presence of the mid- and low-level vortex are key assumptions in the above tropical cyclone motion and genesis studies. Thus, the goal of the analyses of two TCM-92 cases is to document, for the first time, the horizontal and vertical scales in terms of expected structure and evolution of the tropical MCS.

## **II. BACKGROUND**

### **A. OVERVIEW OF TCM-92**

Observations of MCSs during the Tropical Cyclone Motion-90 (TCM-90) experiment and recent research suggest MCSs cause short-duration tropical cyclone track deviations, which provided the motivation for TCM-92. More details of this experiment can be found in Elsberry et al. (1992). A brief discussion is presented here for background.

Studies by Holland and Lander (1991), Willoughby (1992), Flatau (1991) and others have suggested that a MCS may have a significant role in causing meanders in tropical cyclone tracks with amplitudes of 100 km over 1-2 days. However, with only satellite imagery as a means to observe MCSs, these authors have had to make assumptions concerning the structures and physical processes within the MCS. Based on these studies, Elsberry et al. (1992) proposed that the observation platform of an aircraft was necessary to evaluate the mesoscale features of interest in determining track deviations. The major objective of TCM-92 was to obtain *in situ* aircraft flight-level measurements and dropwindsonde observations in tropical cyclones and nearby MCSs to evaluate the interaction mechanisms described in the studies mentioned above. An additional objective was to document the thermal and vorticity structure of tropical MCSs. Motivation for such investigations stems from studies by Frank and Chen (1991), Frank (1992) and Fritsch (1992). They proposed models that describe mesoscale vortex formation in the stratiform rain region within tropical MCSs. Another genesis model proposed by Ritchie and Holland (1992) suggests that the merger of the vorticity centers associated with two or more MCSs may result in the creation of a system with greater vorticity.

### **B. IMPORTANCE OF THE TROPICAL MESOSCALE CONVECTIVE SYSTEM**

The introduction of a MCS into a tropical environment can be thought of as an introduction of a relatively large mesoscale heat source. The hypotheses being explored here relate to how the introduction of such forcing into the environment of a tropical cyclone will produce a distinct effect on the cyclone motion, and a countering effect on the MCS. Such effects are expected to depend upon the strength and the horizontal extent of the tropical cyclone and/or the MCS. Several observational and numerical studies form the basis of these hypotheses. In this section, several hypotheses are



presented to provide background on the importance of MCSs and the effects such a mesoscale mechanism could have on larger scale features and their environment.

#### 1. Track deviations due to asymmetric convection

The idea that an asymmetric distribution of convection near the center of a tropical cyclone could cause track deviations has existed for some time (Elsberry 1987). Early support for this idea came from radar photographs during periods of trochoidal motion. That is, the center of the storm appeared to accelerate and decelerate and have cross-track deviations on the order of the eyewall radius as regions of intense radar echoes rotated about the eye. It is reasonable that an asymmetry in convective latent heat release would produce an associated isallobaric tendency with low surface pressure beneath it, and thus a perturbation on the low pressure core in the center. As this perturbation would rotate with the convection asymmetry, the minimum surface pressure that defines the storm track may also seem to follow the rotation. This combination of a rotation plus an environmental steering results in a trochoidal-type track.

Satellite imagery (Black 1977) occasionally reveals a strong asymmetry in deep convection (which Black calls a "supercell") during the early stages of tropical cyclone development. In addition to modifying the intensification process, the track is deflected toward the convection maximum. Several researchers (Fett and Brand 1975; Lajoie and Nicholas 1974) have studied changes in tropical cyclone track directions in response to a change in orientation of the primary convection areas observed in satellite imagery. However, the empirical rules they developed have not been applied successfully in operational forecasting because of the lack of specificity about when the turning motion may occur (e.g., in 6 h, 12 h, 18 h, etc.). In addition, the rules did not address the ranges of asymmetric convection magnitudes, durations and separation distances that occur in nature. One might also suspect that the intensity (or other aspects of the wind structure) of the tropical cyclone would also be a factor, but this aspect was not included in the empirical rules.

Willoughby (1992) has developed a barotropic, shallow-water model of the track changes in response to a rotating mass source-sink that represents the rotating convection asymmetry just outside the radius of maximum winds. Willoughby's model produces a trochoidal track that has a period equal to the rotation period of the convection. The cross-track deflections due to this process are on the order of 10 km. Consequently, the rotating convection mechanism is compatible with the radar observations of track deviations of this magnitude. Whereas such short-term oscillations in radar center fixes may be critical near landfall, the forecaster would normally smooth the

oscillations to obtain a more conservative, longer term estimate of the present and future track.

A more intriguing result from the Willoughby (1992) model is that a stationary mass source-sink pair relative to the tropical cyclone center causes a track deflection of larger magnitude that may have a persistence beyond the end of the convection asymmetry (Fig. 1). The center is deflected toward the mass sink (which represents the asymmetry in deep convection in the model) due to the divergent wind from the source to the sink that flows across the storm center, and also interacts with the symmetric vorticity pattern. In addition, Willoughby finds the asymmetry triggers the development of a normal mode in his linear model that is in the form of a wavenumber one gyre (Fig. 2). Although the gyre circulation is damped after the mass source-sink is removed, the flow between the gyre centers continues to deflect the storm center relative to the steering as the gyre damps. Consequently, the track deflection may persist and perhaps cause a significant deviation if the asymmetry in convection was strong and sustained.

Flatau (1991) studied the response of a multi-level baroclinic model on imposed asymmetries in convective latent heat release. Whereas Willoughby only considered convection near the cyclone center, Flatau found significant track deviations were produced even when the convection was a few hundred kilometers from the center. Such a persistent convection region might exist along a feeder rainband.

## **2. Nonlinear interaction with adjacent mesoscale convective complex**

Holland and Lander (1991) have examined "meanders" in tropical cyclone tracks on time scales of hours (e.g., the radar-observed track oscillations) to days. They show that characteristics of observed meanders do not agree with a theory that the oscillations are excited by inertial oscillations (Yeh 1949 and Kuo 1950), or a theory representing the tropical cyclone as a rotating cylinder (Kuo 1968).

Holland and Lander propose that medium-scale meanders (on the order of 100 km over 1-2 days) may arise from nonlinear interactions with mesoscale convective complexes (MCC). Specific characteristics of an MCC in terms of spatial scales on the enhanced infrared imagery, ellipticity and durations (greater than 12 h) have been defined by Maddox (1980). Holland and Lander show a case of Typhoon Sarah during 1989 that had a long-lasting MCC (which they code named as Alpha) of similar dimensions to Sarah (Fig. 3). The MCC went through periods of active convection, decay and renewed convection. The tracks of the two systems appear to have a mutual cyclonic orbit around a centroid that is analogous to the so-called Fujiwhara effect in binary cyclone interactions (Fig. 4). This centroid, which was assumed to be the midpoint

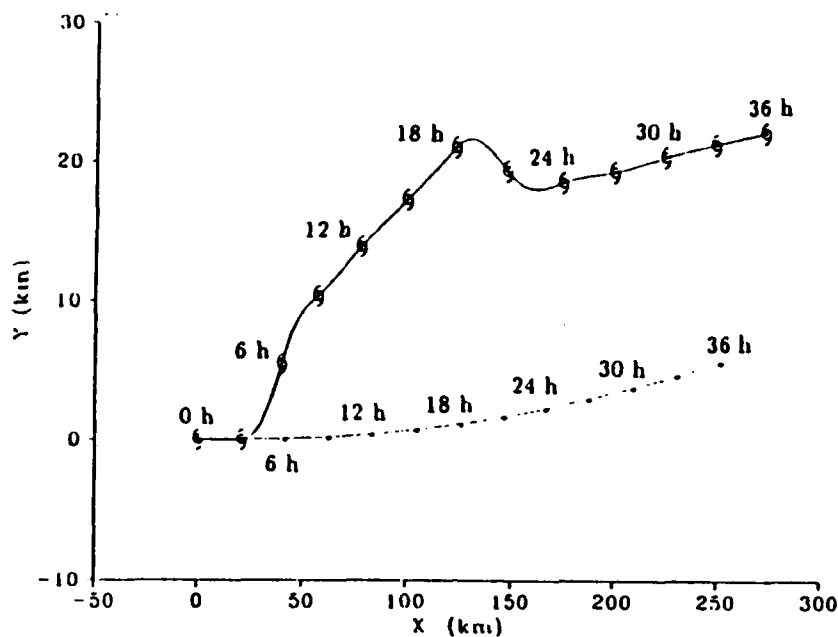


Figure 1. Vortex tracks each 3 h with (6) and without (dots) the inclusion of a fixed mass source-sink relative to the center of the vortex in the Willoughby (1992) barotropic model. The mass source-sink is initiated at  $t = 3$  h and terminated at  $t = 18$  h, and the environmental flow is 2 m/s from the west.

between Sarah and MCC Alpha since the two were about the same size, tracked steadily toward the west-southwest while the two systems orbited cyclonically.

Holland and Lander numerically simulated the potential effect of MCC Alpha on the track of Sarah by assuming it had the same outer circulation as Sarah. Such a circulation did indeed contribute to a southwestward deflection in Sarah's track (Fig. 5). Without direct observations, it is not possible to verify whether MCC Alpha had an independent mesoscale circulation as assumed by Holland and Lander.

Holland and Lander suggest that the track impact due to a particular intensity MCC would decrease as the typhoon intensity increased, which would be consistent with the meander statistics they collected. Since the MCC presently is detected only in the satellite enhanced IR imagery without supporting *in situ* observations, it logically can not be assumed that all MCCs have the same intensity. Holland and Lander speculate that the period and amplitude would decrease as the MCCs form closer to the center, which would be similar to the Willoughby simulations. The key point is that little is

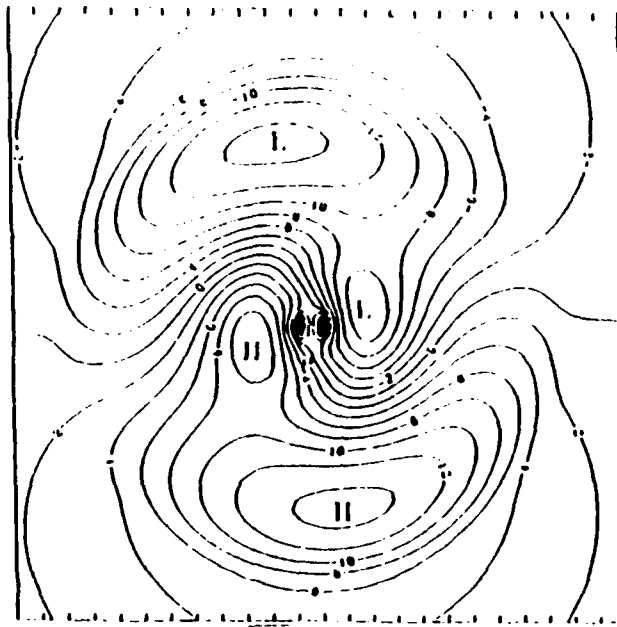


Figure 2. Streamfunction after 18 h of the integration of the Willoughby (1992) barotropic model with the inclusion of a fixed mass source-sink and an environmental flow of 2 m/s as in Fig. 1. Contour interval,  $2 \times 10^4 m^2/s$ .

known about the structure and other characteristics of MCCs within the tropical cyclone circulation that may cause significant deviations from a steady, smooth track.

### 3. Monsoon trough shear influences

Les Carr, who recently served as Deputy Director of the Joint Typhoon Warning Center (JTWC) in Guam, has collected a number of examples of significant track deflections when tropical cyclones form within the monsoon trough. For example, tropical cyclone Caitlin during 1991 exhibited a significant departure from its previous track in possible association with a mesoscale convective system (MCS). The more generic label of MCS is used here because many of these convective systems in the tropics do not satisfy the horizontal spatial specification, duration or ellipticity requirements of the midlatitude MCCs (Maddox 1980). This MCS appeared to be created by the large scale shear effects of a monsoon gyre and formed in the strongest southwesterly monsoon flow to the south and east of Caitlin. The MCS rotated from a position south of Caitlin to a position east of Caitlin (Fig. 6). At this time, Caitlin and the MCS appeared to couple and both systems tracked northward perpendicular to the line connecting them, which was to the right of the previous track of Caitlin. This may or may

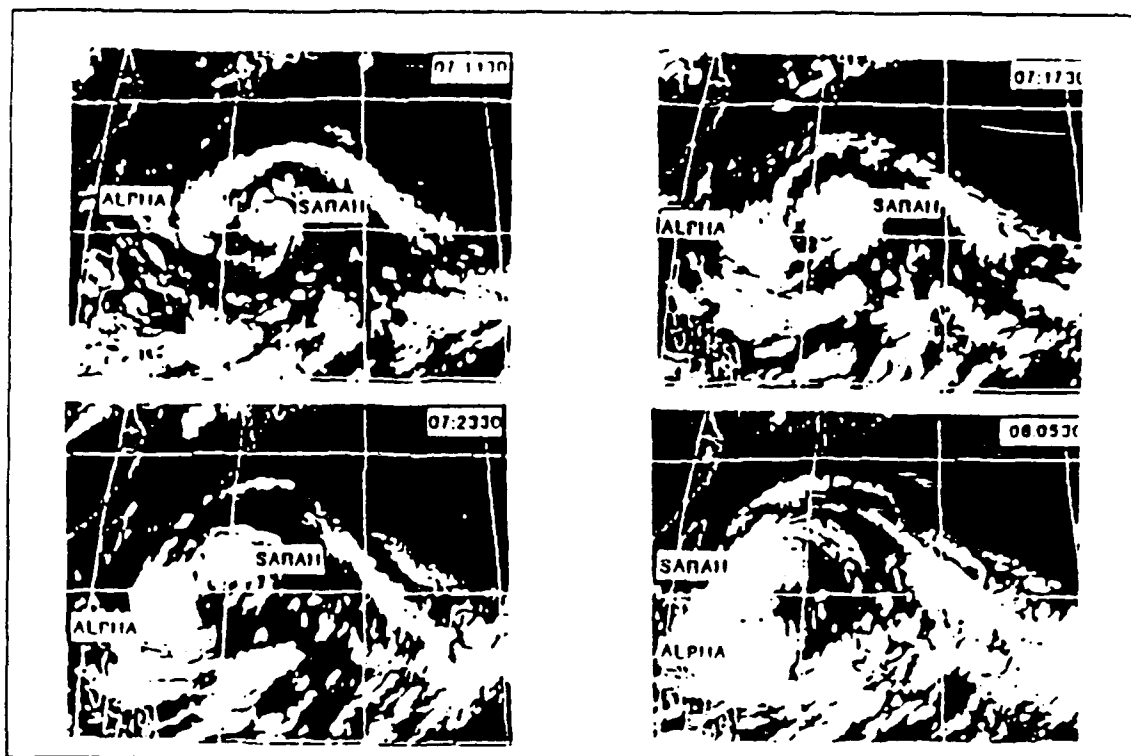


Figure 3. Mutual orbit and horizontal scales of MCC Alpha and Typhoon Sarah as depicted in geostationary satellite infrared imagery. Times are 7 September 1989 at 1130, 1730 and 2330 UTC and for 0530 UTC 8 September starting upper left (Holland and Lander 1991).

not be attributable to the presence of the MCS, that is; the track deviation may be due to larger scale effects. However, without knowing the structure of this type of MCS and its environment, the MCS may indeed be contributing to the deviation.

Two systems at different radial positions from the center of a strongly sheared monsoon trough may appear to have a cyclonic orbit similar to the Fujiwhara effect. One example is the Typhoon Ed and Supertyphoon Flo case during TCM-90 (Elsberry et al. 1990). Even though the two cyclones were separated farther than systems expected to have the Fujiwhara effect, Ed and Flo appeared to rotate cyclonically relative to a centroid position for 2-3 days. However, the westward motion of Ed and the northwestward track of Flo could also be interpreted as being due to their positions within a horizontally sheared monsoon trough.

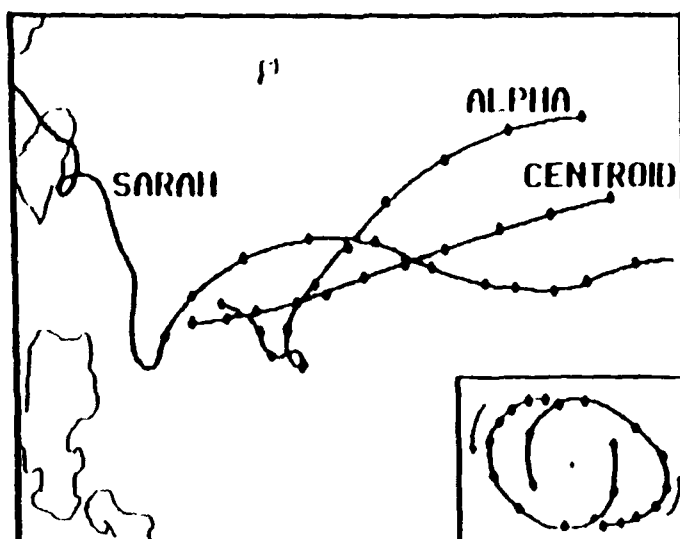


Figure 4. Positions each 6 h of developing Typhoon Sarah, MCS Alpha and the centroid starting at 23 UTC 5 September 1989. The inset contains the centroid-relative motion of Alpha and Sarah (Holland and Lander 1991).

The Holland and Lander case of Sarah and MCC Alpha might also be interpreted to include a sheared monsoon trough influence as well. That is, the motion of MCC Alpha relative to Sarah in Fig. 3 may be due in part to Alpha having been at a greater distance from the center of a monsoon trough in which both systems were embedded. Both the curvature of the long trailing convective band behind Alpha in Fig. 3 and the west-southwestward path of the centroid in Fig. 4 suggest the presence of a large monsoon trough.

The point from these interpretations is that cyclonic rotation about an apparent centroid is not sufficient evidence of an interaction between a tropical cyclone and an adjacent MCS. Since formation of both tropical cyclones and MCSs are favored in a strongly sheared monsoon trough situation, some (or all) of the relative rotation may be due to radial positions within the monsoon trough. This is not to say that a MCS-tropical cyclone interaction may not also be occurring. In the case of Sarah-Alpha, the tropical cyclone Sarah deviated to the left of the expected westward track. In the case of Caitlin, the tropical cyclone apparently deviated to the right of the expected track. Such track deviations are difficult to forecast and contribute significantly to track forecast errors.

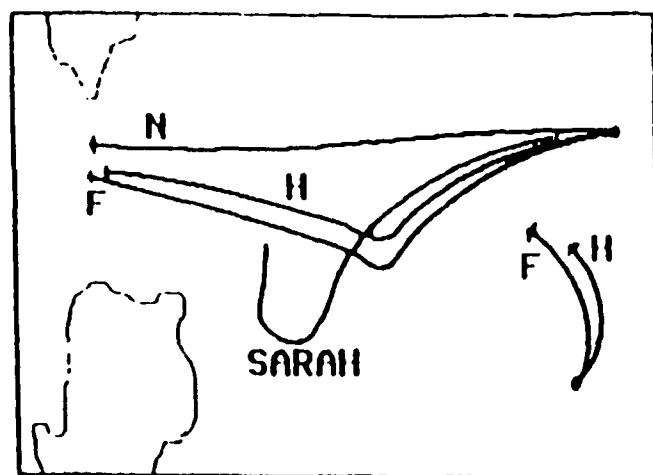


Figure 5. Tracks of Typhoon Sarah and the superimposed mesoscale vortices from 18 h barotropic model experiments starting at 23 UTC on 7 September 1989. Letters indicate forecast tracks with no superimposed vortex (N), with a half strength (H) and with a full strength (F) MCS vortex (Holland and Lander 1991).

Although the presence of a MCS may be detected in the satellite enhanced IR imagery, the structural characteristics of these systems over the tropical oceans are unknown. Understanding the tropical cyclone motion in the presence of a MCS requires *in situ* measurements to provide ground-truth of the structure of the MCS, the structure of the tropical cyclone and the wind structure between the MCS and the cyclone. This was the goal of TCM-92.

### C. PRIMARY MISSIONS OF TCM-92

The primary missions of TCM-92 were based on the theories described above and in further detail by Elsberry et al. (1992). Four hypotheses were posed in relation to these theories and corresponding flight tracks were developed. The hypotheses were:

1. Long-lived tropical MCSs have a three-dimensional wind and thermal structure similar to a midtropospheric vortex in the stratiform rain region of a midlatitude MCS, and have sufficient horizontal extent to cause a mutual interaction with a tropical storm or weak typhoon via a Fujiwhara-type effect that results in track deviations of 100 km over a day.
2. Long-lived tropical MCSs that maintain a quasi-stationary position relative to an associated tropical cyclone cause approximately 100 km deflections in the cyclone track via the divergent circulation and its interaction with the symmetric vorticity field to create a symmetric wavenumber one circulation.

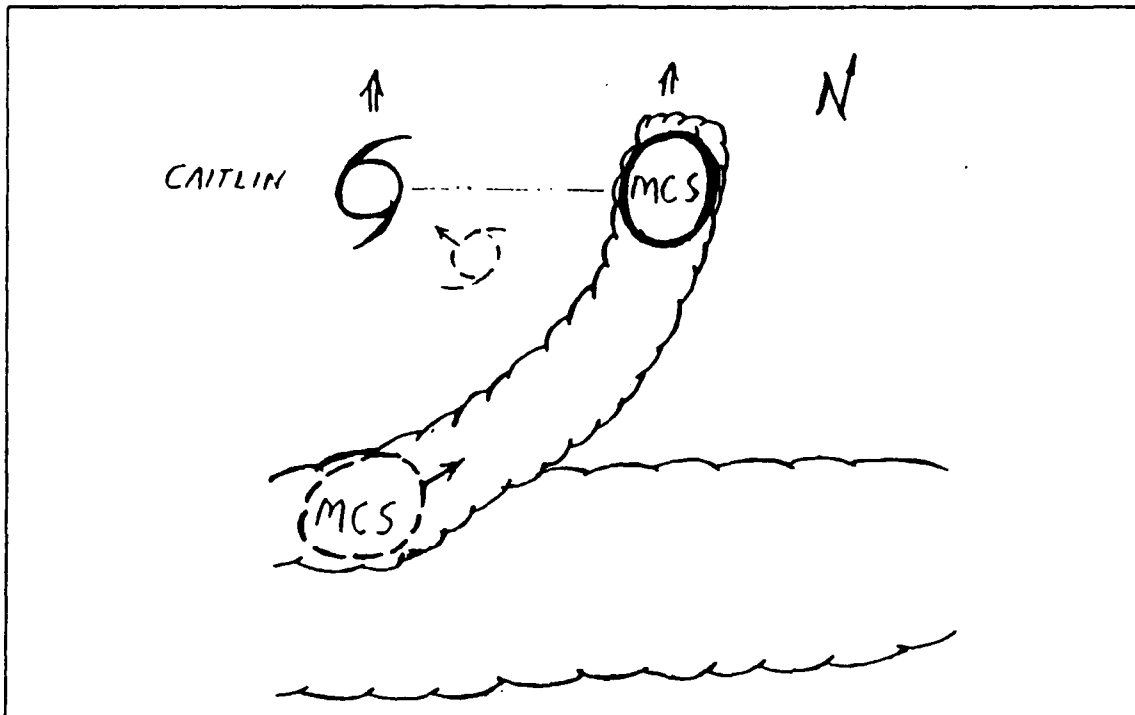


**Figure 6.** Schematic of a curved band of the active monsoon trough cloudiness with the positions of tropical storm Caitlin and a MCS at two times. The attached arrows indicate the track directions before (MCS to south of Caitlin) and after (MCS east of Caitlin) the two systems appear to couple along the dot-dashed line (Elsberry et al. 1992).

3. Relative cyclone track displacements of a MCS and a tropical cyclone can be related to their radial positions within the horizontal wind shear field of an active monsoon trough.
4. Tropical cyclone genesis is caused by the merger of two or more interacting MCSs to create a system with greater vorticity.

Testing these hypotheses requires having at least two vortices, or at least potential vortices, available for investigation. As outlined by M. Lander in Dunnavan et al. (1992), the synoptic regime in western North Pacific (WPAC) was not conducive to producing long-lived MCSs during TCM-92. Rather, short-lived systems tended to prevail until the monsoon trough briefly set up in WPAC late in the experiment. The lack of long-lived systems may be explained due to the lack of background vorticity necessary to spin up potential vortices (Elsberry et al. 1987). Although a few missions



were flown in an effort to examine possible vortex-MCS interaction cases, more opportunities were available to fly alternative or secondary missions.

## D. MCS CHARACTERISTICS

### 1. Formation

Frank and Chen (1991) and Frank (1992) have proposed that the genesis stage of a tropical cyclone may occur in less than one day in association with a MCS. They propose that a mesoscale vortex forms in the stratiform rain region behind a deep convection line due to the organized ascent and latent heat release in the stratiform area (Fig. 7). For certain large-scale conditions, the formation of a large stratiform rain region results in a local reduction of the vertical stability, which reduces the Rossby radius of deformation

$$L_R = C_g[(f + \zeta)^{1/2}(f + 2V/R)^{1/2}]^{-1/2}.$$

Because the group velocity  $C_g$  is reduced to small values in the moist adiabatic stratiform region, the local Rossby radius may be reduced to about 125 km, which is smaller than the area of the stratiform cloud. In the normal tropical atmosphere, the Rossby radius is much larger than the area of convection, so that latent heat release is balanced locally by vertical ascent and the resultant energy is radiated from the region via gravity waves. When the Rossby radius is large, only small net warming and generation of rotational motion occurs.

In the special conditions of Fig. 7, the latent heat release is more efficient at increasing the temperatures and rotational winds than a similar amount of heating would have in a cluster of individual convective clouds in an unsaturated environment. The spinup of the vortex with time, and the descent of the maximum vorticity, in the Frank and Chen model is shown in Fig. 8. Rather than taking days to spinup, the time period is just 12 h, which means the vortex could be developed on the time scale of a diurnal cycle of deep convection. Once the stratiform region becomes well-established (Fig. 7), the vorticity increase is almost entirely due to stretching. That is, the vertical motion associated with the latent heating in the stratiform region is being converted into rotational motion rather than propagated away via gravity-inertia waves.

The model-generated mid-level cyclonic vorticity and anticyclonic vorticity aloft are shown in Fig. 9. Notice that the horizontal scale is of the order of 100 km at 500

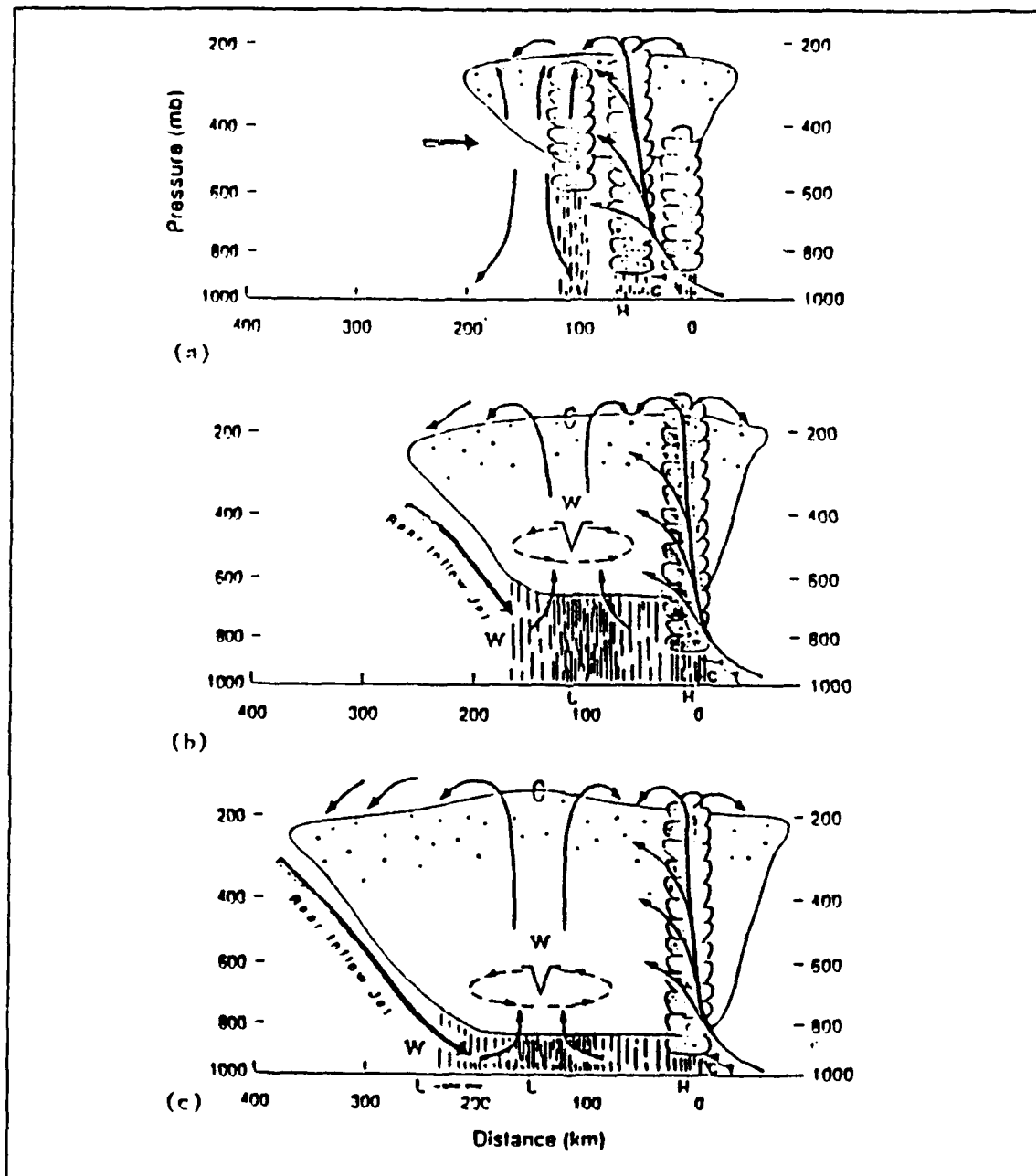


Figure 7. Schematic diagrams of the structure of an MCC and the associated mesovortex at (a) initial stage, (b) mesovortex genesis stage, and (c) mesovortex intensification stage (Frank and Chen 1991).

mb and about twice that at 200 mb. Frank and Chen propose that the formation of such a mesoscale vortex may occur in tropical maritime cloud clusters via this process of

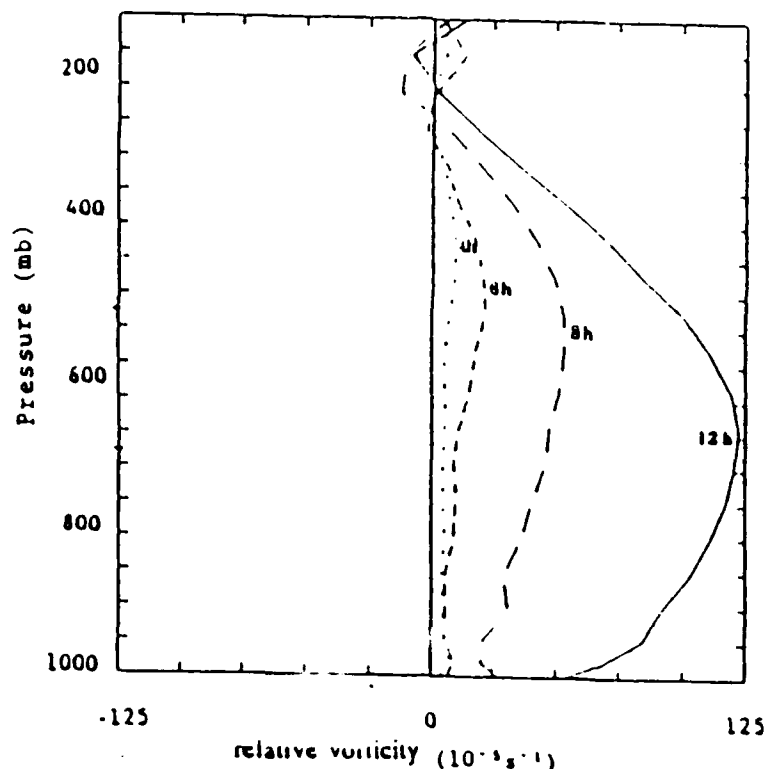


Figure 8. Downward displacement of the relative vorticity maximum in the stratiform rain region at selected times during the numerical model integration of Frank and Chen (1991).

reduced Rossby radius in the stratiform cloud region. Although the details regarding the necessary and sufficient environmental conditions (and possible role of ice microphysics) are not known, the Frank and Chen model provides a plausible explanation for why a satellite-observed MCS may contain a mesoscale circulation that could interact with a tropical cyclone.

Evidence supporting the Frank and Chen proposal may be found in a case documented by Menard and Fritsch (1989) in what they term a mesoscale convectively-generated vortex (MCV) associated with a mesoscale convective complex (MCC) that formed over Oklahoma on 6-7 July 1982. This complex was a large and intense area of convection forming in a region of high convective available potential energy (CAPE) and relatively stable synoptic conditions. Within this MCC, a three layered structure became evident: a warm core mid-level cyclonic vortex; an upper-level anticyclone of larger scale than the mid-level vortex; and a rain-cooled mesoscale high with a trailing low at the

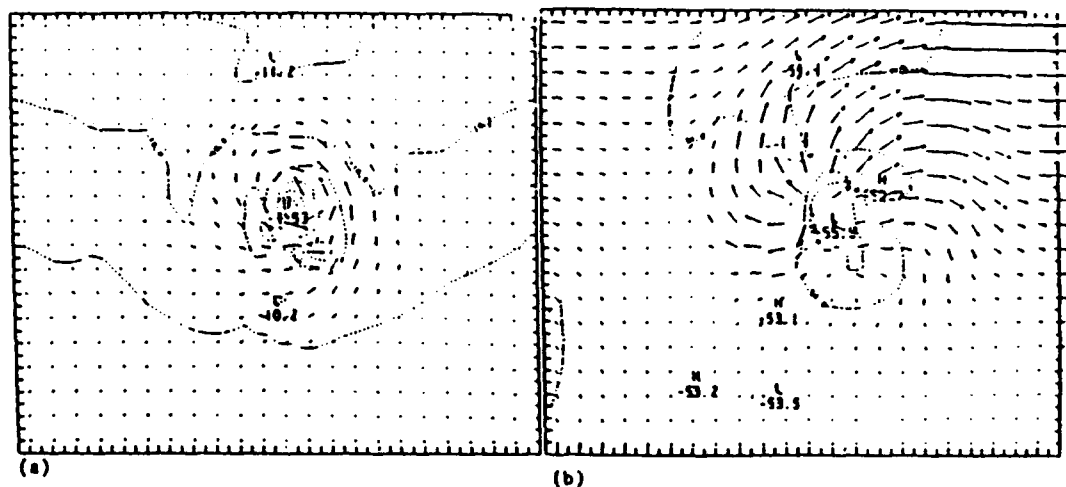


Figure 9. Relative wind vectors in a coordinate system moving at the speed of the vortex and temperature ( $^{\circ}$  C, dashed lines) at (a) 500 mb and (b) 200 mb. Each grid point is 25 km (Frank and Chen 1991).

surface (Fig. 10). Particularly intriguing was the persistence of the mid-level cyclone for two days in a relatively undisturbed synoptic regime.

## 2. Maintenance

A relatively unknown aspect of the long-lived tropical MCS is the source of its longevity. This is an important feature to assess when attempting to understand how the MCS can interact with a tropical cyclone long enough to significantly alter its track. Since the maximum cyclonic vorticity is in the midtroposphere and the anticyclonic vorticity is aloft (Fig. 9), the thermal structure must be cool in the lower and upper troposphere, with a warm core in the midtroposphere. A long-standing problem in understanding tropical convection is what maintains the convection above a cool near-surface layer. In the Frank and Chen (1991) model, the convective line remains coupled to the stratiform region (Fig. 7). In combination with the rear inflow jet, the mesoscale ascent is maintained provided adequate (but evidently not too large) values of CAPE are provided to the stratiform region.

After the MCC had dissipated in the Menard and Fritsch case, the mid-level vortex was found to exhibit a 5-10 m height depression over a horizontal distance of 250 km. The surface mesohighs exhibited pressures of 1-3 mb higher and temperatures of

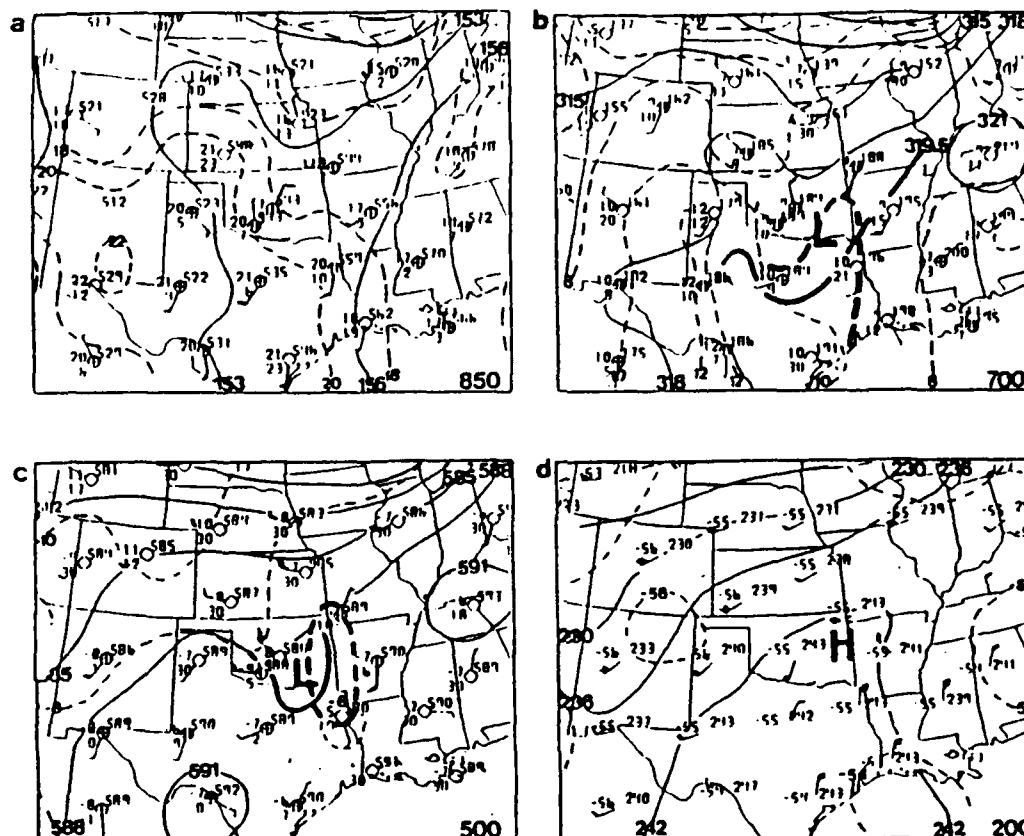


Figure 10. Upper-level analyses for: (a) 850 mb, (b) 700 mb, (c) 500 mb and (d) 200 mb, 1200 UTC 7 July 1982. Solid lines are heights (dm) and dashed lines are isotherms ( $^{\circ}\text{C}$ ). Heavy lines indicate subjective analysis. Full wind barb = 5 m/s (Menard and Fritsch 1989).

3-8  $^{\circ}\text{C}$  cooler than environmental values. This structure was accompanied by a vertical profile of positive relative vorticity from the surface to 350 mb, with a maximum between 750 and 550 mb (Fig. 11). A negative maximum could not clearly be discerned in rawinsonde data evaluated throughout the period and Menard and Fritsch suggest that the upper-level anticyclone dissipated rapidly due to inertial instability aloft. They further suggest the dominating feature of this case was the high  $\theta_e$  air being supplied at the low levels producing large amounts of CAPE in a region of weak vertical shear and upper level-diffuence (Figs. 10 and 12).

One explanation Menard and Fritsch suggest for the maintenance of the vortex is that the MCV was coupled to the low-level mesolow with mesoscale frictional convergence, and therefore associated mesoscale ascent being created during daytime

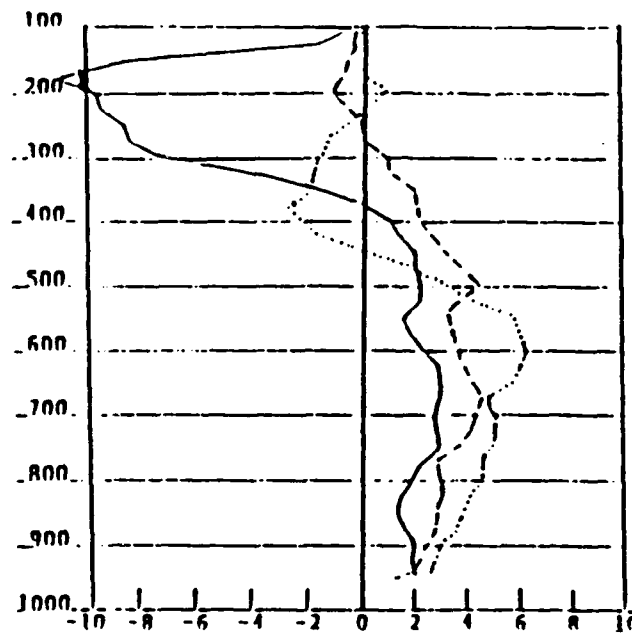


Figure 11. Vertical profiles of relative vorticity ( $10^{-3}/s$ ) for 1200 UTC 7 July (solid), 0000 UTC 8 July (dashed) and 1200 UTC 8 July (dotted) 1982 (Menard and Fritsch 1989).

heating. Resultant condensation heating could then act to maintain the vortex. Their study suggests that a mesoscale feature such as the MCC can alter the environment significantly given the appropriate synoptic regime. Such alteration may result in long-term effects (such as the development of a tropical cyclone) if the warm-core cyclone extends down to the surface.

Raymond and Jiang (1990) have proposed a theory for long-lived MCSs in the midlatitudes that might also be relevant to the TCM-92 observations. Their mechanism involves an interaction between quasi-balanced vertical motions and the diabatic effects of moist convection (Fig. 13). A low-level inflow is hypothesized to provide a continual source of water vapor that ascends over the raised isentropic surfaces. Such surfaces are found in the evaporatively cooled downdraft region below the midtropospheric positive potential vorticity anomaly. In the midlatitudes, cold highs below the MCS are quite intense and the lifting of the warm air at the boundary of the cold high is sufficient to cause condensation. The Raymond and Jiang model produces a cyclonic circulation in the lower troposphere (Fig. 14a) such that air parcels ascend on the east side and descend on the west side. an anticyclonic circulation is created at 10 km (Fig. 14b).

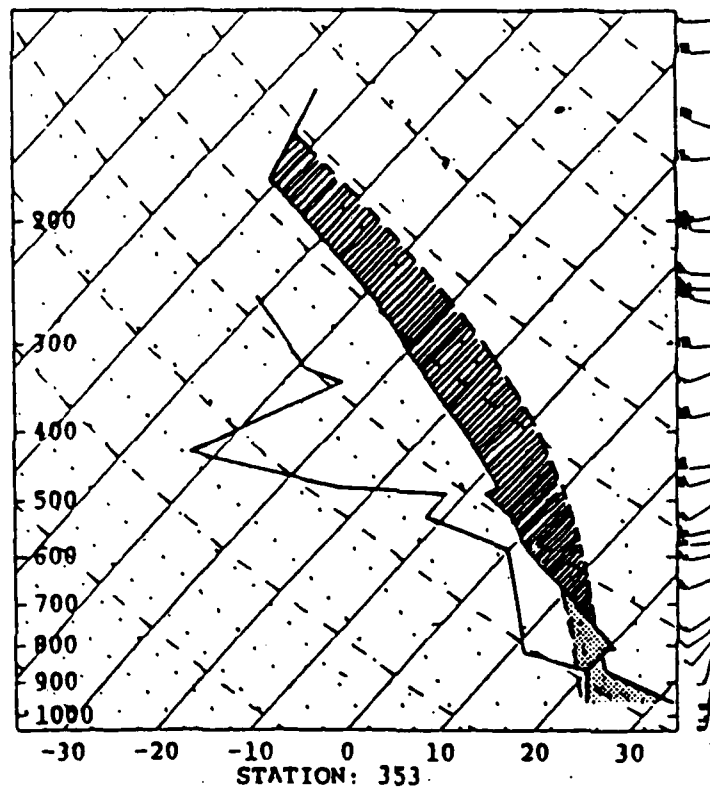
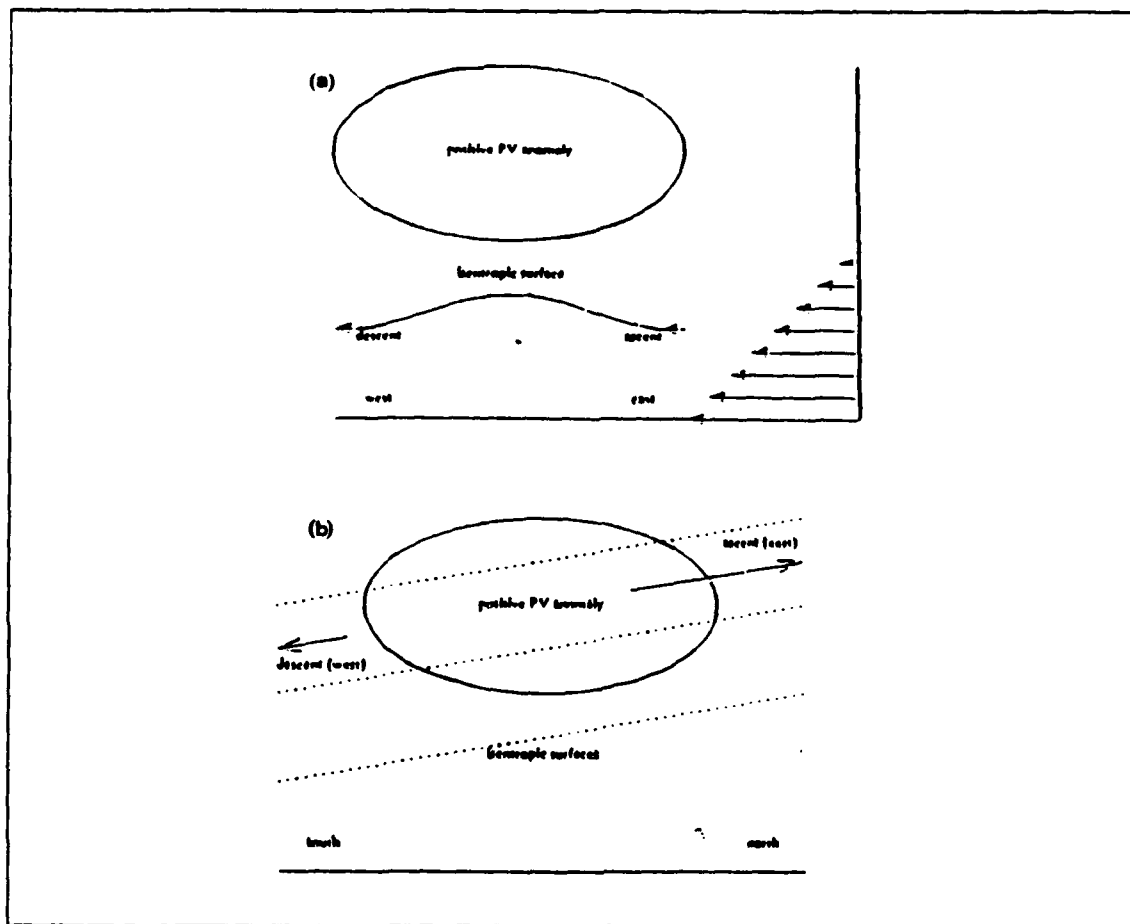


Figure 12. Sounding for Oklahoma City 0000 UTC 7 July 1982. Hatched area is the positive convective energy of an undiluted updraft; shaded area is the negative convective energy of a saturated downdraft. Full wind barb = 5 m/s; flag = 25 m/s (Menard and Fritsch 1989).

Between these vortices, the air is relatively warmer than the air above and below. The Raymond and Jiang model provides a long-lived, self-contained MCS because the interactions within the convection are between a mesoscale lifting mechanism associated with potential vorticity anomalies of a strength comparable to the ambient potential vorticity.

Hertenstein and Schubert (1991) have also modeled diagnostically the potential vorticity anomalies in the wake of midlatitude squall lines. Based on observations from the PRE-STORM experiment, they suggest that squall lines with trailing stratiform regions may be associated with large, positive midtropospheric potential vorticity anomalies in their wake. Unlike the squall line, the trailing stratiform region can be represented by a diabatic heat source due to condensation, with an underlying layer acting as a diabatic heat sink due to evaporation. The lengthy time-span and broad regional



**Figure 13.** Sketches of mechanisms by which lifting might occur in the presence of a potential vorticity anomaly in shear confined to below the anomaly on an east-west plane. (a) In a frame in which the anomaly is stationary, the relative environmental wind induces ascent and descent on the perturbed isentropic surface created by the potential vorticity anomaly. (b) Potential vorticity anomaly viewed from the east with tilted isentropic surfaces (dashed lines) associated with uniform ambient westerly shear through the depth of the illustration. The cyclonic circulation around the anomaly causes ascent in the northward-moving air on the east side and descent in the southward-moving air on the west side (Raymond and Jiang 1990).



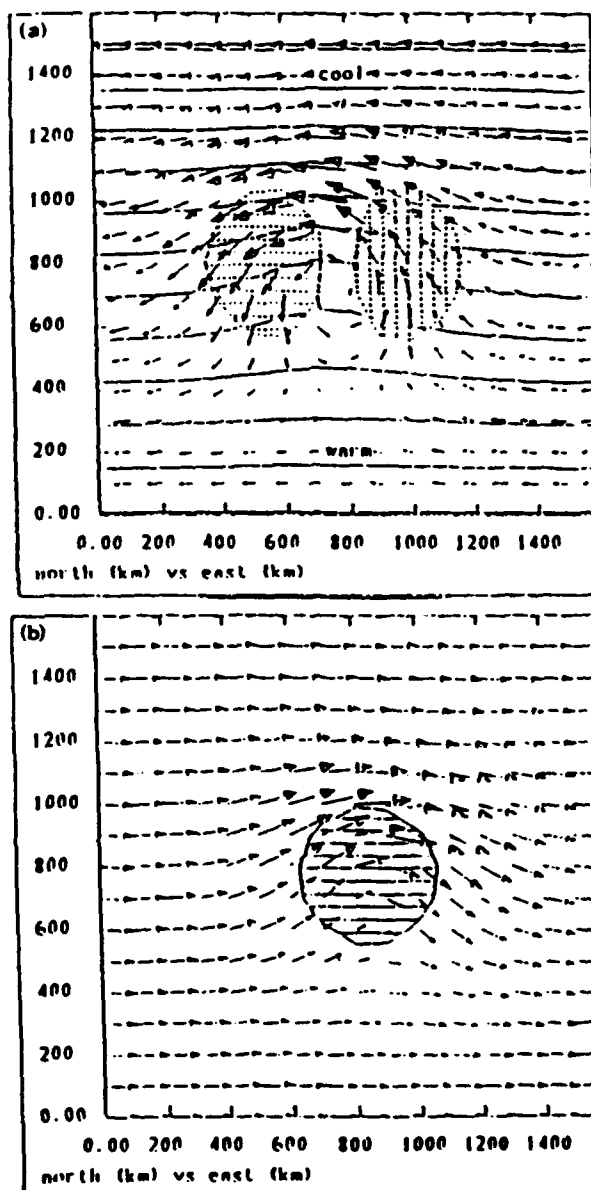


Figure 14. Flow on horizontal sections at (a)  $z = 3$  km and (b)  $z = 10$  km. Flow is generated after  $10^4$  s of integration of the Raymond and Jiang (1990) model. Potential temperatures at  $1^\circ$  K intervals and updrafts/downdrafts exceeding  $0.5$  cm/s are indicated in (a). Region of negative potential vorticity anomalies exceeding  $0.33$  pvu is hatched in (b). Wind vectors of  $100$  km length correspond to  $3$  m/s in (a);  $5$  m/s in (b).

coverage of the stratiform region present a strong midtropospheric potential vorticity signal. This signal is eventually stronger than that found in the more intense line of convection associated with squall lines.

Hertenstein and Schubert force a two-dimensional semi-geostrophic model in isentropic and geostrophic coordinates with an apparent heat source corresponding to the trailing stratiform-type squall line. A strong cyclonic potential vorticity maximum is simulated in the midtroposphere with a broad but shallow anticyclonic maximum aloft (Fig. 15). Notice that the wind maxima ( $\pm 5$  m/s) associated with the midtropospheric cyclone are separated by about 250 km, the wind maxima ( $\pm 9$  m/s) associated with anticyclone are about 450 km apart. Thus, the horizontal scale of the anticyclonic vorticity region aloft is about twice that of the cyclonic region. Lower temperatures below, higher temperatures above, and the midtropospheric vorticity maximum are simulated in the Hertenstein and Schubert model. This diagnostic model suggests that diagnosed midtropospheric vortices in the stratiform region are quasi-balanced wind and mass fields associated with convectively produced potential vorticity anomalies in the midlatitudes.

Fritsch (1992) has proposed a mechanism in which new deep convection may form within the cool region of a MCS, and specifically does not require any frictional convergence. Although his observational study was of a midlatitude MCS, Fritsch proposed this mechanism can create an inertially stable warm-core vortex that can lead to tropical cyclone genesis. Fritsch analyzed the development-decay cycle over three days of a long-lived MCS over land. New convection developed in the interior over the cold pool rather than on the boundary as in the Frank and Chen or Raymond and Jiang models. The net MCS intensification during the convectively active phase appeared to be well correlated with the strength of that convection. The potential vorticity cross-sections were similar to the MCS models described above in that the positive maximum was at 550 mb and negative maximum was at 250 mb, and positive anomaly was approximately half as wide as the negative anomaly. The positive anomaly increased from 100 km diameter on the first day to 200 km on the second day.

An essential difference in Fritsch's observational study relative to the Raymond and Jiang model is that the air trajectories originated upstream of the MCS rather than on the leading edge (Fig. 16). The MCS, which was translating with midtropospheric winds, moved slower than the air in the low-level jet that was providing the continual moisture source. However, the lifting mechanism is still the isentropic ascent over the evaporatively cooled downdraft air as in the Raymond and Jiang model (Fig. 13).

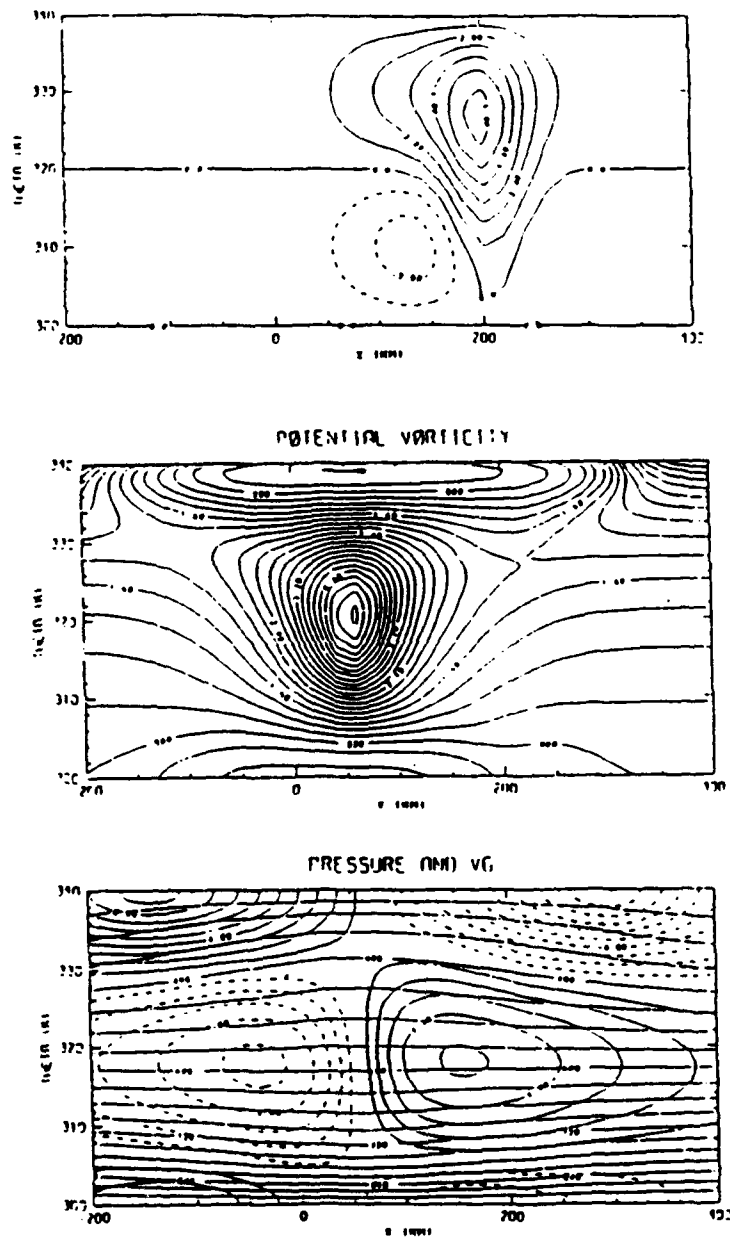


**Figure 15.** Heating function (top), potential vorticity (middle), wind speeds and isotherms (lower) diagnosed in the Hertenstein and Schubert (1991) model. Heating function corresponds to a squall line with a trailing stratiform rain region and is indicated by solid contours while dashed lines represent cooling. Note that the contour interval for the potential vorticity fields is 0.2.

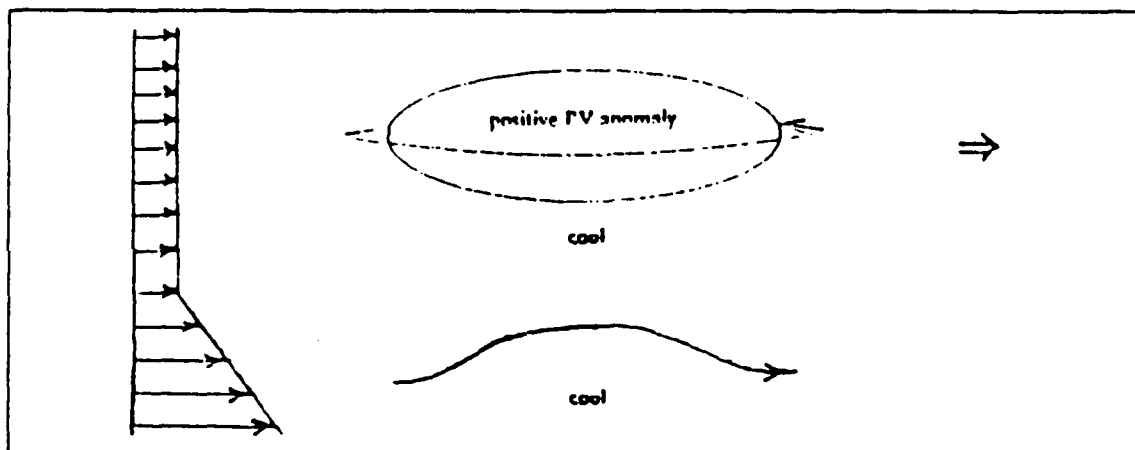


Figure 16. Schematic of the sheared environmental wind profile and low-level trajectories of air parcels in a rear-inflow case deduced in an observational study by Fritsch (1992).

## E. EXPECTED MCS STRUCTURES

With most study of mesoscale convective systems being concentrated on midlatitude systems, background on tropical MCS structure is limited. However, a discussion of climatological observations of tropical mesoscale systems is provided. In addition, the relation of the above theories to the tropics is presented.

### 1. The Western Pacific Region (WPR) MCS

A 1983-1985 climatology of WPR MCCs is provided by Miller and Fritsch (1991). Within this climatology, a comparison is made between midlatitude MCCs of the Americas and those of the WPR. Miller and Fritsch define WPR MCCs using the same definition offered by Maddox (1980). Using similar blackbody temperature threshold values on IR imagery, they classify MCCs based on geographic areas encompassed by the MCC cloud shield. These thresholds consisted of  $-33^{\circ}\text{C}$  and  $-56^{\circ}\text{C}$ . Although this was useful for consistency, they have limitations due to tropical MCCs exhibiting much colder cloud top temperatures than midlatitude versions. Nevertheless, they found overall cloud shields very similar in size ( $200,000 - 300,000 \text{ km}^2$ ) and duration (10 - 11 h). A similar diurnal cycle could also be discerned in the development of WPR MCCs (Figs. 17a and 17b).

Evaluation of preferred zones of development indicated similar requirements (e.g., low-level advection of high  $\theta_e$  air and upper-level diffluence) necessary for the MCCs of the Americas applied in the WPR. They found the WPR MCC was usually

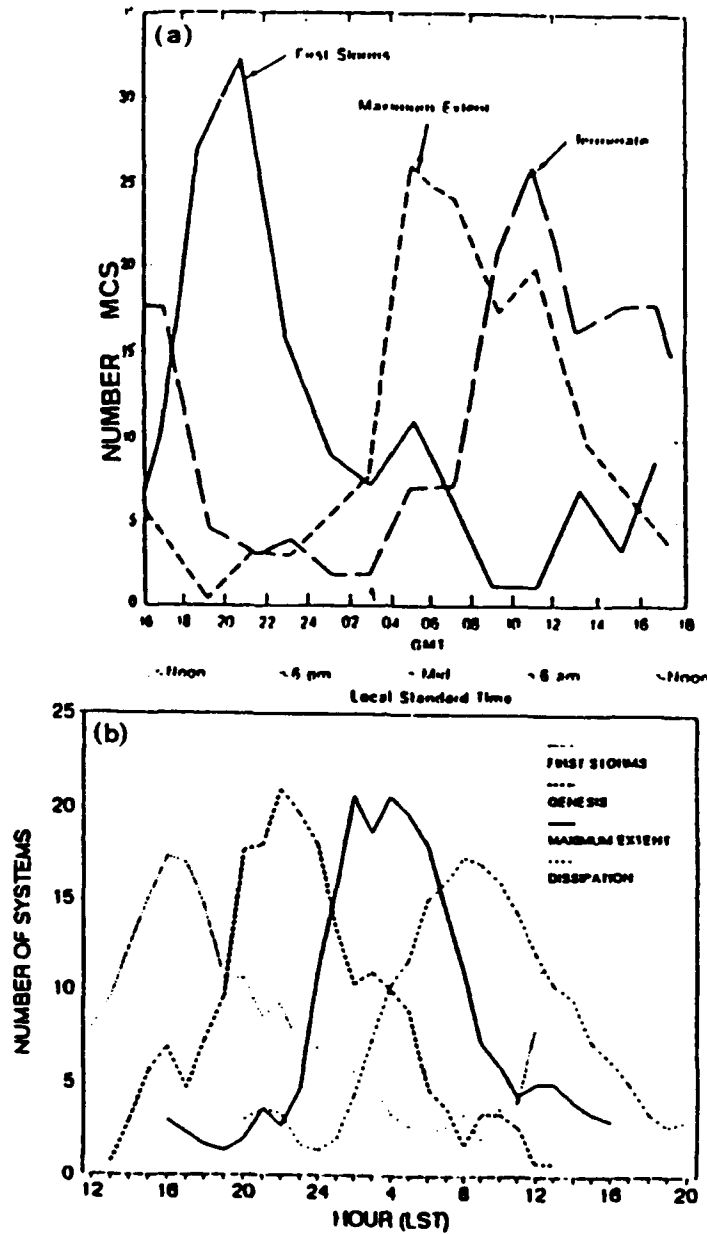


Figure 17. Comparison of MCS life cycles in U.S. and WPAC. (a) Diurnal variation in the number of MCCs observed in the mid-western United States, from 1600 UTC (1000 LST) to 1800 UTC (1200 LST) the next day (Maddox et al. 1986). (b) Life cycle of western Pacific region MCCs. Frequency curves were smoothed with a three-point running mean (Miller and Fritsch 1991).

tied to either land masses or large islands. Very few MCCs were found over the open water within the period studied (Fig. 18). Further, it is noted that several MCCs that developed over near land have then moved over water and developed into tropical cyclones. Although many similarities exist between the MCCs of the Americas and the WPR, it is difficult to suggest midlatitude MCCs are the same as over-water MCCs MCSs of the tropics, based on climatology alone.

## **2. Application to Tropical MCS**

As indicated above, few observations exist to describe the structure and evolution of MCSs in the tropics. Indeed, this was a primary motivation for the TCM-92 mini-field experiment. As presented, the basic physical mechanisms for formation of a mesoscale vortex within the stratiform rain area would appear to operate as well in the tropics as in the midlatitudes. The requirement for a vertical wind profile that has higher velocities at low levels than in the midtroposphere (Figs. 13 and 16) would be satisfied in the monsoon trough region (Fig. 19). Strong southwesterly winds often are found at low levels on the equatorward side. Although strong tradewind flows are found on the poleward side as well, some limited experience suggests that the MCSs are more prevalent on the equatorward side (Elsberry et al. 1992). The lower inertial stability, and the higher equivalent potential temperatures, of the air approaching from the equatorward side would tend to favor MCSs in that branch. Multiple MCSs are common in this equatorward branch and a common forecast problem is to decide which of these MCSs might intensify into a tropical cyclone. Again based on limited personal observation, the poleward MCS tends to be favored, perhaps because of the larger Coriolis parameter being more favorable to induce rotational motion for the same low-level convergence. Mark Lander of the University of Guam is developing a climatology of MCS occurrences that will provide a more quantitative basis for discussion of the spatial distribution and intensification characteristics.

When the poleward MCS develops into a tropical cyclone, or any MCS within the equatorward branch develops a significant organization and moves poleward, the convective band may be curved cyclonically into a "fishhook" shape (Fig. 19). Continuation of this trend can lead to the convective band extending cyclonically around the poleward branch of the monsoon trough as in Fig. 4. The key concept related to the MCS models is that a low-level speed maximum is likely to be sustained over a period of days. Thus, the continual moisture flux into the rear of the MCS as in the Fritsch conceptual model (Fig. 16) would seem to be possible. Consequently, conditions for the MCS to be sustained during each diurnal minimum in convection, and for MCS

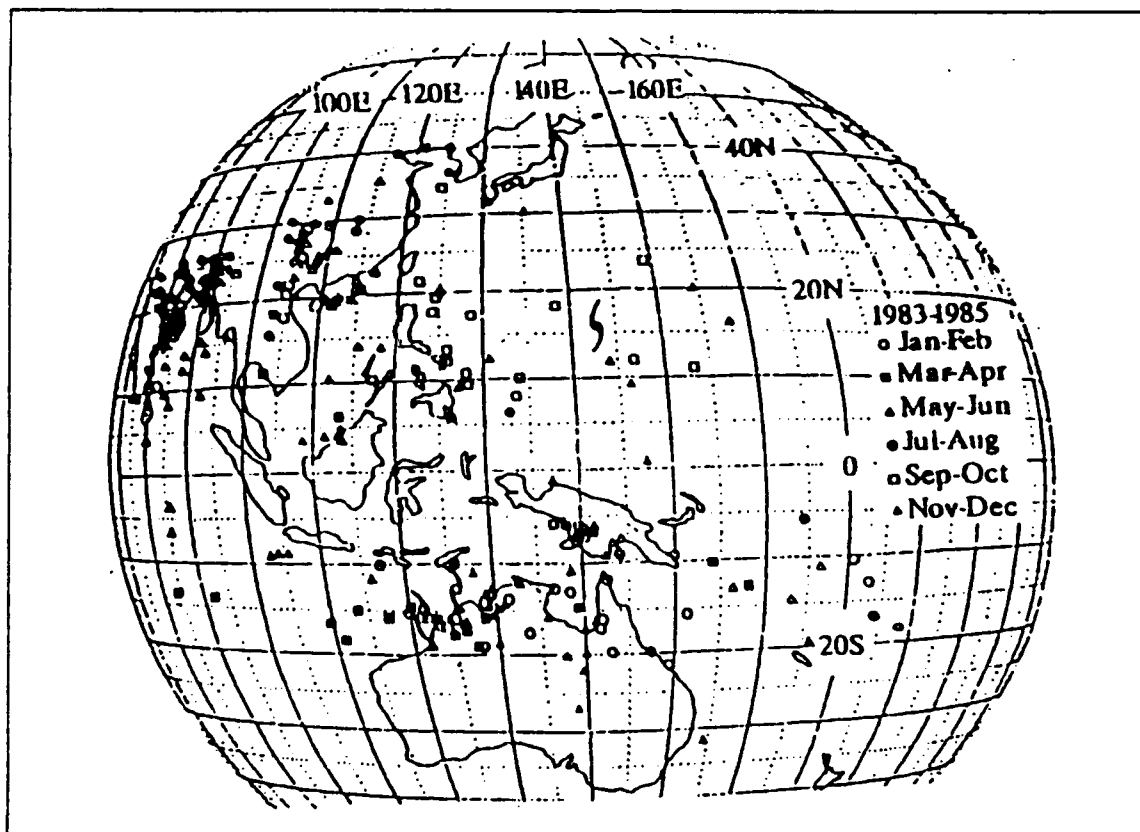


**Figure 18.** Geographical and monthly distributions of MCCs in the western Pacific region. Locations are for the MCC at the time of maximum extent of the cold-cloud shield. Hurricane symbols indicate MCCs that developed into tropical storms (Miller and Fritsch 1991).

rejuvenation and growth during the subsequent diurnal maximum in convection, would seem to exist in the monsoon trough. As indicated previously, such long-lived MCSs are required for significant deflections of an adjacent tropical cyclone.

One different aspect of the tropical maritime MCS versus the observations and models of the MCS over land in the midlatitudes is the likely magnitude of the isentropic lifting at low levels. In the midlatitudes, the rain-induced cooling below the high cloud bases can lead to strong downdrafts. Over land, this cold air may be little modified by surface fluxes, and strong cold highs may persist. In the tropics, the cloud bases of the convective cloud are lower and low-level rain cooling is smaller. However, saturated mesoscale downdrafts adjacent to the convective cloud do reach the ground and spread forward to form the lifting mechanism in tropical squall lines. The mesoscale downdrafts

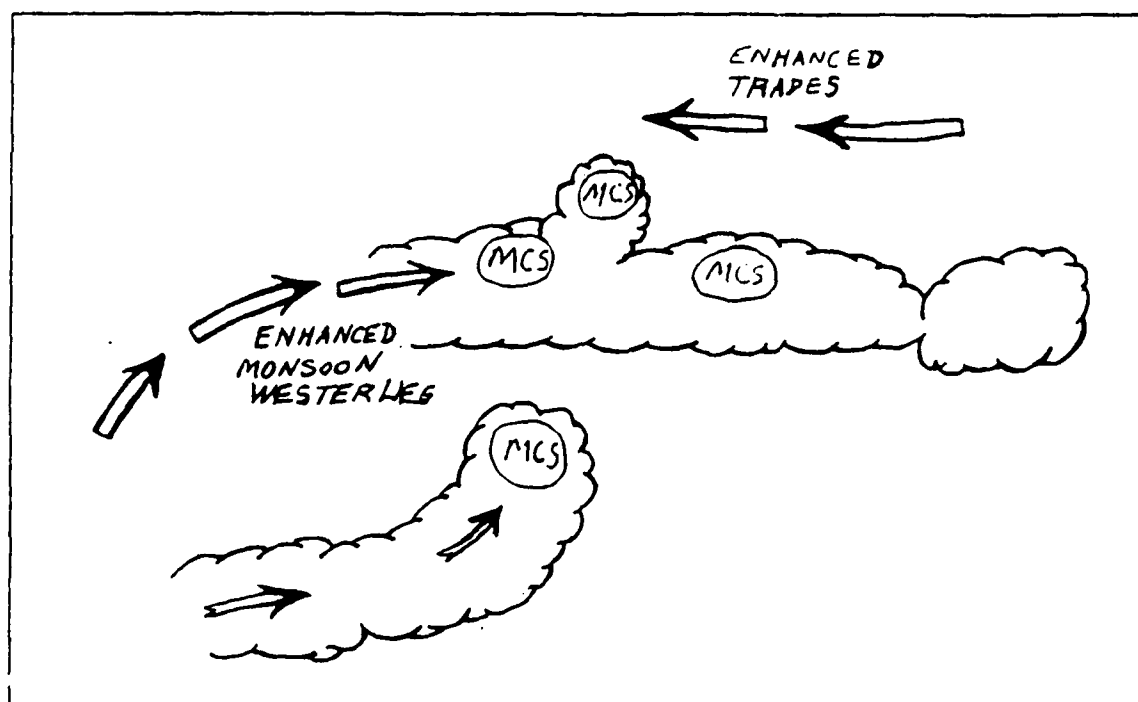


Figure 19. Schematic of early stage (top) and later stage (bottom) of multiple MCSs in an active monsoon trough region between enhanced monsoon westerlies and enhanced trade wind easterlies. In the later stage, development and/or translation of a MCS northward has resulted in a fishhook shape to the monsoon trough convection with sustained low-level flow into the rear of the MCS as in Fig. 16 (Elsberry et al. 1992).

create substantial cold pools with significant isentropic slopes as in the midlatitudes (Fig. 13). However, high  $\theta_e$  values of tropical air do not require as much vertical lifting to trigger convection. Consequently, the feasibility of the Fritsch rear-inflow mechanism for sustaining ascent and latent heat release in the stratiform rain region must be demonstrated from observations of tropical MCSs. The alternative may be an internal mechanism (perhaps related to the ice microphysics) that sustains the mesoscale updraft within the stratiform rain region, and thus the possibility for continued intensification of the midtropospheric vortex.

At least in the early stages of the MCS, little reflection of such a midtropospheric vortex can be found in the surface winds or pressures. This is highlighted in the two separate cases evaluated by Hertenstein and Schubert. Their first case



consisted of a squall line with no or little stratiform rain region. In this case, no vortex was found and positive vorticity anomalies were strongest in the low levels. Their second case, a mature squall line with stratiform region, had the features previously discussed. Thus, frictional Conditional Instability of the Second Kind (CISK) does not play an essential role during the early stages. Tapping into the surface oceanic energy source locally requires a downward extension of the vortex and high winds into the surface layer. Frank and Chen (1991) note that they are searching for the conditions under which the MCS circulation is extended downward since the frictional CISK plus the local oceanic heat source would provide two additional mechanisms for intensification to the tropical depression or tropical storm stage. Although TCM-92 was intended to provide observations necessary to understand tropical cyclone motion, these observations will be of interest to understand genesis as well. Thus, additional flight plans were developed for TCM-92 to understand the structure of MCSs when a tropical cyclone-MCS situation had not developed yet.

#### **F. ALTERNATE MISSIONS OF TCM-92**

With the limited time-frame of TCM-92, both in duration (30 days) and time of year (early within the typhoon season), alternative missions had to be developed. These missions were of vital importance to experiment objectives in that theories and conceptual models described above were an integral part of designing the alternate mission profiles. Thus, the alternate missions concerned documenting the structure of tropical MCSs and were essential to testing the hypotheses posed under TCM-92's primary missions. As discussed in the operations plan (Elsberry et al. 1992), these structure missions were to consist of flying through MCSs at multiple levels (700 mb, 500 mb, 300 mb). Both aircraft observations and the omega dropwindsondes were desirable to examine the horizontal and vertical structures of these features. Because only one aircraft was available, it was impossible to document long-lived MCSs throughout their life cycle (18-24 h). Thus, the MCS structure missions captured either the early or late stages of long-lived MCS life cycles. Short-lived MCSs ( $< 10$  h) primarily were observed and one Aircraft Observation Period (AOP) captured a system's entire life cycle. The majority of TCM-92 missions encountered non-interacting MCSs and these missions accounted for five of the nine missions. A composite of these individual missions at different stages of development will be attempted to formulate a model of the life cycle.

### **III. DATA SUMMARY**

With the short time-frame in which TCM-92 was formulated, arrangements for data collection had to be restricted to standard data bases. Observing the convective systems of interest required relatively high spatial and temporal data resolution. As previously discussed, the primary platforms available for such coverage were the aircraft and the geostationary satellite. Thus, most data collection efforts centered on these platforms. Additional data include the Special Sensor Microwave Imager (SSM/I) imagery plus the data sources normally available on the Automated Weather Network (AWN). The latter encompassed standard synoptic data and the Fleet Numerical Oceanography Center (FNOC) analyses and forecast fields. Very few FNOC fields and standard data were missing in the data collection effort. These data and analyses have a coarser resolution than is desirable for mesoscale analysis. However, they provide background fields for the aircraft data, which often was contained within an area of only 300 n mi in diameter. Some of the dropwindsonde data were transmitted from the aircraft to the JTWC, and from there entered into the real-time AWN data base.

#### **A. AIRCRAFT DATA**

For the purposes of this section, aircraft data consists of flight-level (automated and manual) observations and dropwindsondes (sondes). Whereas flight-level observations are essential to detect the horizontal structure of the MCSs and interacting tropical cyclones, the sondes are critical to link the various levels together into a coherent vertical structure. Flight-level observations in one minute and ten second formats were automatically compiled and stored by the Improved Weather Reconnaissance System (IWRS) onboard the WC-130. Manual (Recco) observations were also made by the Aerial Reconnaissance Weather Officer (ARWO) during each sonde launch. The Reccos served as important quality control checks on any suspect sondes, as well as indicating visually sensed phenomena such as surface winds, radar observations, icing, etc.

##### **1. Improved Weather Reconnaissance System (IWRS) measurements**

IWRS senses data parameters eight times per second and averages these values into ten second data files. These ten second files are subsequently averaged to produce one minute files. The one minute files will be the primary flight-level data in the analyses of this study because they are of sufficient density and have been averaged to produce representative fields. The following information on the IWRS is taken from technical

manuals on IWRS and its subsystems (Omega Dropwindsonde System (ODWS) and Satellite Communication System (SATCOM)), which are maintained by the 815th Weather Squadron, Keesler AFB, MS 39534-5000. Further details concerning IWRS should be directed to that organization.

## 2. Flight-level data

As suggested above, IWRS flight-level data were highly effective in both accuracy and density. The periods when these data are believed to be unreliable are relatively few. Generally, these are the times when the aircraft was turning and shortly thereafter. Although this action does not necessarily affect the temperature and dew point measurements, the wind direction, speed and geopotential heights may be degraded as described below.

Degradation in the IWRS winds increases dramatically as the environmental wind speed decreases to less than 10-15 kt. Typically, ARWOs will consider an IWRS-produced wind of 10 knots or less as light and variable. However, this is probably an overly pessimistic view in situations with relatively constant wind fields, in which accuracy may be maintained in winds as light as 5 kt. Winds computed by IWRS are estimated from differential pressures sensed by three probes on the exterior of the aircraft (Fig. 20). In addition, navigation information and aircraft speed are provided through an interface with the inertial navigation system on the aircraft. If any of the probes are presented with an aircraft attitude other than straight-and-level flight, errors of varying magnitudes will be introduced. Degraded performance will also occur if the probes become covered with ice. Altitudes flown throughout TCM-92 were between 20,000 and 30,000 feet, which are prime regions for aircraft icing in MCSs and tropical cyclones. Thus, suspect data is removed from the data set for the analyses.

Geopotential heights will also suffer possible degradation during aircraft turns. The relative magnitudes of the errors are not as large as in the wind measurements. Geopotential heights are calculated using a pressure altimeter set to standard atmosphere (1013.25 mb) and a radar altimeter that measures height above ground. Typically, the radar altimeter aboard the WC-130 has an accuracy of about 1% of flight altitude. Thus, the system errors become very significant at the TCM-92 flight-levels (i.e., 20,000 to 30,000 feet). In addition, the system occasionally is unable to "lock on" to the surface at these high altitudes and in a turn.

Fluctuations in height values were detected in both AOPs, especially AOP 7 where the autopilot during this period was inoperable. Maintaining a constant aircraft attitude of a WC-130 at high altitudes is a difficult task without an autopilot. The result

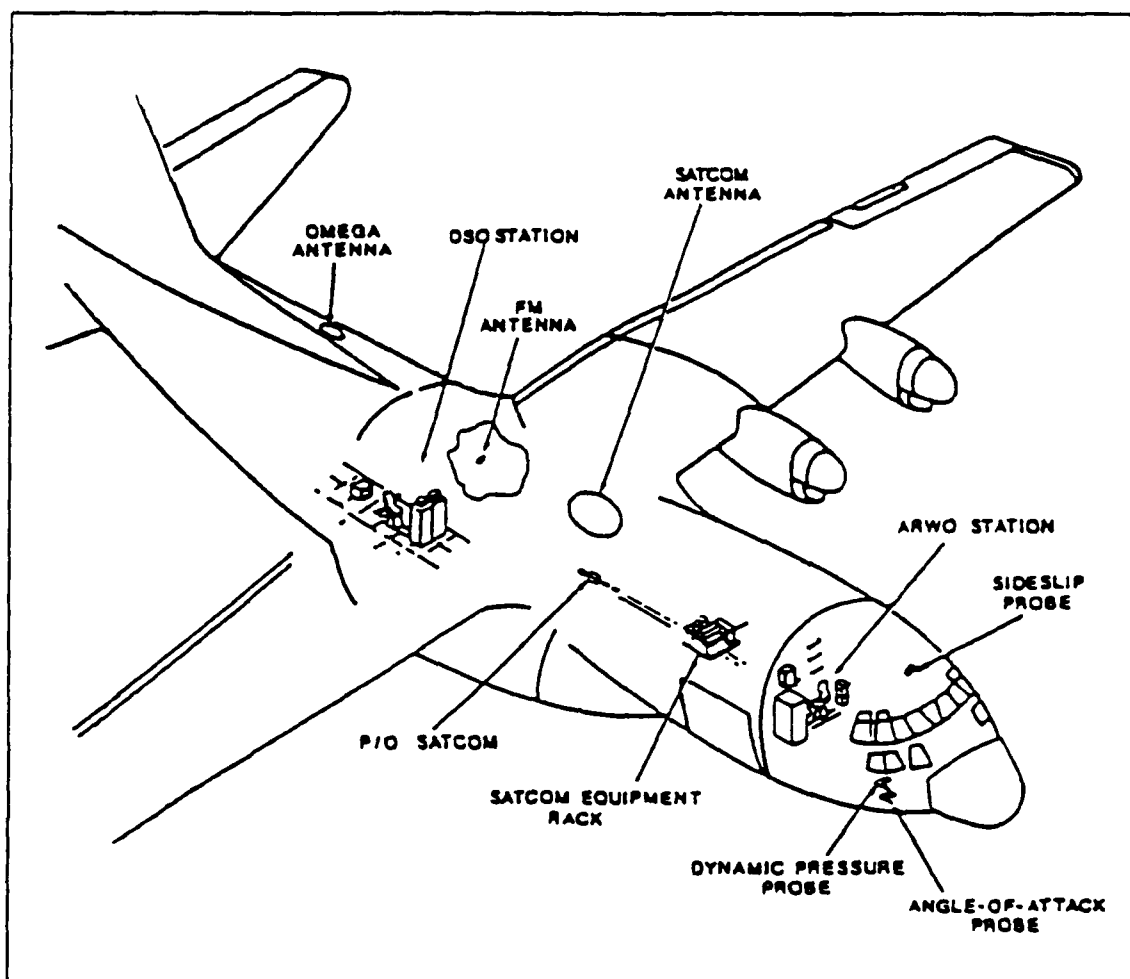


Figure 20. Location of primary Improved Weather Reconnaissance System (IWRS) components on a WC-130. Sideslip, dynamic pressure and angle-of-attack probes are used for sensing winds.

was fluctuating radar and pressure altitudes that were too large for the IWRS averaging to smooth. Thus, many of the geopotential heights were erroneous.

Another important aspect of the flight-level data collection was the methodology for normalizing all observations to a single reference pressure level. Generally, flight level data within  $\pm 25$  mb of a mandatory or significant level are combined into that level. For example, all measured parameters from 525 mb to 475 mb were grouped into the 500 mb level. This did not appear to create a problem for the winds. However,

unrealistic horizontal gradients in temperature, geopotential and humidity observations result from the aircraft ascending or descending through a 50 mb layer.

Because the aircraft temperature probe had anti-icing heating, application of this heating occasionally created temperature spikes in the data. Such spikes were few and minor in the two cases examined. The dewpoint probe is not as susceptible to icing and no noticeable degradation was found.

### **3. Omega dropwindsonde data**

Sonde requirements during TCM-92 severely tasked the ODWS since two sondes were in the air at most times, with a total 17 to 30 sondes per mission. These demands tended to overload the ODWS, and data frequently would be lost (Dunnavan et al. 1992). This section will provide further details on the ODWS data system to illustrate the potential error sources.

Omega dropwindsondes provide wind speed and direction, temperature, humidity and geopotential height data. The ODWS calculates the geopotential heights using temperature, humidity and associated pressure levels. Wind direction and speed are calculated by the ODWS software using 13.6 kHz worldwide omega transmissions to triangulate position and speed on the falling sonde, which falls at a rate of 1,000 feet per minute. Real-time wind calculations use the most recent three minutes of the omega signals. Every 30 seconds, the ODWS performs a least-squares, second-order fit to each of the three-minute data sets, and computes signal rate values at a time near the midpoint of the three-minute interval. A wind vector is then produced along with a confidence rating for the three minutes based on the omega signal strength. Since the sondes fall at a rate of approximately 1,000 feet per minute, the interval is approximately 3,000 feet between calculated wind values. The ODWS software encodes the calculated wind at the lowest altitude of each 3,000 foot interval.

Temperatures from the sensor on the sonde are received at the aircraft and the ODWS quality control software ensures temperature changes of  $\pm 3^{\circ}\text{C}$  of the preceding value are not encoded. Sondes will be rejected prior to launch unless the accuracy of the temperature sensor is within  $\pm 2^{\circ}\text{C}$  of a verification temperature. Temperatures at mandatory levels are automatically produced and significant levels are provided using temperature change thresholds. The dropwindsonde operator has an option of manually deleting unrealistic values. Such deletions were typically accomplished during all TCM-92 missions.

Humidity is also measured by a sensor on the sonde. In addition to the temperature check discussed above, the accuracy of the humidity sensor is evaluated prior

to launch and must be within 2% of a calibration value, or the sonde is rejected. Once the ODWS has quality controlled temperatures from the sonde, humidity levels are selected. A humidity level will not be encoded by ODWS unless the actual humidity deviates by 10% or more from a trend line resulting from humidity values of the two preceding adjacent levels. As a result, humidity profiles on the sondes appear quite smooth and provide little detail in terms of dry layers of smaller magnitude, which may be frequently found on rawindsondes. Thus, the sondes may not have the desired ability to accurately measure the mesoscale systems of interest. However, personal experience has shown that the sondes respond reasonably well when dropped through varying humidity levels found in cloud layers, inversions, etc. The ODWS software converts the humidity into a dewpoint depression for encoding on the dropsonde messages entered into the AWN.

Geopotential heights are produced from the hypsometric equation using the temperature and humidity profiles as a function of pressure, and is accomplished by the ODWS software. The integration of this equation is started at the aircraft altitude and is iterated downward to the surface. Thus, heights are most accurate at the aircraft altitude and decrease in accuracy down to the surface. ARWOs are required to ensure that data at the lowest levels deviate no more than  $\pm 30$  m from an independent verification height (when available). These calculated heights are naturally very sensitive to errors in the temperature profiles, and especially to the initial height data provided at sonde launch by the ARWO. The height data consist of a flight-level temperature, dewpoint, wind speed/direction and geopotential altitude. The latter consists of contributions from absolute (radar) altitude of the aircraft and the correction necessary to convert this value to a standard reference pressure level (e.g. 500 mb), both of which may be a source of error. If geopotential altitude is too high or low, the corresponding heights calculated by the ODWS from the sonde will also be erroneous. As suggested above, the fact that the aircraft was tasked to fly at much higher altitudes than normal proved to be a major factor in introducing fluctuating initial launch data and subsequent erroneous sonde heights.

Aircraft and dropwindsonde data underwent standard quality control checks during collection and then a post-experiment check using a program developed by LCDR D. Titley of the Naval Postgraduate School (NPS). Flight-level observations were compared with adjacent observations and considered good if within  $\pm 15$  degrees and  $\pm 5$  knots for winds,  $\pm 2$  ° C for temperature and dewpoint, and  $\pm 10$  m for geopotential height. These standards are also applied in the vertical soundings to ensure

overall data consistency. They are based on personal experience and observed behavior of the aircraft instrumentation during TCM-92. Dropwindsondes were further evaluated against rawindsondes from nearby land stations to ensure reasonable temperature and pressure profiles. This comparison does not necessarily validate the dropwindsonde due to the rapid and dynamic changes taking place within the mesoscale systems the sondes were probing. Geopotential heights proved to be the most erratic and it is suggested a large tolerance be applied when using this data in thermodynamic analyses.

## **B. SATELLITE DATA**

Satellite imagery from two separate systems was collected to ensure complete coverage. These systems were the Meteorological Information Data Analysis System (MIDAS) developed by NASA Goddard Space Flight Center and the Naval Satellite Display System-Geostationary (NSDS-G), which are both in operational use at JTWC. The primary enhancement curve used by the TCM-92 EOC was a modified version of the Dvorak "BD" curve (Fig. 21). This was done for consistency with JTWC practice and a desire to select an enhancement that is widely utilized in tropical centers. As the raw image files do not have an enhancement curve applied, the choice of the enhancement is an option for the user to select during post-experiment analysis.

Polar orbiting imagery from NOAA satellites was not collected because it was rare that a low-orbit satellite would pass over the vicinity of a target system. However, SSM I images were collected for possible use in conjunction with the TCM-92 aircraft data or conventional data. Though not used in this analysis, examination of rainfall rates and surface wind speeds using SSM I is expected to be useful for determining convection and circulation intensities.

### **1. MIDAS imagery**

Full resolution (2.7 n mi) infrared (IR) images were collected on 4 mm "dat" tapes throughout the experiment with few gaps in the archived imagery. This imagery is sectorized and covers an area from 5 ° S to 50 ° N and 115 ° E to 160 ° E. The image files are 1024 x 1024 pixels and are in the original satellite projection. Thus, no mapping of the image is accomplished and navigation of the grid is based on pixel locations relative to the sub-satellite position on the Earth.

Due to the data file size of the MIDAS visual imagery, which has a resolution roughly four times higher than that of the NSDS-G visual imagery, it was unfortunately necessary to reduce the resolution to the 2.7 n mi resolution of the IR imagery. The

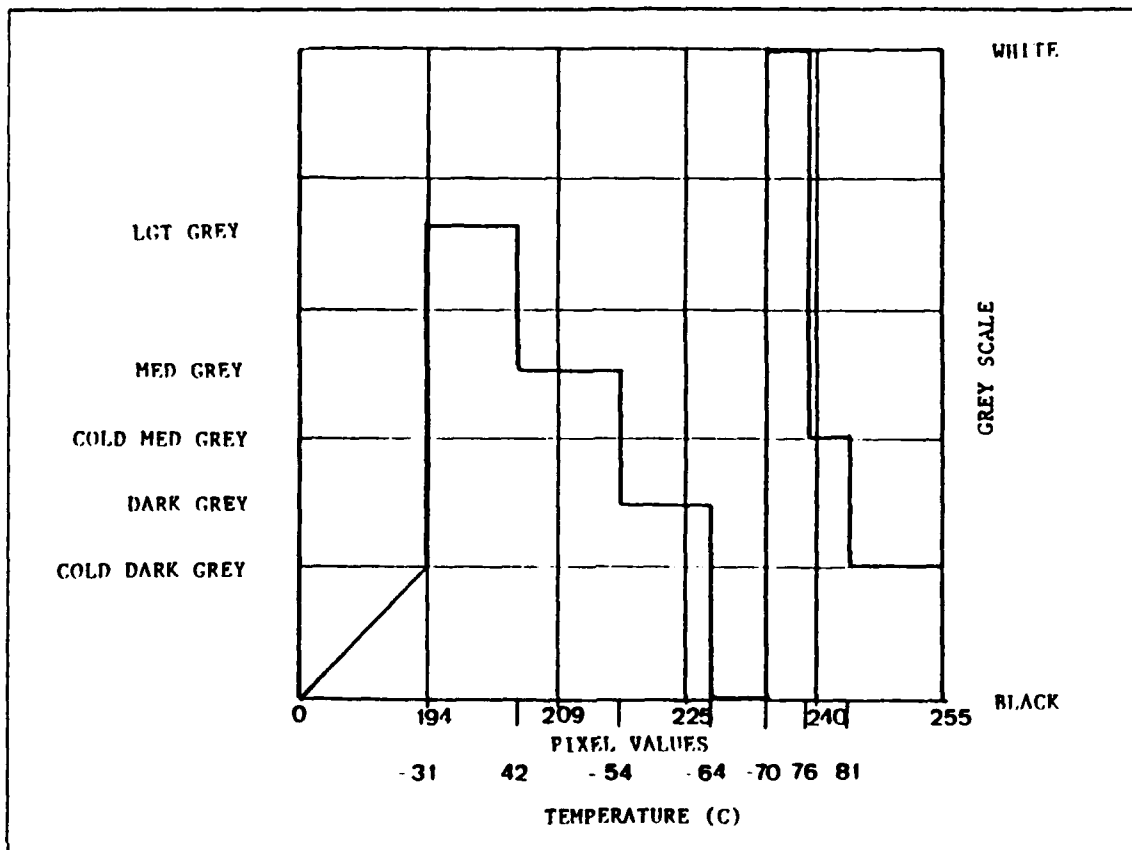


Figure 21. Modified Dvorak "BD" infrared enhancement curve for geostationary imagery. Enhancement employs continuous greyscale to -31 ° C.

larger data files would have required more time for archival on the MIDAS system than was available without adversely impacting JTWC operations.

## 2. NSDS-G imagery

IR imagery was also collected from a NSDS-G terminal at JTWC and loaded onto standard 5 1/4" floppy disks. Resolution of this imagery is the same as the MIDAS system (2.7 n mi). The goals for collecting this imagery were twofold. First, a viable back-up to the MIDAS imagery had to be considered in case a failure in collection occurred. Second, this system was openly accessible to the EOC members during the experiment for real-time decisions, whereas the MIDAS was not. This imagery format allows determination of useful motion vectors for systems of interest as well as providing large-scale views of WPAC convection.



Regional images were produced throughout TCM-92 usually covering the area of 5 ° N to 35 ° N and 120 ° E to 170 ° E. During each AOP, blow-ups of the target MCS interacting cyclone were made and archived as separate image files. Two different image coverages centered on the target system were selected: 15 ° lat. by 25 ° long. and 5 ° lat. by 10 ° long. Due to the limited amount of storage space on the NSDS-G and an inability to man the terminal on a 24-h basis, several gaps appear in the archived NSDS-G imagery.

### **3. Special Sensor Microwave Imager (SSM/I) data**

The DMSP satellite passes were automatically collected when they occurred within the area of 5 ° S to 35 ° N and 110 ° E to 150 ° E. SSM/I data were collected to provide the intensity of convection through use of rainfall rate algorithms. A frequent problem encountered during every AOP was that IR and or visual imagery suggested extremely widespread and strong convection when the aircraft personnel were observing considerably less convection visually or by the aircraft radar. The microwave imagery may provide a better representation of the convection under the cirrus shield detected in the IR and visual imagery.

## **C. CONVENTIONAL DATA**

Conventional data for the purposes of this discussion consist of: synoptic station data, ship and buoy data, sounding data, reconnaissance reports and FNOC gridded analyses and forecast fields. Times collected are from 16 July 1992 to 22 August 1992. These files were all stored on nine track magnetic tapes at NPS. They are usable in GEMPAK 5.0 format and provide coverage over WPAC from 5 ° S to 40 ° N and 100 ° E to 180 ° E. The primary use for these data is for analyzing the synoptic regime during TCM-92.

Unfortunately, satellite cloud track winds could not be stored on tape. However, hard copies were saved and copies of the JTWc hand-plotted analyses were made throughout the experiment, which routinely contain cloud track winds for the 200 mb and gradient levels. In addition, a series of surface pressure analyses accomplished by M. Lander, University of Guam, have been copied. There is at least one surface analysis per day of the experiment and the coverage is of the entire WPAC region. Finally, LCDR L. Carr, NPS, hand-analyzed 200 and 850 mb WPAC charts throughout most of TCM-92. The majority of these analyses contain all data available from the AWN in real-time.

#### IV. ANALYSIS

Two tropical MCSs observed during TCM-92 will be analyzed in terms of horizontal and vertical profiles following the approach of Maddox et al. (1986). Hand analyses of the wind, temperature and dewpoint depression fields are generated at the pressure levels of 300 mb, 400 mb, 500 mb, 700 mb, 850 mb and at the surface. Although the hand analyses were prepared by overlaying the concurrent satellite imagery, the imagery will be presented separately for clarity.

Most Aircraft Observation Periods (AOPs) during TCM-92 provided potential data sets containing a tropical MCS. Due to time constraints, just two AOPs (1 and 7) are selected for analysis. The primary objective is to produce an analysis of the most ideal MCS structure case (AOP 7) observed during TCM-92, and then contrast it with a less intense case (AOP 1) for comparison. These preliminary analyses are presented in terms of the expected characteristics of MCSs primarily based on midlatitude cases as presented in the background section (Table 1). For example, the primary structural feature expected is a mesoscale mid-level cyclone, referred to as a vortex. Such a vortex of sufficient intensity is required if the MCS is to alter the track of an adjacent tropical cyclone in support of the first TCM-92 hypothesis. In addition, the existence of a warm, moist mid-level would provide evidence as to the presence of a region with a small Rossby radius of deformation, as hypothesized by Frank and Chen (1991).

The following sections will provide descriptions of the two MCSs and their environments during AOPs 7 and 1. Satellite imagery used in the AOP 7 and 1 descriptions, as well as for this chapter, are compiled in Figs. A-1 through A-6 and A-7 through A-11 of Appendix A. In addition, the flight tracks flown and significant events that occurred in each system are discussed. Further details concerning the TCM-92 cases and the data characteristics can be found in Dunnavan et al. (1992).

##### A. AIRCRAFT OBSERVATION PERIOD 7 OVERVIEW

The objective of AOP 7 from 1642 UTC 14 August to 0237 UTC 15 August was to investigate a large circular MCS near 14 °N, 139 °E. During maximum extent at 1330 UTC 14 August (Fig. A-2a, Appendix A), cloud-top temperatures of -54 ° to -63 °C in this MCS encompassed an area of approximately 160,000 km<sup>2</sup>. In addition, a region of approximately 20,000 km<sup>2</sup> with temperatures less than -80 °C existed in the center of this MCS. Satellite imagery showed convection within the MCS to be very concentrated

Table 1. EXPECTED CHARACTERISTICS OF MCS STRUCTURE

Feature	Position Relative to MCS	Convective Growth Stage	Horizontal Scale
<i>Mid-Level Vortex</i>	Stratiform Rain Region	Early Mature to Decaying	100 n mi to 125 n mi
<i>Low-Level Vortex</i>	Under Stratiform Rain Region	Late Mature to Decaying	200 n mi to 250 n mi
<i>Upper-Level Anticyclone</i>	Outflow Layer Above MCS	Mature and Decaying	175 n mi to 225 n mi
<i>Mid-Level Warming</i>	Stratiform Rain Region	Formation to Decaying	Minimum 100 n mi
<i>Low-Level Cold High</i>	Under Convective Rain Region	Formation to Mature	Order of 100 n mi
<i>Low-Level Warm, Moist Rear Inflow</i>	Into Rear of MCS (With Direction of Movement)	Formation to Mature	Of Similar Proportions to MCS
<i>TD Development</i>	Under Mid-Level Vortex	Mature to Decaying	Similar to Low-Level Vortex

and circular. Thus, this AOP had captured a seemingly ideal case of a long-lived (18-24 h duration) tropical MCS in its mature and decaying stages.

For the two days prior to AOP 7, a large monsoon gyre dominated the synoptic circulation in the region surrounding the MCS development area. Typhoon Kent was to the north, a tropical disturbance (soon to become TS Lois) was to the west, and a broad area of diurnally active convection associated with convergent flow into Kent was on the east end of the gyre (Fig. 22). Low-level southwesterly flow of 10-15 kt extended to roughly 13 °N. North of 13 °N, low-level wind fields weakened and the area between 135 °E and 145 °E appeared to be influenced by speed convergence. Upper-level northeasterly winds of 35-55 kt created significant vertical shear south of 13 °N (Fig. 23). North of this region, the upper-level wind field was weak and diffuse. Upper-level anticyclonic flow had persisted for several days in a large area to the southeast of Kent. Weak ridging also extended toward the west-southwest to approximately 135 °E. Thus, it appeared that this low vertical shear environment in the region of AOP 7 was the cause of the circular and quasi-stationary nature of the ensuing MCS developments.

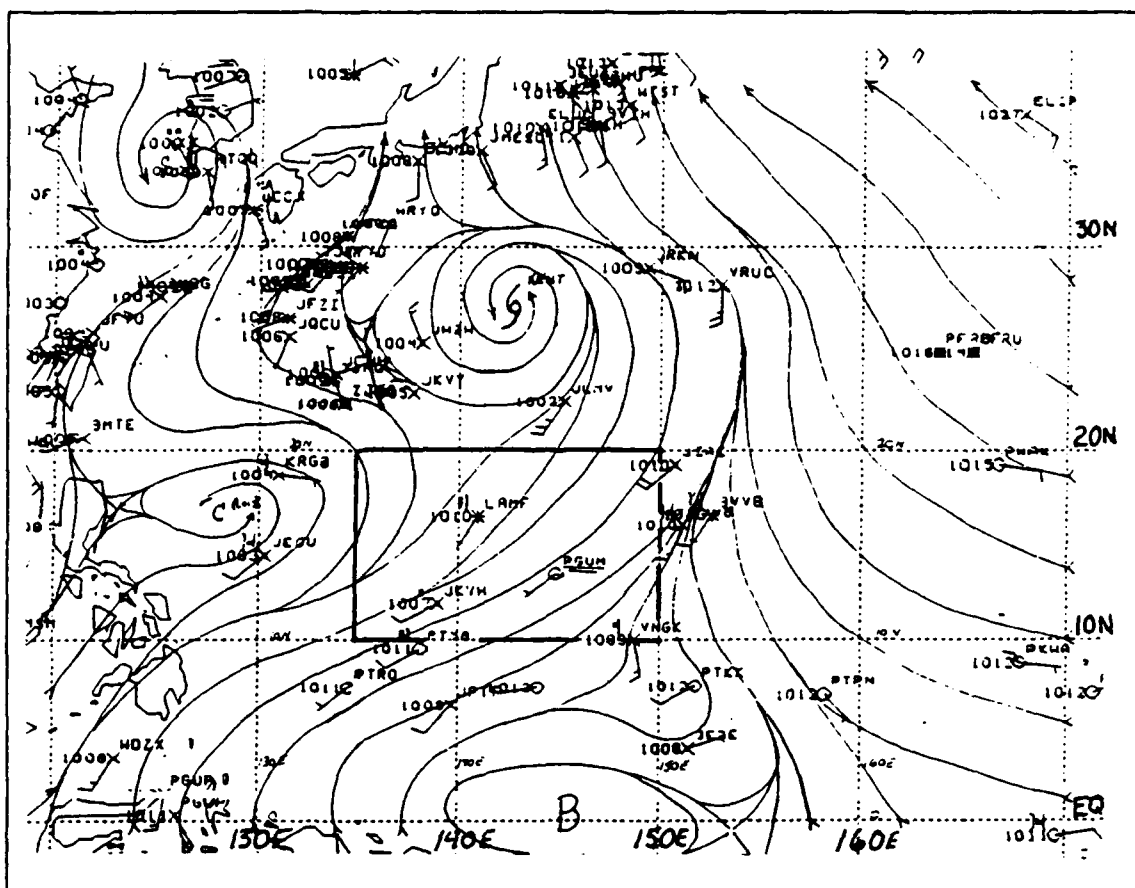


Figure 22. 1200 UTC 14 August 1992 gradient-level analysis of WPAC. AOP 7 region is within bold outline.

At 1400 UTC 14 August, the center of the MCS was near 14 °N, 139 °E. The flight track included data collection at 500 mb and 300 mb (Fig. 24). Aircraft data coverage in the region of the first MCS encompassed an area of approximately 350,000 km<sup>2</sup>. Convection, turbulence, precipitation and icing were all significant throughout most of the 500 mb track. Around 2100 UTC, these features began to decrease in frequency and intensity and heavy stratiform rain and light rime icing were prevalent.

At about 1830 UTC, the rapid development of a second MCS over Guam was detected. Because of the desire to collect a full data set on the first system, the aircraft completed full coverage of the first system and used the remaining fuel to make a single west to east pass through the second system. Consequently, data collected in the vicinity of the second system was sparse. Overall, dropwindsondes were deployed every 60 to

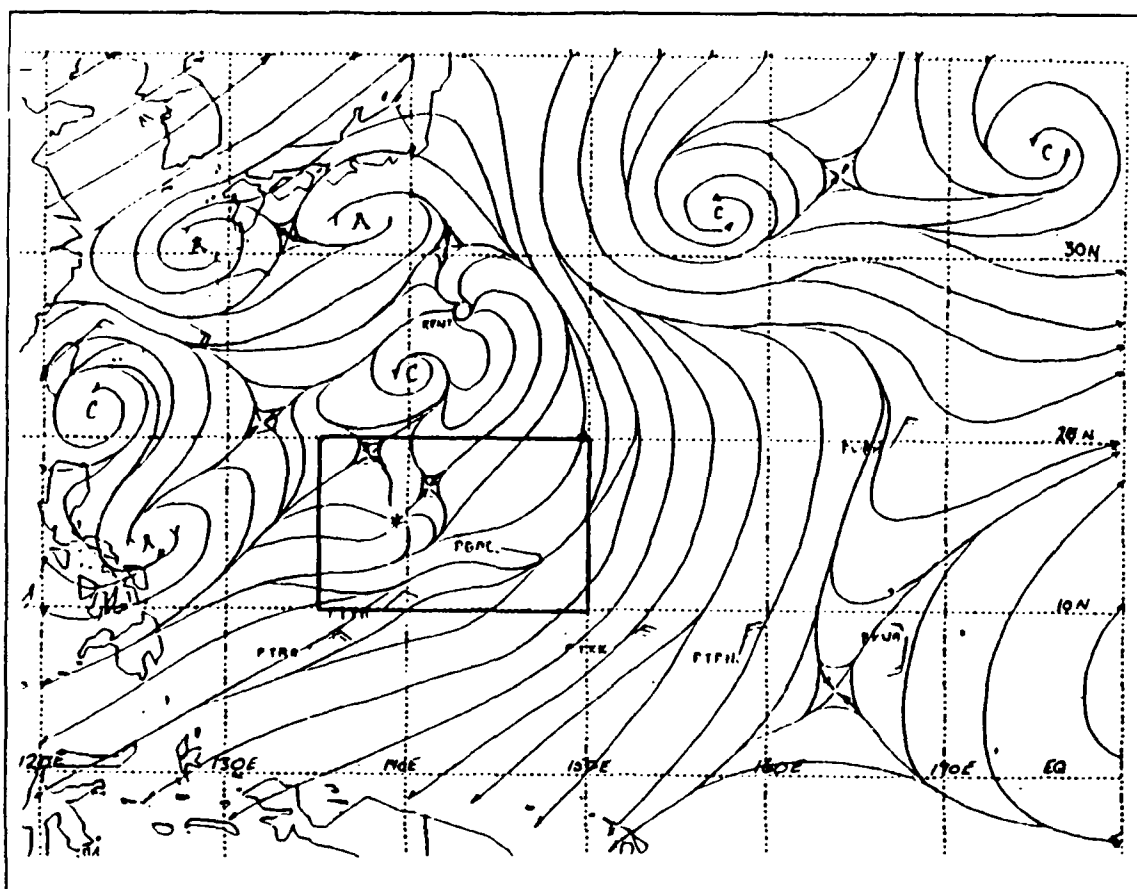


Figure 23. 1200 UTC 14 August 1992 200 mb analysis for WPAC. AOP 7 region is within bold outline.

120 n mi within the primary MCS region with two along the west to east leg approaching the second MCS. Proximity to the island of Guam prohibited the deployment of further dropwindsondes.

Development of the first MCS appeared to be very rapid (3-6 h) for the size of this system. After achieving maximum extent, gradual 'rainout' of the system over large stratiform rain regions occurred. These regions remained very centralized. At the same time, a mid-level mesoscale vortex slightly north of the main convective region was clearly evident in the aircraft observations and later in the satellite imagery (Fig. A-5a, Appendix A). As this first system approached maximum extent, the second MCS began to develop over Guam and attained similar dimensions as the first by 2330 UTC 14 August (Figs. A-2b and A-3b, Appendix A). Over the next 12 to 18 h, convection

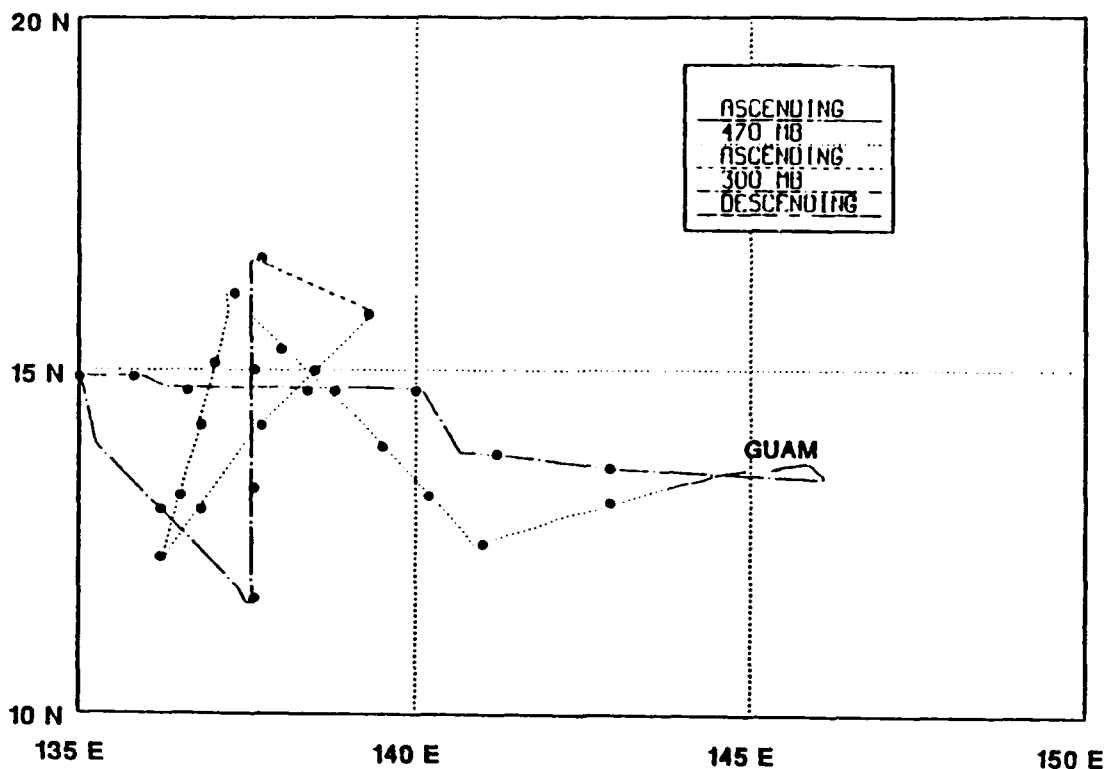


Figure 24. WC-130 flight track during AOP 7. Circles mark dropwindsonde locations.

associated with both systems dissipated. However, vortices were detected in the curved bands of low-, mid- and upper-level clouds on the satellite imagery. Furthermore, anticyclonic outflow could be analyzed in the 200 mb wind fields (not shown) during and shortly after the occurrence of these MCSs. Because this outflow was observed in the area of the MCSs, these systems apparently were significant mesoscale features of sufficient intensity and duration to alter the large-scale regime for over 24 h.

Although the vortex structure of these systems suggested that a TD should have developed within the area, such a development did not occur. The initial hypothesis was that a lack of a well-defined monsoon trough at low levels in conjunction with a northward encroachment of upper-level northeasterlies (increasing vertical shear) were the primary causes preventing TD development.

## B. AIRCRAFT OBSERVATION PERIOD 1 OVERVIEW

The first mission flown during TCM-92 was an investigation of the structure of a loosely organized MCS located about 450 n mi south-southwest of Guam. The aircraft departed Guam at 1920 UTC 23 July and returned at 0600 UTC 24 July after having spent roughly 10 hours in the MCS region.

Even though a convective outbreak near the dateline on 19 July had dissipated, a mid-level circulation had persisted and propagated westward. Surface pressure values were quite high (1009 to 1011 mb) for tropical disturbance development in the region. Beginning at 1200 UTC 21 July, and for the next 3 days, a low-level circulation could be analyzed, apparently in conjunction with the mid-level circulation. Seven hours before take-off, the low-level circulation was south-southeast of Guam and upper-level winds were producing little vertical wind shear (Figs. 25 and 26). Since the convection continued to flare periodically, the circulation region appeared to support a persistent MCS.

Although the surface circulation was centered near  $8^{\circ}$  N,  $140^{\circ}$  E at the time of aircraft departure, the flight track focused on the cloud cluster southwest of the circulation center (Fig. A-7a, Appendix A). Flight-level data were collected at 700 mb, 500 mb and 300 mb within the MCS region (Fig. 27). Dropwindsondes were deployed with the same spacing as in AOP 7 with an additional launch along both the inbound and outbound legs to the area.

Satellite imagery throughout the mission revealed that the main convection area was slightly south of the planned target area. Two hours after take-off, cloud-top temperatures in the region were lower than  $-80^{\circ}$  C. Satellite imagery at 2230 UTC revealed that the convection was organizing into a circular region of roughly  $4^{\circ}$  lat. in diameter and centered near  $6^{\circ}$  N,  $139^{\circ}$  E. By 0030 UTC 24 July, satellite imagery indicated a return to two smaller convective areas located at  $6^{\circ}$  N,  $138^{\circ}$  E and  $6^{\circ}$  N,  $140^{\circ}$  E, as well as a convective line from  $8^{\circ}$  N,  $140^{\circ}$  E to  $7^{\circ}$  N,  $143^{\circ}$  E (Fig. A-8b, Appendix A). However, impressive convective areas on satellite imagery throughout this mission were often dispelled by aircraft reports of merely "cirrus above and cumulus below."

Wind and height data indicated different flow patterns at various levels as will be discussed in detail in the AOP 1 MCS structure section. Although surface wind reports from ships and islands were weak, preliminary analysis of the winds from sondes indicated reasonably strong low-level winds (20-25 kt at 960 mb) from the southwest. At 500 mb, speeds of 25-30 kt were observed in the northern sector and only light and variable winds in the southern sector. Finally, flight-level winds at 300 mb were

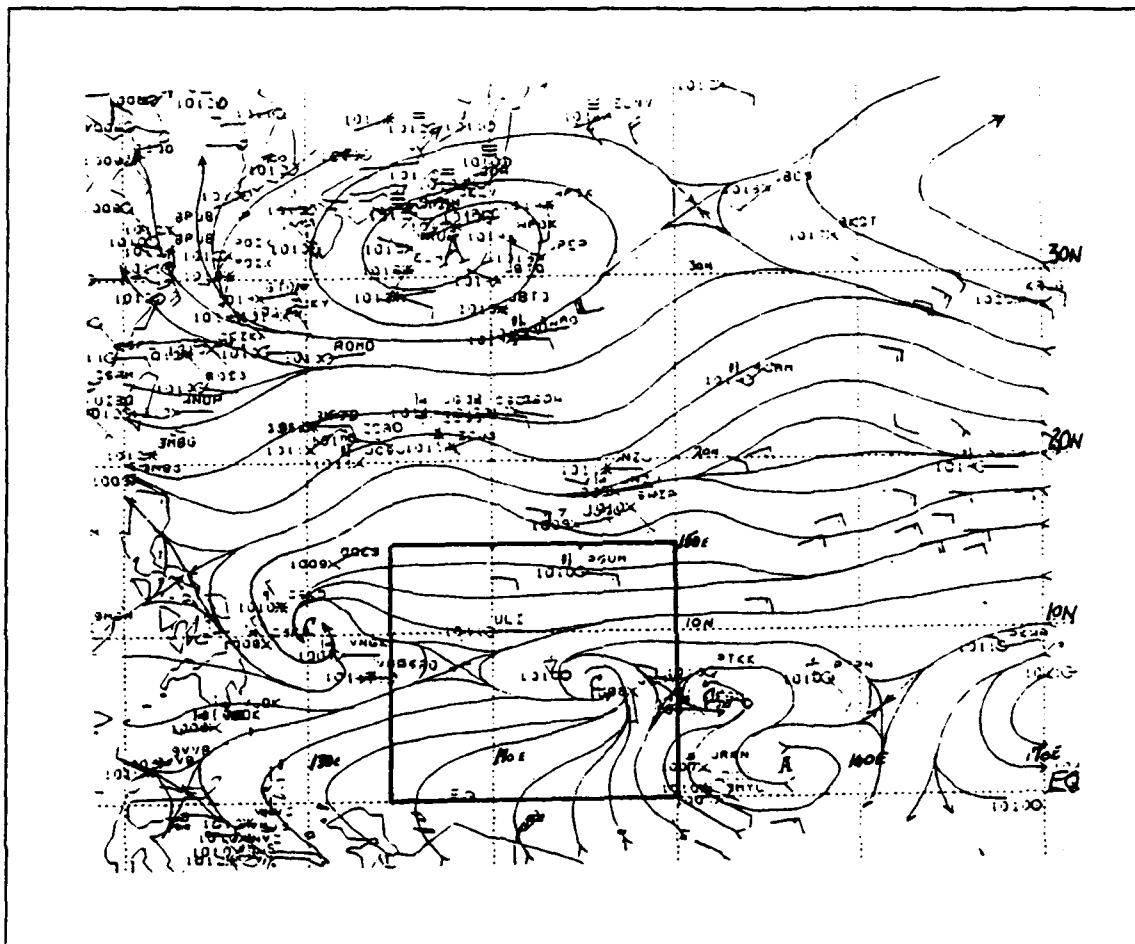


Figure 25. 1200 UTC 23 July 1992 gradient-level analysis for WPAC. AOP 1 region in within bold outline.

predominantly northeasterly with indications of shear vorticity that had a similar orientation as at 500 mb. However, the lowest height values were observed in the northeast quadrant rather than the southwest. In summary, the system appeared to have a large circulation near the surface that tilted southward and diminished in size and strength with height.

The strong low-level southwesterly flow measured during AOP 1 suggested that this MCS had the potential to develop into a significant tropical cyclone. Satellite imagery from 0630 UTC 24 July indicated a comma-shaped convective flareup to the north-northeast of the original target area. Low-level analyses continued to carry the circulation west-northwestward until its dissipation near the Philippines on 26 July.



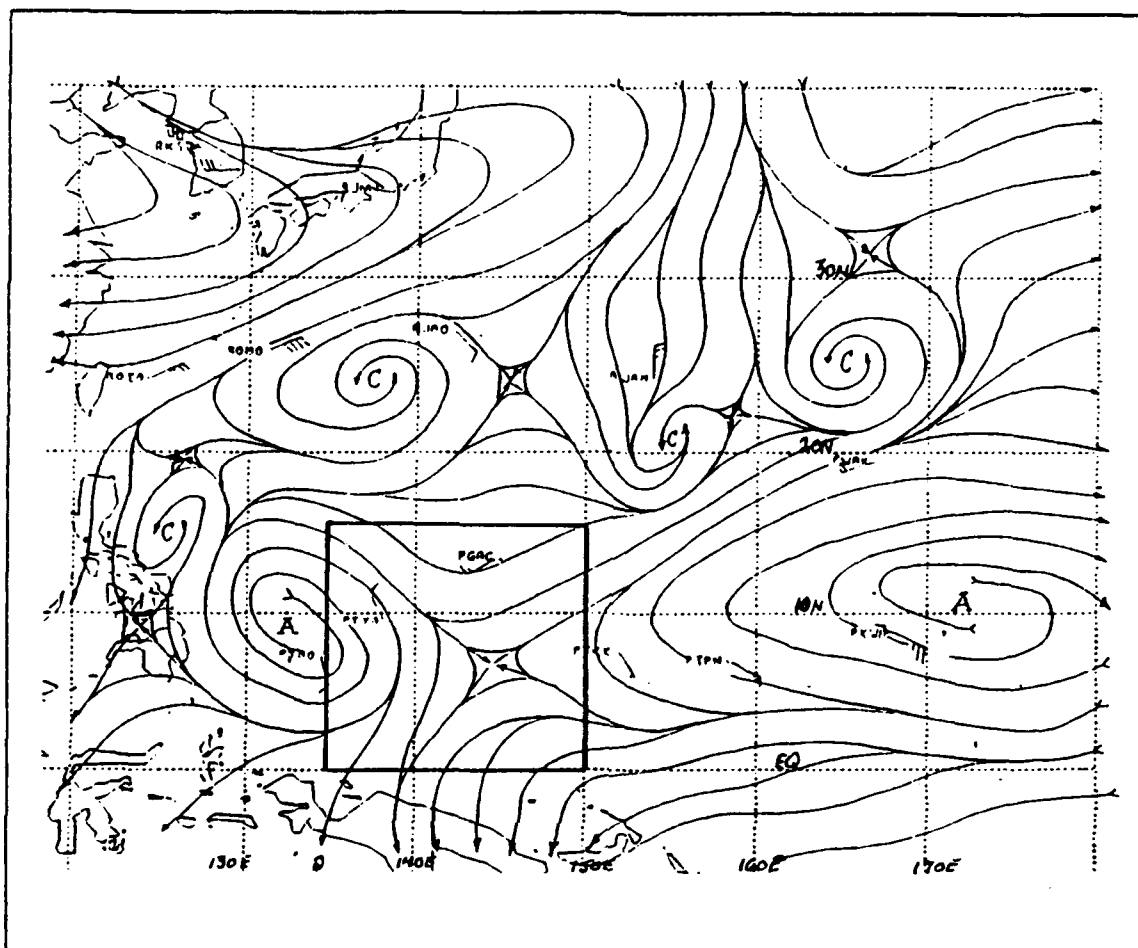


Figure 26. 1200 UTC 23 July 1992 200 mb analysis for WPAC. AOP 1 region is within bold outline.

### C. ANALYSIS OF WPAC

The domain over which the aircraft data was collected was relatively small. Therefore, it was necessary to use standard synoptic data and FNOC analyses to produce an environmental analysis for the AOP region. These analyses were accomplished for the gradient and 200 mb levels and provided both a background to facilitate the mesoscale analyses of aircraft data as well as determine whether the MCS had sufficient strength to alter the synoptic regime.

A major component of this analysis is the satellite imagery, which is crucial for determining locations of both synoptic and mesoscale features. Verification of features in the FNOC analysis fields was possible using this hourly imagery. For example, the 0000

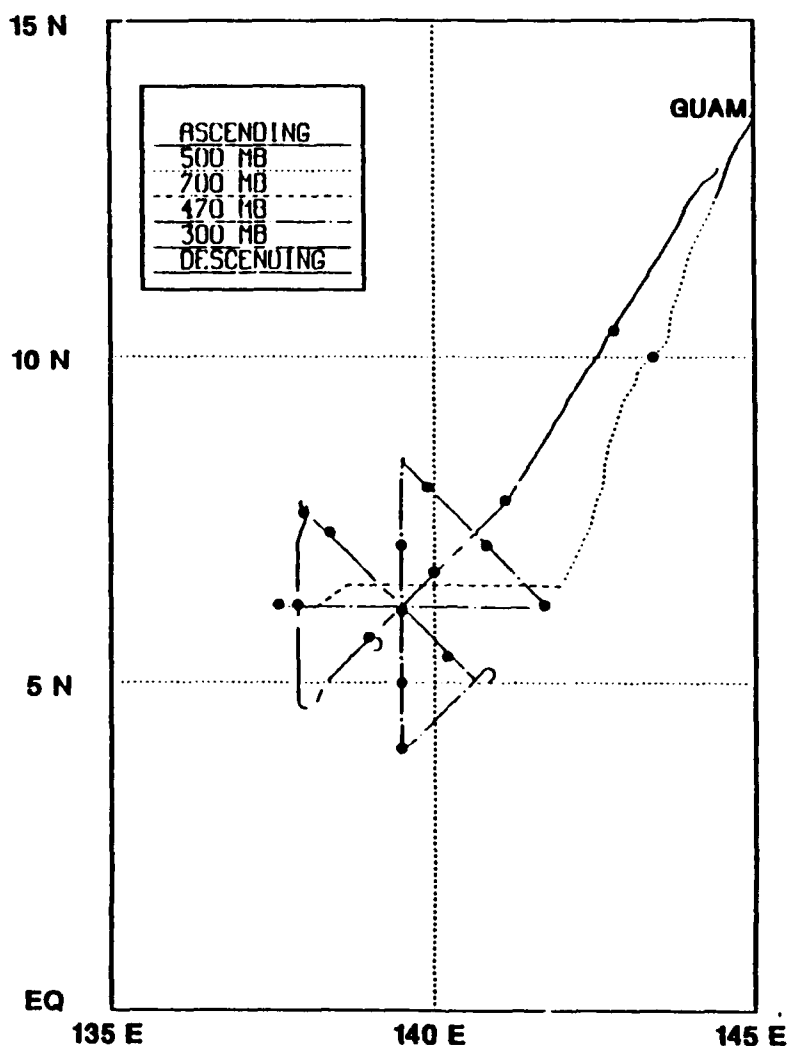


Figure 27. WC-130 flight track during AOP 1. Circles mark dropwindsonde locations.

UTC 15 August FNOC fields suggest southwesterly flow into Supertyphoon Kent up to 300 mb, and the hourly imagery strongly supports such flow patterns.

#### D. AOP ANALYSIS APPROACH

##### 1. Satellite imagery

As mentioned above, Figs. A-1 through A-11 of Appendix A provide both IR and visual imagery sequences so that the evolution of the AOP 7 and 1 MCSs is depicted. The MCS evolution in both cases took place prior to, during and after the aircraft was flying within the region. Thus, gaps in the aircraft data can be filled by

inferring information from both the IR and visual imagery. After examining the evolution of the MCSs, one image is chosen to best represent the entire AOP. The selection of this image is based on how well it represented the feature(s) of interest within the AOP in relation to the observed aircraft data. In both AOPs, an image around the midpoint of the AOP is chosen, and a nephanalysis is subsequently accomplished using enhanced IR temperature contours overlaid on the aircraft data. The selected center times for the AOPs were 2000 UTC 14 August for AOP 7 (Fig. 28) and 0000 UTC 24 July for AOP 1 (Fig. 29). The nephanalyses actually were made from two hourly images a half-hour prior to and after these center times.

A detailed nephanalysis of the  $-70^{\circ}$  to  $-75^{\circ}$  C cloud-top temperatures is performed every two to three hours of imagery for each AOP. This temperature interval is used because it represented the most significant cells within the MCSs observed during the AOPs. These analyses are presented in five hour increments such that a rough motion vector can be observed on various cells within the MCSs (Figs. 30 and 31).

## 2. Hand analyses

All aircraft data are plotted with respect to the center time that corresponds to the nephanalyses described above. In addition, synoptic data for the time closest to each center time (0000 UTC 15 August for AOP 7 and 0000 UTC 24 July for AOP 1) such as soundings and ship reports are added to the aircraft data plots. These data are checked to ensure they were consistent with the analysis based on the aircraft data. Because the synoptic regime may also be evolving due to the presence of the MCS, the closest synoptic time to the center time may not necessarily be the most valid for the AOP analyses.

Hand analyses are accomplished for the wind, temperature, dewpoint depression and some height fields in the horizontal over a relatively small area, usually  $10^{\circ}$  lat. by  $10^{\circ}$  long. squares. Detailed streamline analyses are possible at levels with aircraft flight-level winds. Aircraft flight-level and dropwindsonde winds are given the most weight in the streamline analyses. As indicated in the data summary, aircraft flight-level winds are removed from the data set if the aircraft was in a turn, orbiting or in a significant climb or descent. This ensured the least amount of contamination by erroneous winds created during these unusual aircraft attitudes. Synoptic soundings or surface data are weighted less than the aircraft observations. Finally, FNOC wind analyses are used primarily to ensure the mesoscale analyses were appropriately blended with the larger synoptic analysis.

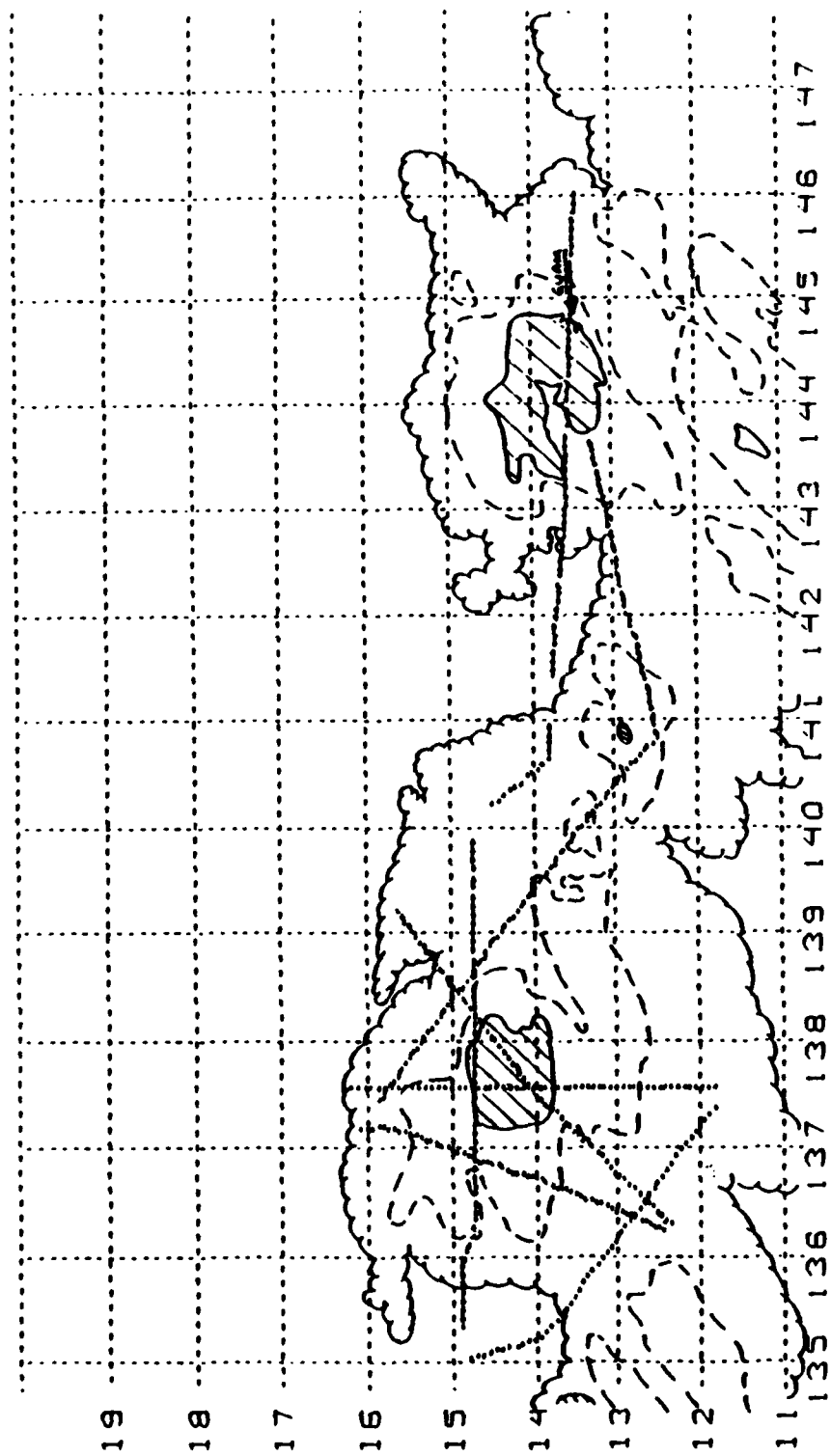


Figure 28. AOP 7 nephanalysis for center time (2000 UTC 14 August 1992) with flight track overlaid. Area within scalloped line defines cloud-top temperatures of  $< -30^{\circ}\text{C}$ ; within dashed line,  $-70^{\circ}$  to  $-75^{\circ}\text{C}$ ; within cross-hatched,  $< -80^{\circ}\text{C}$ .

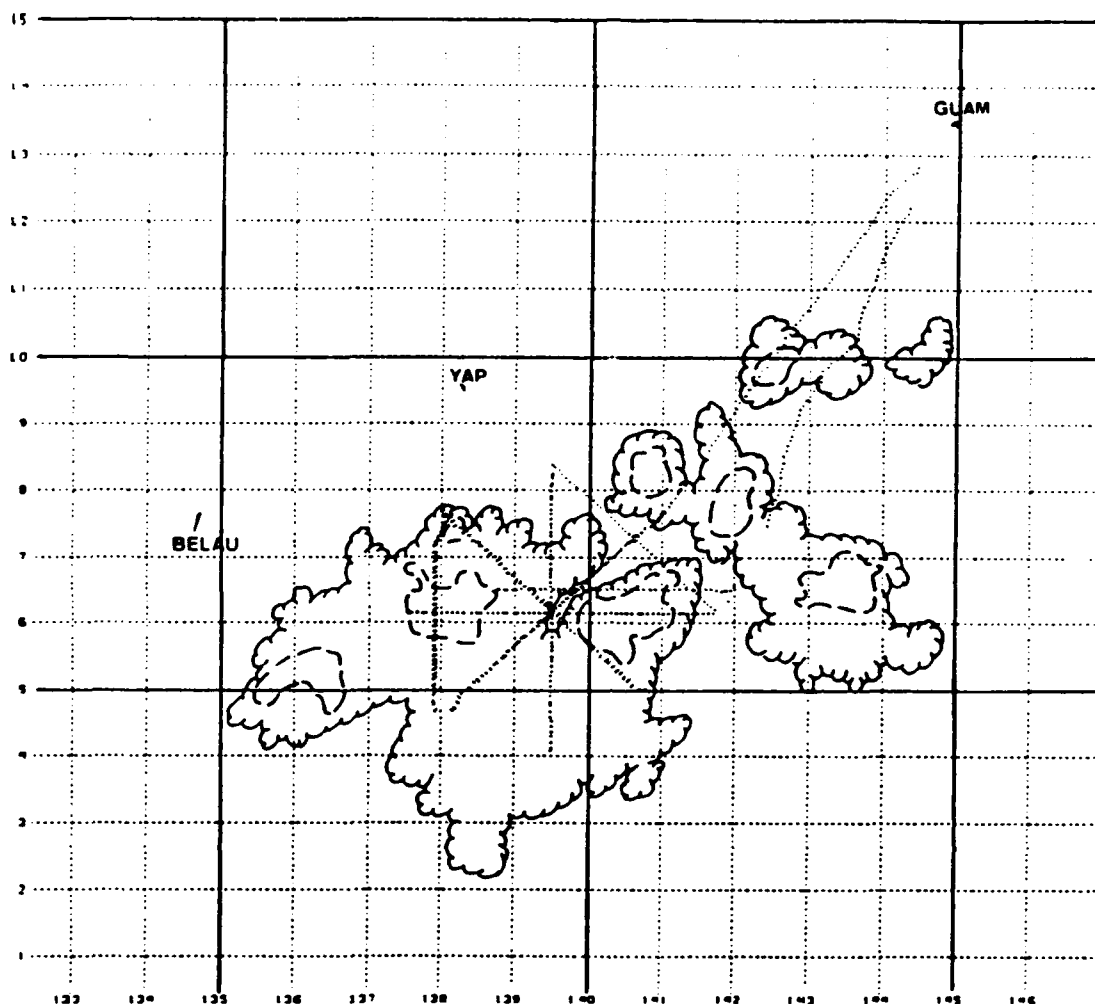
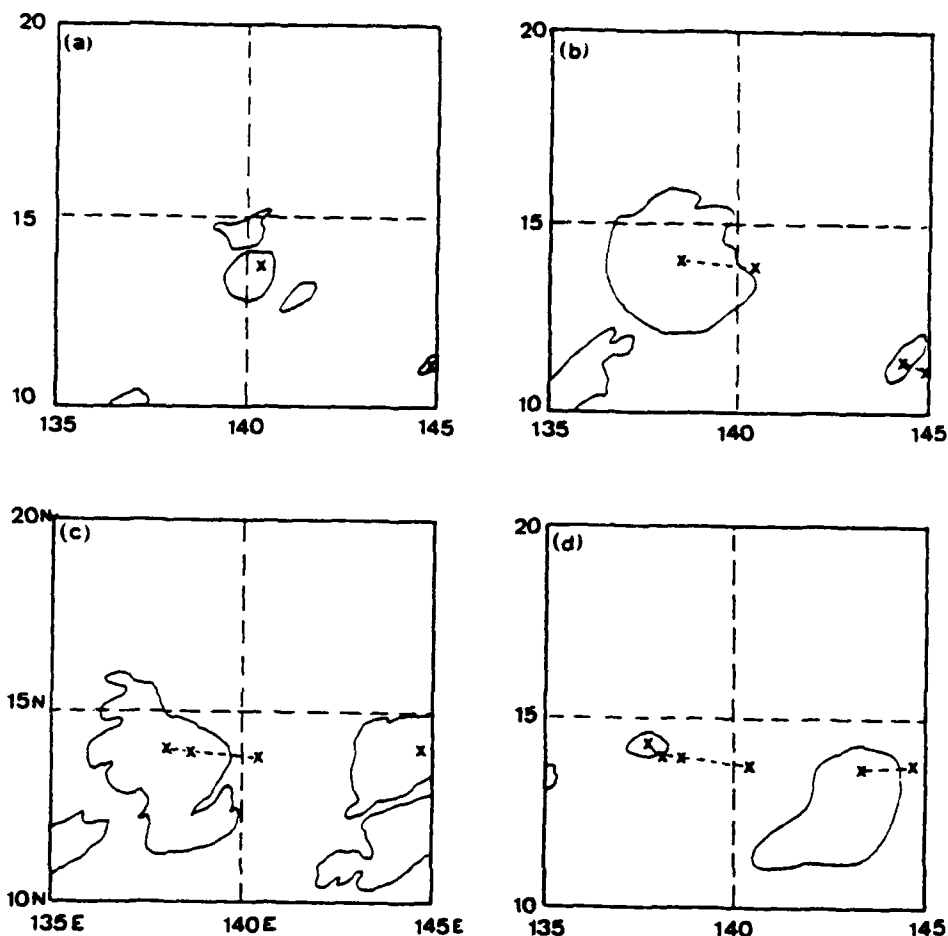


Figure 29. AOP 1 nephanalysis for center time (0000 UTC 24 July 1992) with flight track overlaid. Area within scalloped line defines cloud-top temperatures  $< -30^{\circ}\text{C}$ ; within dashed line,  $-70^{\circ}\text{C}$  to  $-75^{\circ}\text{C}$ . Temperatures  $< -80^{\circ}\text{C}$  did not exist in this MCS at the center time.

Temperature and dewpoint depression analyses are accomplished in the same manner as the winds. However, more credence is given to the dropwindsondes rather than the flight-level data because the aircraft was often flying 1,000 to 2,000 feet above the mandatory pressure level to ensure the sondes would fall through the mandatory level of interest. Consequently, flight-level temperatures and dewpoints are typically  $1^{\circ}$  to  $4^{\circ}\text{C}$  lower than measured by the sondes at the mandatory level. Such temperature offsets preclude a single analysis of both data sets. Thus, separate temperature dewpoint



**Figure 30.** Time sequence of  $-70^{\circ}$  to  $-75^{\circ}$  C cloud-top temperatures for AOP 7. Center positions (x) of most intense convection are connected by dashed lines: (a) 0930 UTC 14 August, (b) 1430 UTC 14 August, (c) 1930 UTC 14 August, and (d) 0030 UTC 14 August.

analyses are accomplished using just the flight-level data (not presented) and using the dropwindsonde, synoptic and FNOG data.

Finally, geopotential heights are only analyzed roughly because of the anticipated lack of accuracy in the measurements. As discussed in the data summary, the aircraft was unable to provide adequate baseline data for the dropwindsondes launched from higher altitudes (e.g., 400 mb or 300 mb). Such heights frequently had to be removed from the data sets. Thus, these geopotential height analyses often do not provide mesoscale detail. In cases in which the changes encountered within the MCSs are very dynamic, areas of increased or decreased heights can be discerned in the data.

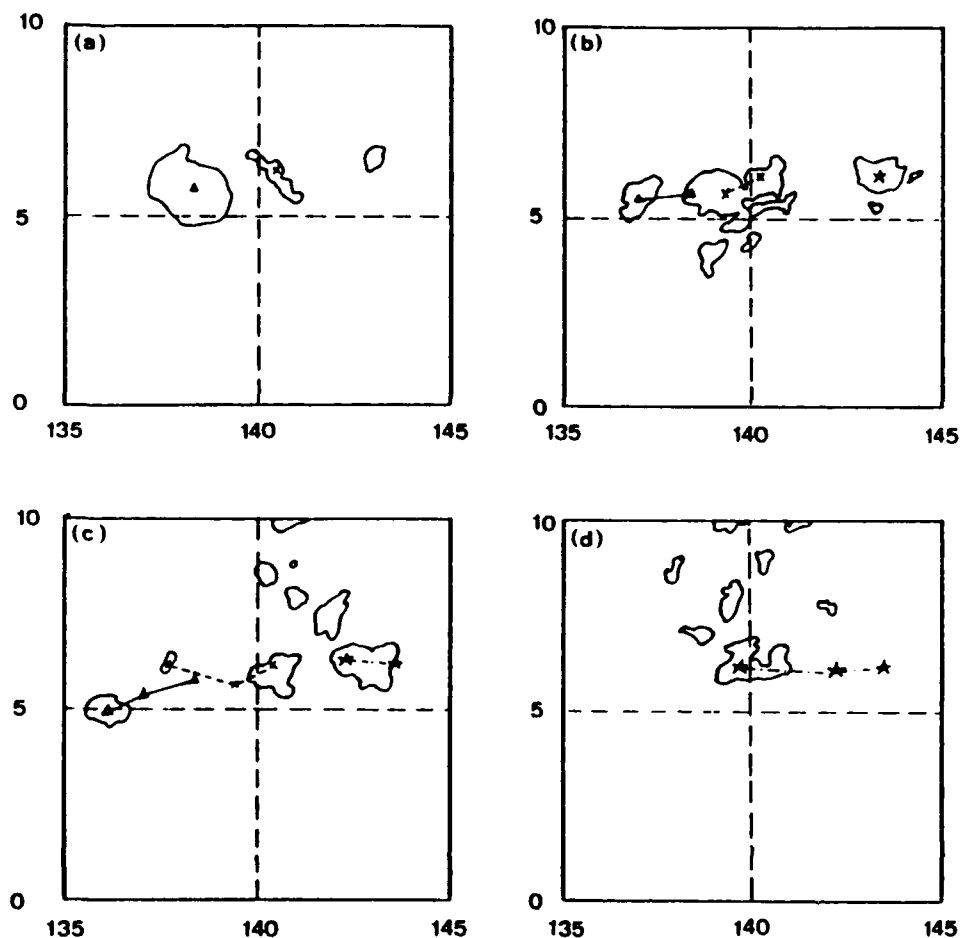


Figure 31. As in Fig. 30 for AOP 1. Triangles, stars and x define separate cells that are connected by solid, dot-dashed, and dashed lines respectively: (a) 1530 UTC 23 July, (b) 2030 UTC 23 July, (c) 0130 UTC 24 July, and (d) 0630 UTC 24 July.

Vertical profiles of temperature and dewpoint are produced from the dropwindsondes. Recent proposals by Emanuel (1992) suggest the moisture content of the air in the lower levels may be a key factor in determining subsequent development of MCSs into tropical cyclones. Levels of subsident warming and drying are present in these data sets. As these warm and dry "pockets" did not necessarily coincide with the mandatory levels, additional horizontal levels are analyzed to discern a pattern in relation to the satellite nephanalyses.

Ideally, an analysis of this type would include vorticity and  $\theta_e$  fields to better evaluate the theories posed in the background section. However, this is a preliminary analysis accomplished in a short time-frame.

## **E. STRUCTURE OF AOP 7 MCS**

As mentioned above, two very large circular MCSs developed over a short period of time during AOP 7. Both MCSs had a life-span of 17-18 h from first detection to total dissipation. As previously shown, the satellite imagery using the modified BD enhancement curve (Fig. A-1 through A-4a, Appendix A) highlight this life cycle. Corresponding visual imagery is shown in Figs. A-4b through A-6b, Appendix A. In addition to the large spatial extent of the coldest cloud tops in the IR imagery, note that much lower temperatures are often found in the tropical MCS compared to the midlatitude MCC/MCS (Maddox 1980). In the following sections, the circulation features in AOP 7 are related to the signatures in the satellite imagery.

### **1. Horizontal structure**

The most striking and significant feature in the 500 mb and 300 mb analyses is the presence of vortices in both aircraft and satellite data (Figs. 32 and 33). The most significant (primary) vortex located near  $15^\circ \text{N}$ ,  $139^\circ \text{E}$  at 500 mb is directly related to the primary MCS west of Guam. In addition, the primary vortex is found as low as 700 mb, although slightly northeast of the 500 mb location (Fig. 34). While this may imply vertical tilt, movement of the MCS during the AOP accounts for most of the displacement. In addition, the position of the 700 mb center is not well-resolved by observations on the eastern side. At lower levels, a relatively strong warm and moist southwest flow of 15-25 kt exists, but no closed vortex is detected (Figs. 35 and 36).

The vortices in this case are of similar horizontal scale as those outlined in Table 1. The primary vortex at 500 mb is on the order of 200 n mi in diameter and slightly less at 300 mb. The 700 mb vortex is broader (roughly 250-300 n mi in diameter). Thus, these vortices are quite close to what was expected from the models by Frank and Chen (1991), Fritsch (1992), etc. The section on vertical structure will provide more detail on the horizontal displacements of the vortices in the vertical.

Satellite imagery, especially the visual images from 2130 UTC 14 August to 0330 UTC 15 August, support the development of the primary vortex. When the 500 mb and 300 mb flight-level data are analyzed relative to the center time image of 1930 UTC 14 August, other secondary vortices can be analyzed that appear to be directly related to areas of strong convection. For instance, the second MCS over Guam, an area near



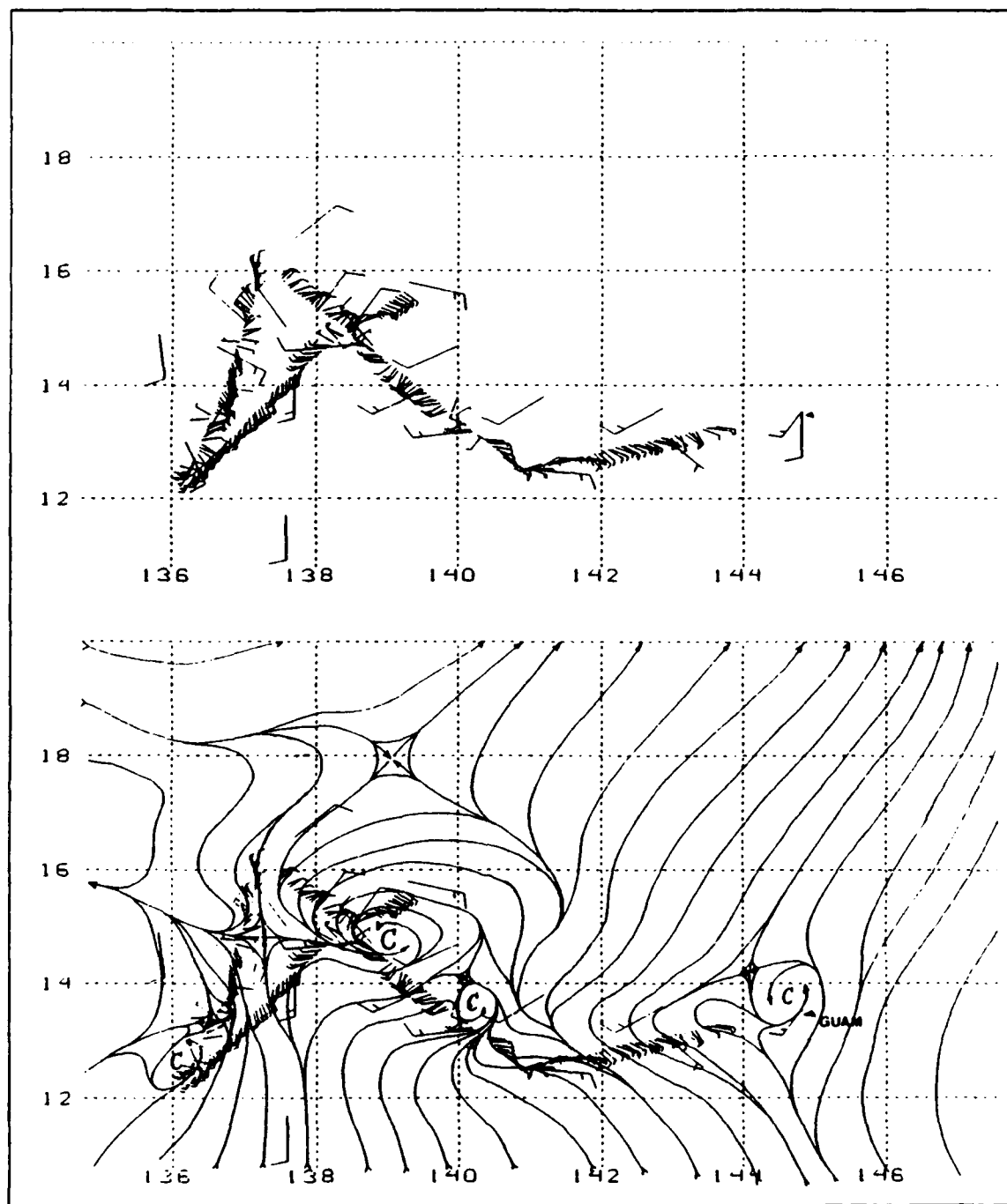


**Figure 32.** AOP 7 500 mb aircraft flight-level, dropwindsonde and 0000 UTC 15 August Guam rawwindsonde winds (kt) (top), with streamline analysis (bottom). Large barbs are dropwindsonde winds.

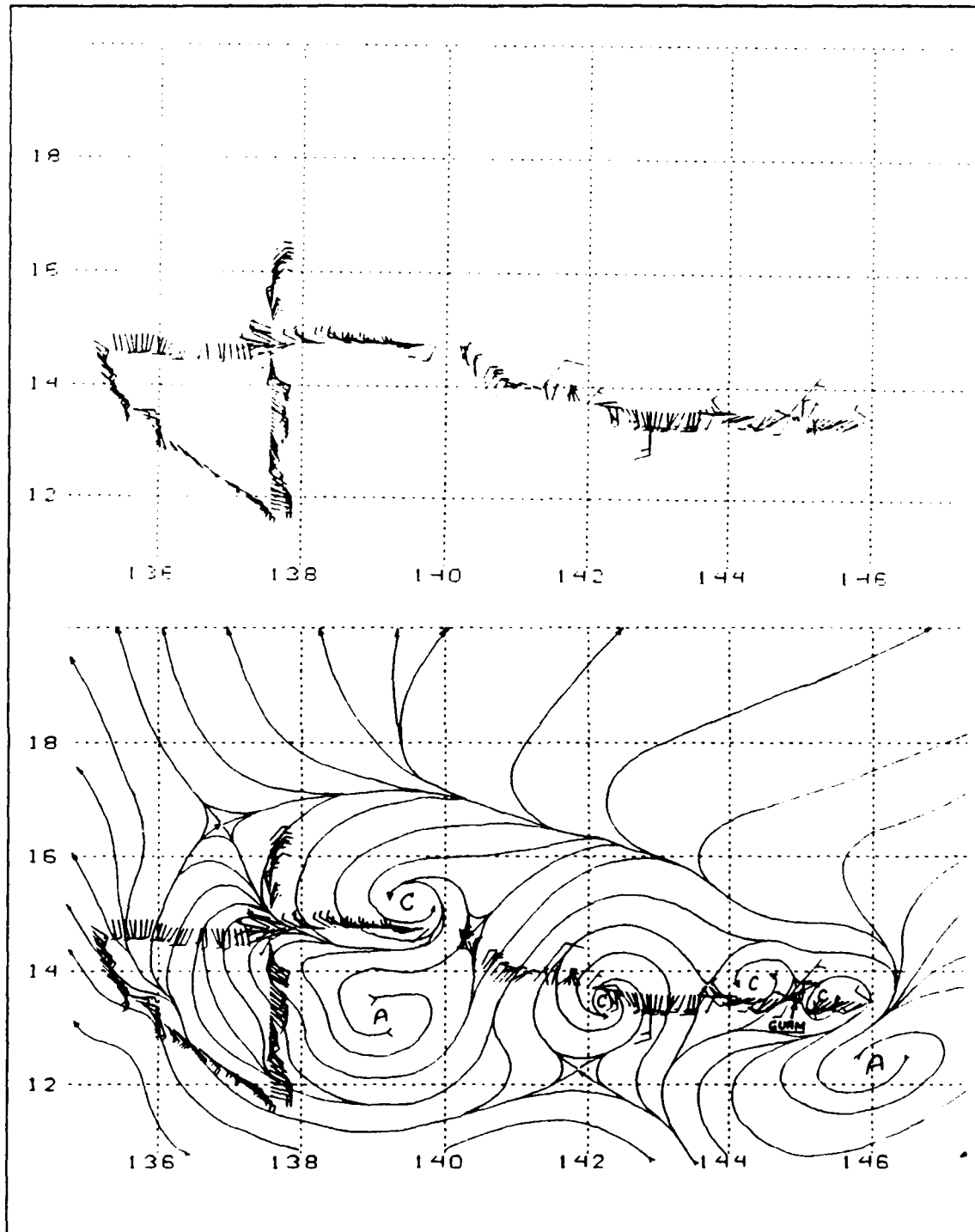


Figure 33. AOP 7 300 mb winds and analysis as in Fig. 32.

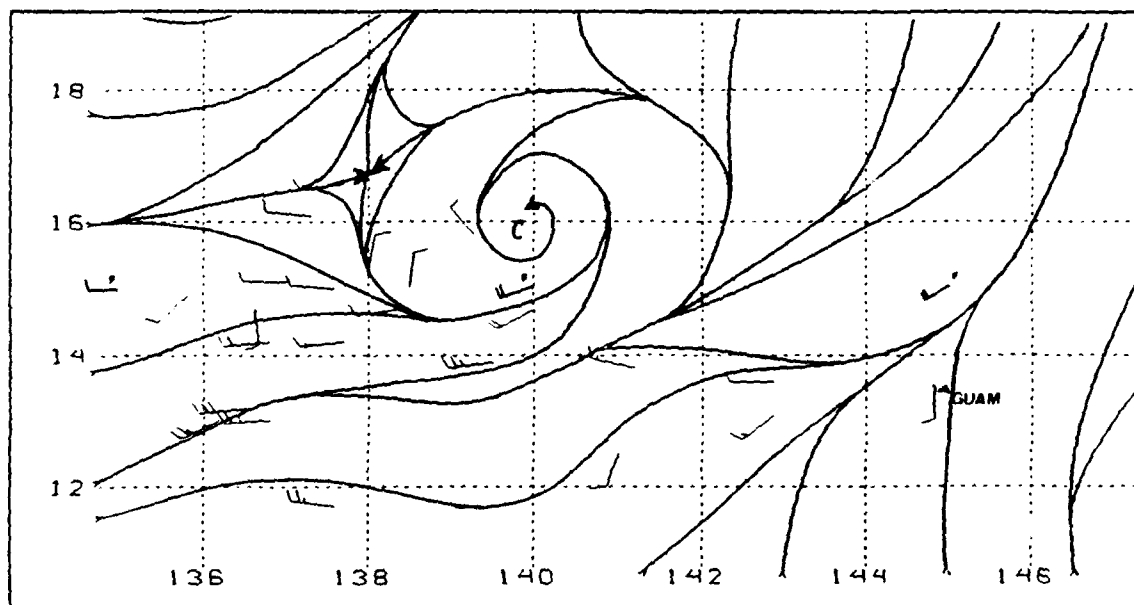


Figure 34. AOP 7 700 mb streamline analysis of dropwindsonde and 0000 UTC 15 August Guam rawinsonde winds (kt).

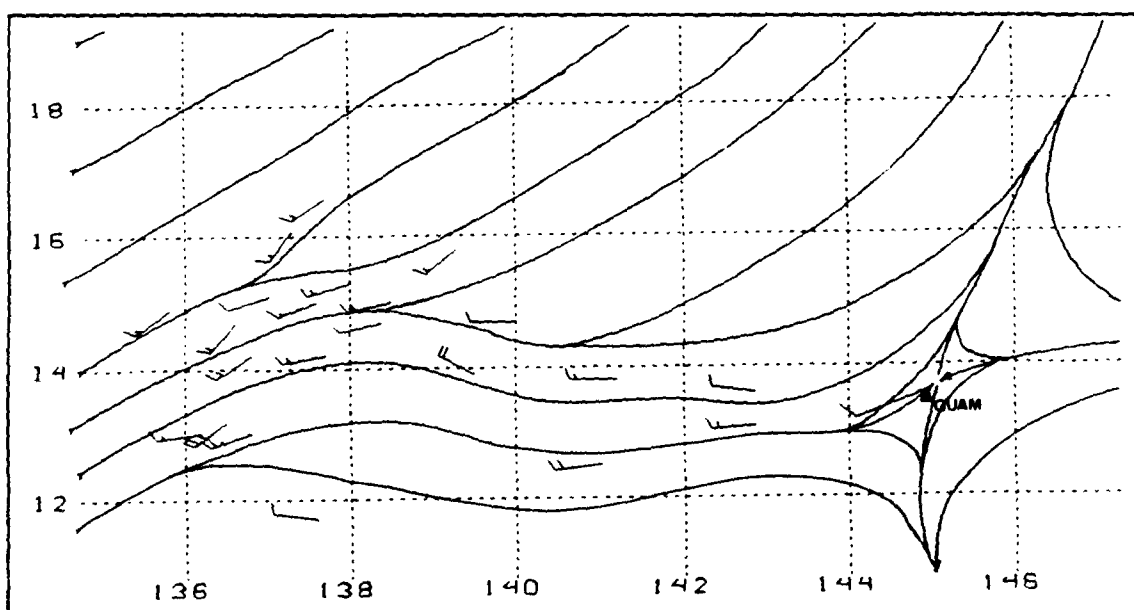


Figure 35. AOP 7 850 mb streamline analysis of dropwindsonde and 0000 UTC 15 August Guam rawinsonde winds (kt).

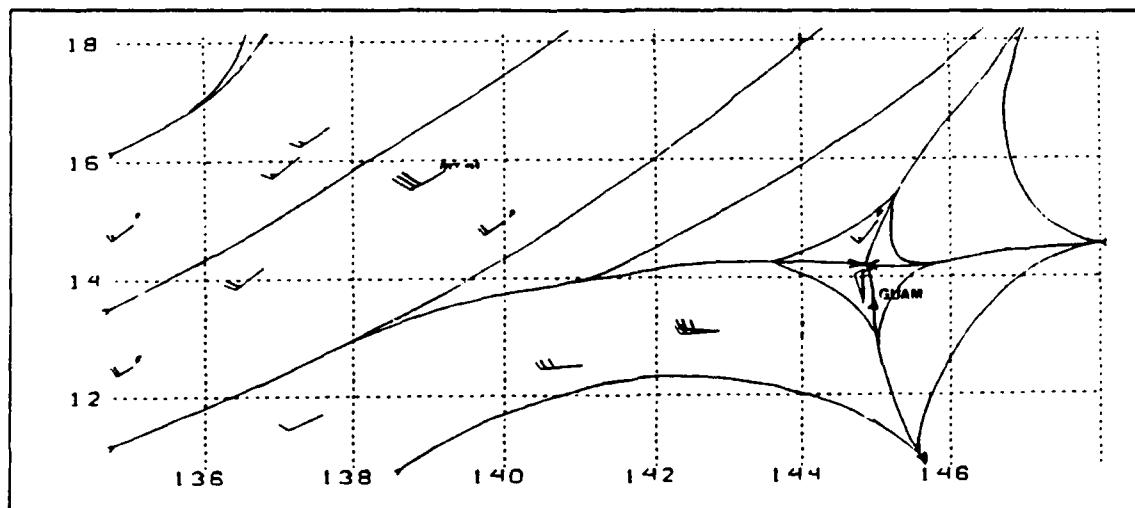


Figure 36. AOP 7 gradient level (960 mb-surface) streamline analysis of dropwindsonde, 0000 UTC 15 August Guam rawindsonde. Also included are visually observed surface winds from aircraft (ACFT OBS) and 0000 UTC 15 August FNOC analysis (F) winds (kt).

14 ° N, 140 ° E, and a feature resembling a squall line to the southwest of the primary MCS all can be tied to either vortices or cyclonic turning in the aircraft data at 500 mb (Fig. 32). This is not to say that every deep center of convection observed during the AOP contains a vortex. However, a definite connection appears to exist between the vortices that have been analyzed and broad regions of stratiform rain/cloud where convection had been intense. Given the sparsity of the data around the other analyzed vortices, the analyses of such vortices is subjective.

These vortices are not coincident with the maximum convective region of the MCSs (i.e., the coldest cloud tops). This is important because the theories suggest the vortices are initially formed in the stratiform rain regions of such systems. Upon examination of the evolution of the MCSs in the satellite imagery, there is strong indication that the vortices are in the dense stratiform cloud regions, after the convection had either decayed or propagated away. Aircraft reports support the imagery in that stratiform cloud and precipitation were frequently observed in these regions. The primary vortex is north of the lowest cloud-top temperatures of the primary MCS and is very well revealed as an exposed circulation late in the AOP (Fig. A-5b, Appendix A). Furthermore, both visual and instrument observations also support a vortex in the main convection region of the MCS over Guam (Figs. A-5a and A-5b, Appendix A; Figs. 32 and 33).

This suggests that vortex formation may begin before the large stratiform rain region develops fully.

Most of the temperature analyses have departures from the environment of 3 ° to 4 ° C over the entire MCS region. Although these temperature variations are rarely continuous gradients leading to either a 4 ° C cool or warm pocket of air, gradients in several analyses are significant. Correlation of the temperature and dewpoint depression fields with the satellite imagery is not as clear-cut as the streamline analyses, probably due to the disparity between where the convection was inferred from the satellite imagery and where it was actually encountered by the aircraft. Nevertheless, a definite correlation exists in the lower levels up to 700 mb between cold pockets within the MCS region and saturated areas (Figs. 37 through 39). The gradient-level analyses have a warm and dry region of air surrounding the MCS regions, which suggests that large areas of subsidence and associated drying had occurred. Some pockets of cooler (2 ° to 3 ° C) moist air are found as well. As indicated in Table 1, these cooler pockets may be responsible for lifting very warm moist air into the low levels of the MCSs. Mid-levels (500 mb and 400 mb) contain a definite warming and associated concentration of moisture in the MCS regions, especially at 400 mb (Figs. 40 and 41). Finally, as would be expected from the massive anvil blow-off observed from the cells of the MCS, analyses at 300 mb reveal a relatively weak warm, saturated pool of air throughout the area of the AOP (Fig. 42).

## **2. Vertical structure**

As suggested above, some of these vortices are not limited to the mid-levels, but are found to have extended over substantial vertical depths. The vortex at 15 ° N, 139 ° E associated with the primary MCS had apparently extended upward to 300 mb and downward to 700 mb. The primary question is: where did the vortex initially form in the vertical? The presence of other (secondary) vortices at the 500 mb level that are not detected at lower levels might suggest that the vortices tend to form no lower than 500 mb. Other possibilities are that either the convection was not over a large enough area to provide the environmental conditions necessary as posed by Frank and Chen (1991) to extend the secondary vortices to lower levels, or the data density from dropwindsondes at the lower levels is not sufficient to confirm such vortices.

The satellite imagery does not allow differentiation of vertical levels of the clouds below the cirrus shield. However, examination of the series of visual imagery obtained as the primary MCS was decaying suggests that the primary vortex consisted of just mid- and upper-level cloud (about 2130 UTC 14 August, Fig. A-4b, Appendix

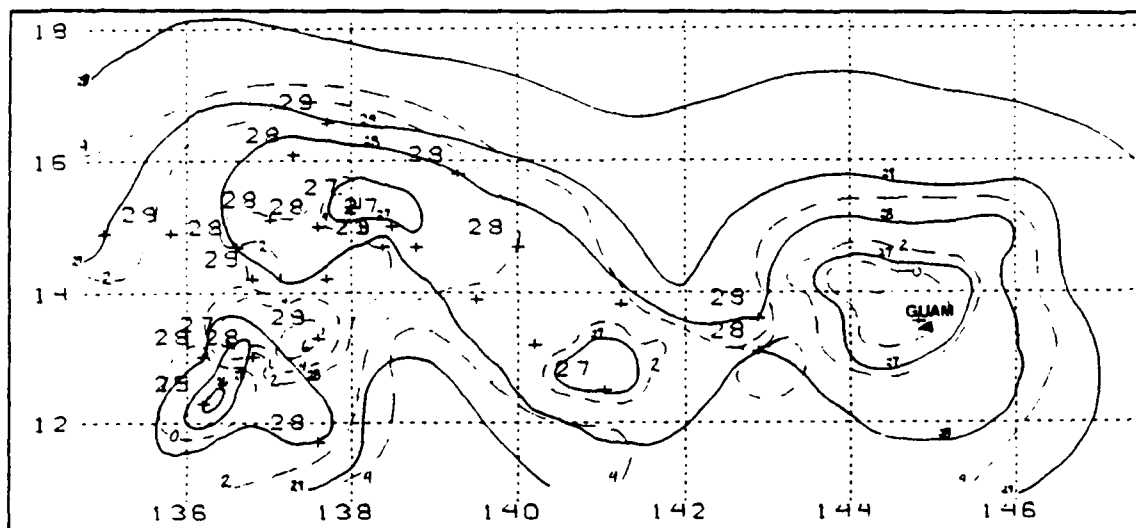
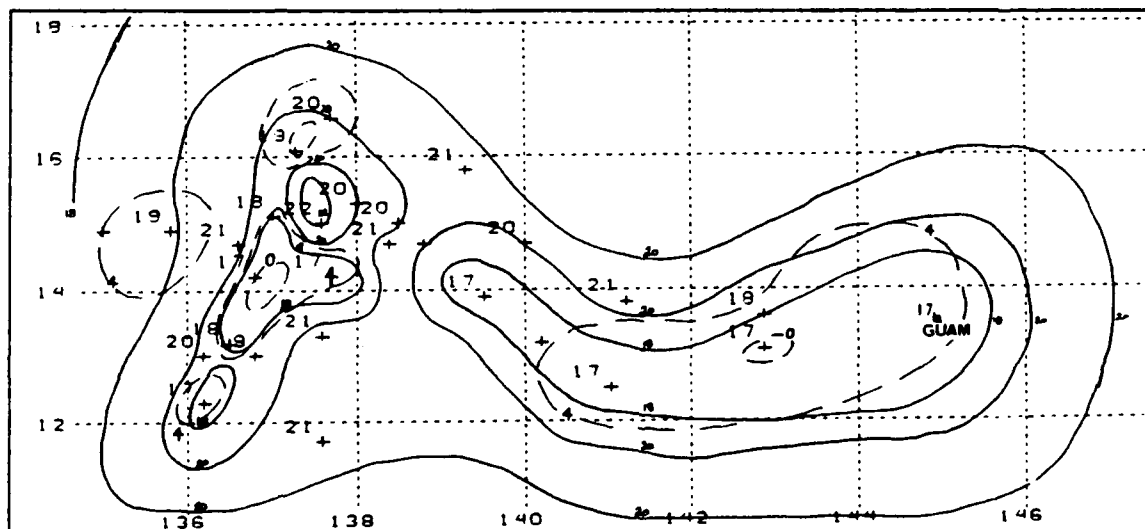


**Figure 37. AOP 7 Surface temperature and dewpoint depression analysis.** Solid lines are isotherms of 1 ° C increments, dashed lines are dewpoint depressions in 2 ° C increments. Environmental temperatures for 0000 UTC 15 August are 28 ° to 29 ° C.

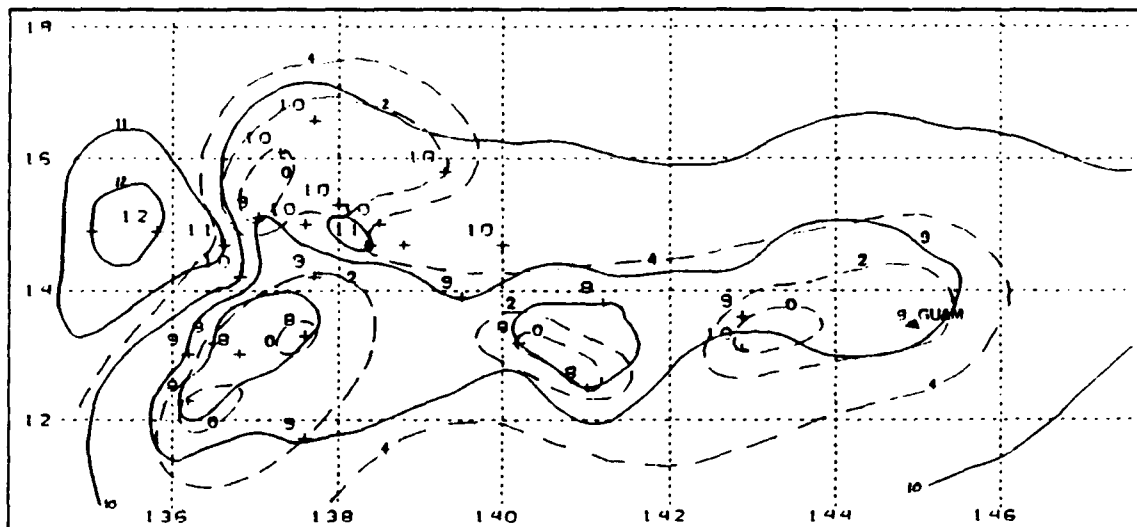
1). Later in the series (about 0130 UTC 15 August, Fig. A-5b, Appendix A), low-level cumuliform cloud is cyclonically spiralling into the primary vortex, which confirms the downward extension of the vortex. Such low-level cyclonic inflow could not be seen in the imagery for the vortex located near Guam.

Vertical profiles for dropwindsondes deployed within the primary MCS of this AOP provide an interesting result. Upon examination of the 25 dropwindsondes: 10 have very moist and somewhat cooler low-level temperatures; 11 others have relatively strong subsidence that both warms and dries the low levels below 720 mb to 680 mb; and the last four have weak mid-level subsidence (Figs. 43 through 45 respectively). Horizontal plots of these dropwindsondes (Fig. 46) reveal a somewhat random location of subsident and moist soundings within the MCS region. However, the majority of the moist soundings are from early in the mission, before the total decay of the primary MCS, whereas the soundings with strong subsidence are prevalent later in the mission. Notice also that the last dropwindsonde and the Guam 15 August 0000 UTC (Fig. 47) sounding both have relatively moist profiles, which are representative of the time of maximum extent of the second MCS that formed over Guam.

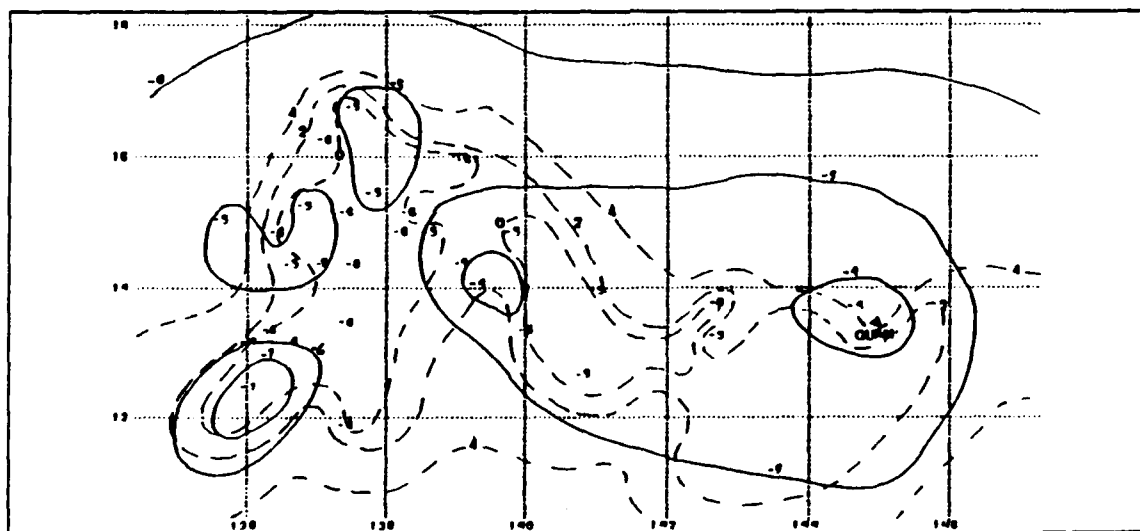
The moisture profile evolution may explain why this MCS with its associated vortices did not continue to evolve into a tropical cyclone. Theories posed by both Frank and Chen (1991) and Emanuel (1992) suggest that TD development should follow if such a vortex exists within a column of moist cool air. Evaluation of where the moist soundings are located with respect to the vortices within the MCS reveals that (with one exception) they are not found in the vicinity of the vortices. As discussed above, the exception is the vortex analyzed near Guam (Fig. 32). Although these two soundings are moist down to the surface, the vortex is in the region of very low cloud-top temperatures and apparently intense convection, which conform to the early stages of vortex formation in the Frank and Chen model. Thus, the profiles are not inconsistent with the expectations of Table 1. The explanation why the vortex revealed in the data and satellite imagery did not continue to develop may lie in the timing of the vortex development and thermodynamic transformations. Given the intense nature of the MCS, and the massive uplift of air in the convection, the subsequent mesoscale downdrafts may have been of such an intensity as to dry the lower levels almost completely. Further intensification of the vortex is thus not possible due to cut-off of the energy source.



**Figure 38.** AOP 7 850 mb temperature and dewpoint depression analysis. Solid lines are isotherms of 2 °C increments, dashed lines are dewpoint depressions in 4 °C increments. The 0000 UTC 15 August Guam rawinsonde is included in the analysis. Environmental temperatures for 0000 UTC 15 August are 18 ° to 19 ° C.



**Figure 39.** AOP 7 700 mb temperature and dewpoint depression analysis. Solid lines are isotherms of  $1^{\circ}\text{C}$  increments, dashed lines are dewpoint depressions in  $2^{\circ}\text{C}$  increments. The 0000 UTC 15 August Guam rawinsonde is included in the analysis. Environmental temperatures for 0000 UTC 15 August are  $10^{\circ}$  to  $11^{\circ}\text{C}$ .





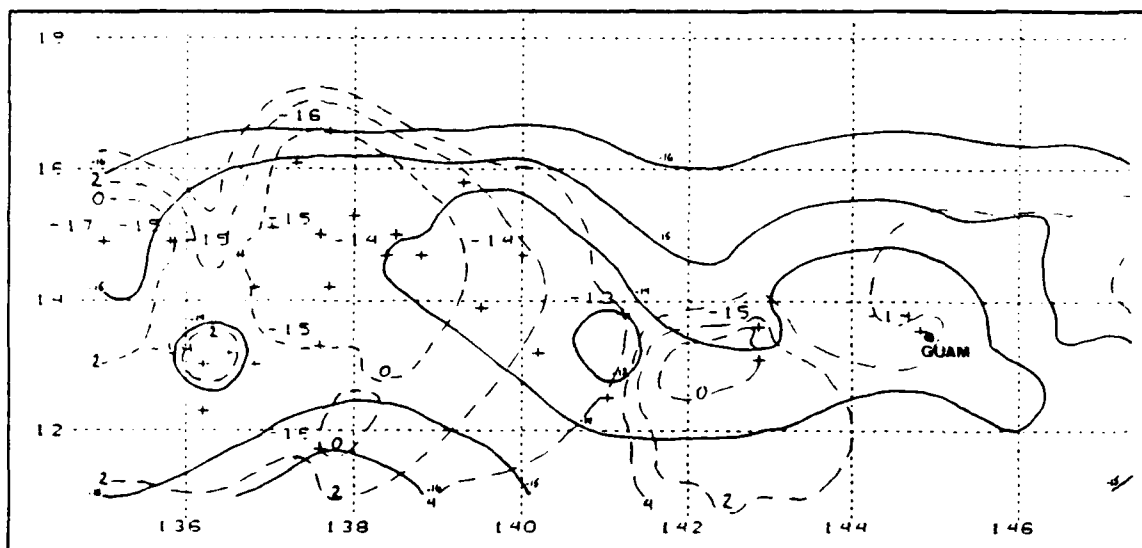


Figure 41. AOP 7 400 mb temperature and dewpoint depression analysis. As in Fig. 39, except environmental temperature for 0000 UTC 15 August is  $-16^{\circ}\text{C}$ .

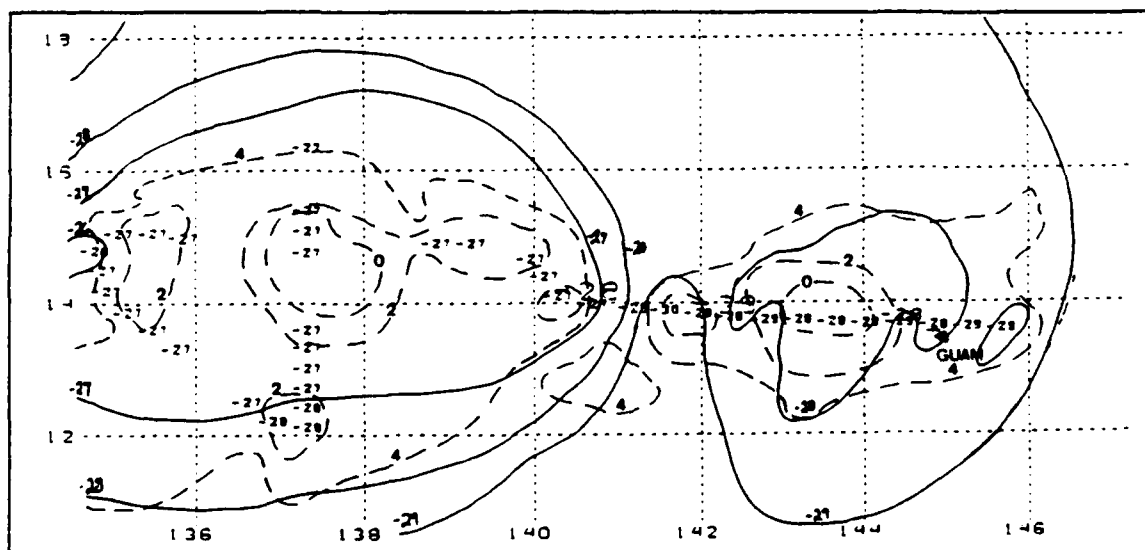


Figure 42. AOP 7 300 mb temperature and dewpoint depression analysis. As in Fig. 39, except environmental temperatures for 0000 UTC 15 August are  $-29^{\circ}$  to  $-30^{\circ}\text{C}$ .

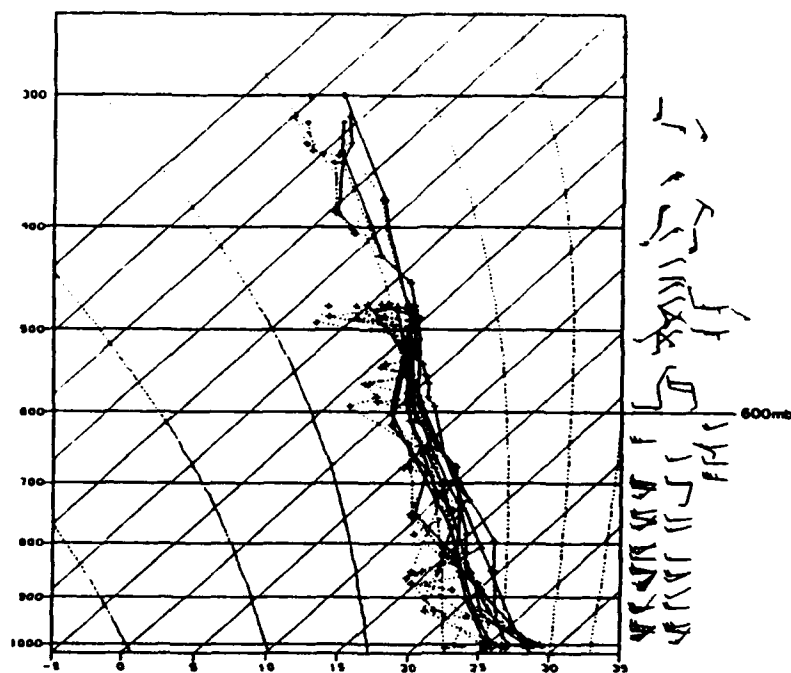


Figure 43. Ten AOP 7 dropwindsonde temperature and dewpoint profiles representing moist and cool conditions through all levels. Note the westerlies extend up to about 600 mb.

The vertical profiles of wind speed and especially direction in the dropwindsondes describe another interesting feature (Figs. 43 and 44). In both the moist and dry sounding regions, west to southwesterly flow is found up to about 690 mb. Above this level, lighter winds and widely varying directions prevail, thus defining the mid-level circulations in the region. In the moist soundings, the level at which these westerly winds change to light and variable is about 600 mb. Recall that these dropwindsondes were deployed in the early stages of the mission. Upon examining the later dry soundings, the transition from westerly to variable flow is found to be at about 690 mb, which supports a descent with time of the layer with light and variable winds that defines the vortex circulations. These soundings also show the depth of the vortices found within the MCS region to be no lower than the 700 mb level, which is consistent with the 850 mb and surface gradient level streamline analyses (Fig. 35 and 36). In addition, a relatively strong inflow to the system is readily evident. As shown above (Fig. 30), the average motion of the MCSs was relatively slow (3 to 5 m/s) toward the west-northwest. Thus, the low-level flow was a front- and/or side-inflow to the primary MCS, rather than a rear-inflow as suggested by Fritsch (1992).

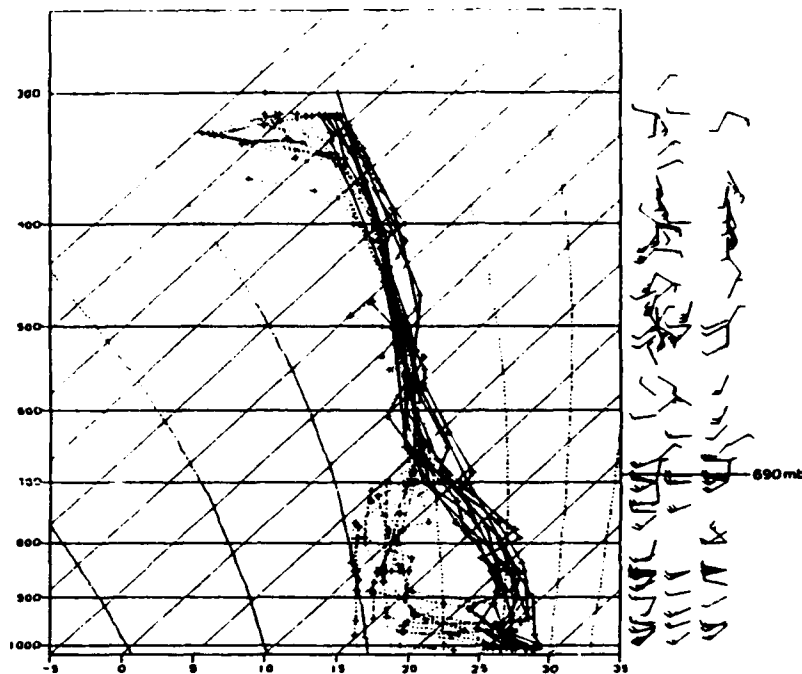


Figure 44. Eleven AOP 7 dropwindsonde temperature and dewpoint profiles that are warm and dry at low levels due to subsidence. Note the westerlies extend only up to 690 mb.

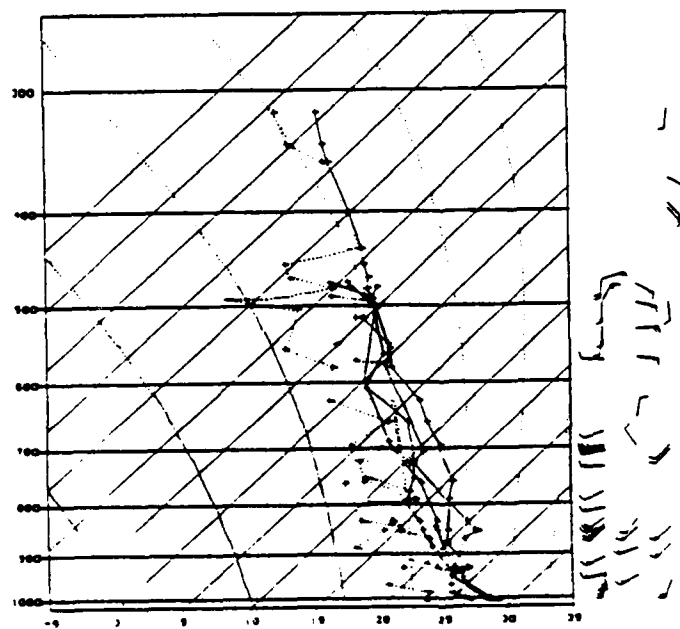


Figure 45. Four AOP 7 dropwindsonde temperature and dewpoint profiles with varying mid-level warm and dry layers due to subsidence.

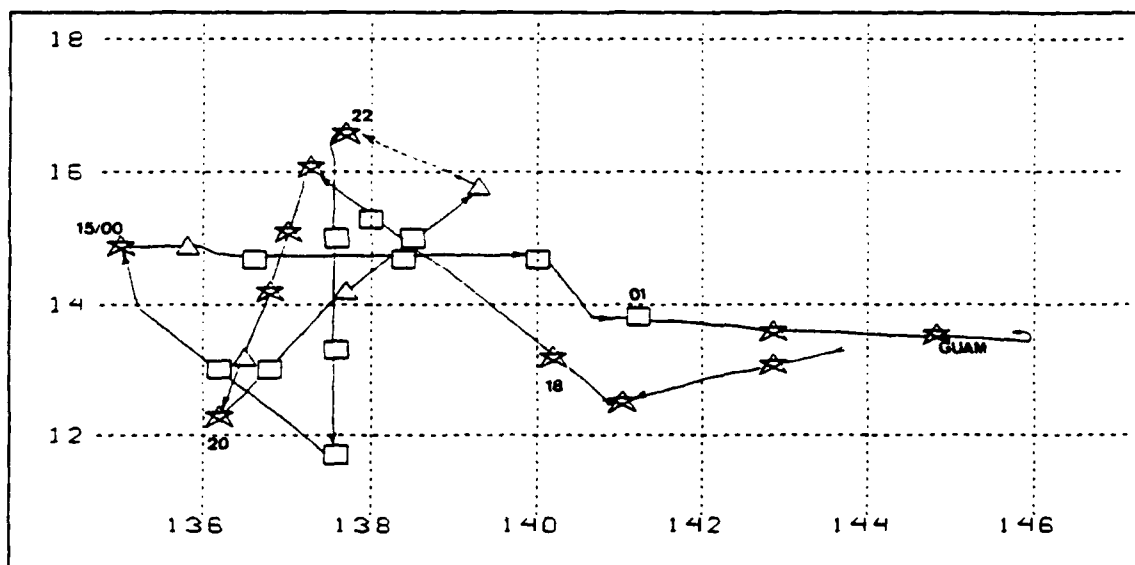


Figure 46. Locations of AOP 7 dropwindsondes in relation to vertical profile: stars represent moist soundings; squares, dry low-levels; and triangles, dry mid-levels. Flight track is overlaid and numbers next to track indicate approximate time (UTC) when aircraft was at that position. AOP 7 mission time was from 1642 UTC 14 August to 0237 UTC 15 August.

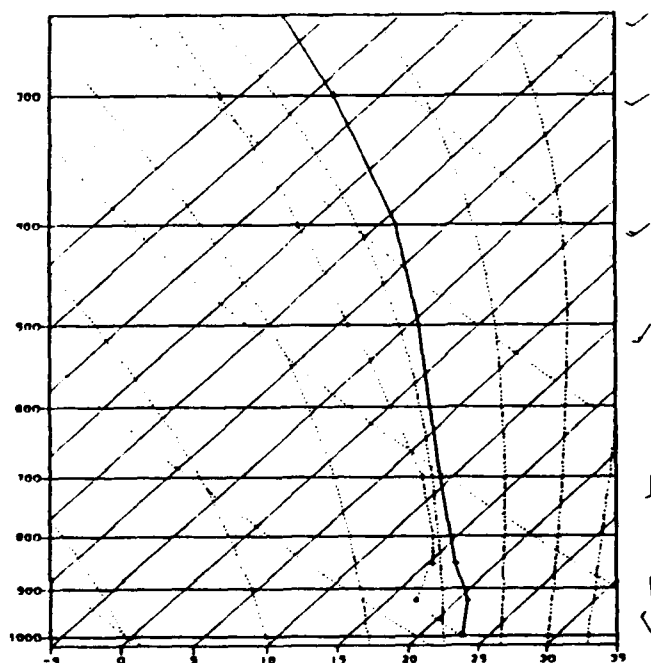


Figure 47. Skew T-ln p plot of 0000 UTC 15 August Guam rawinsonde.

## F. STRUCTURE OF AOP 1 MCS

The AOP 1 MCS differed from the AOP 7 case in several ways. The primary difference is that the AOP 1 MCS was not as centralized. Figs. A-7 through A-9 and A-10 through A-11 of Appendix A describe the IR and visual evolution of this case. One significant aspect is the relatively rapid rate at which cells within the MCS of interest develop and decay while moving westward. In addition, the rapid development and movement of another MCS in the northern portion of the AOP region becomes strongly associated with the low-level circulation of the AOP. The analysis of the data set from this AOP will reflect these differences and some similarities.

### 1. Horizontal structure

As in AOP 7, mid-level vortices are present at 500 mb and 300 mb (Fig. 48 and 49). However, the horizontal scale of these vortices is slightly smaller (approximately 80-100 n mi in diameter) than expected (Table 1). The primary vortex center is near  $5^{\circ}$  N,  $139^{\circ}$  E at 300 mb and  $5^{\circ}$  N,  $140^{\circ}$  E at 500 mb based on both the aircraft and flight-level dropwindsonde data. The circulations analyzed near  $6^{\circ}$  N,  $137^{\circ}$  E and  $6^{\circ}$  N,  $141^{\circ}$  E at 500 mb are only partially revealed in the aircraft flight-level data. Confirmation of mesoscale mid-level vortices within other areas of similar convection in the AOP region provides the basis for closing off these features.

Three circulation centers are also analyzed at 700 mb (Fig. 50). The circulation center analyzed at  $6^{\circ}$  N,  $140^{\circ}$  E is considered the primary vortex. The other two are based on limited data, and there is a lack of vertical consistency with vortices analyzed at the higher levels. That is, an extreme tilt toward the south with increasing elevation would be required in the levels below 700 mb. The validity of such a tilt will be addressed below in the vertical structure section.

The 850 mb and surface wind analyses (Figs. 51 and 52) are remarkably different from the corresponding wind fields in the AOP 7 case. Instead of broad west-southwesterly flow, the low-level flow in AOP 1 is dominated by the presence of a circulation center near  $9^{\circ}$  N,  $140^{\circ}$  E. In addition, this broad center (approximately 400 n mi in diameter) is well north of the main convection of the MCS. Late in the AOP, this low-level center becomes the dominant feature of the area, with the convection spiralling cyclonically around it (Fig. 48). Such characteristics of the low-level circulation suggest that the mid-level vortices are independent of the low-level center. This conclusion is further supported by the gradient-level analyses for the days prior to the AOP, which indicate a low-level circulation propagating westward across the WPAC. However, this preexistent low-level circulation may have provided a favorable

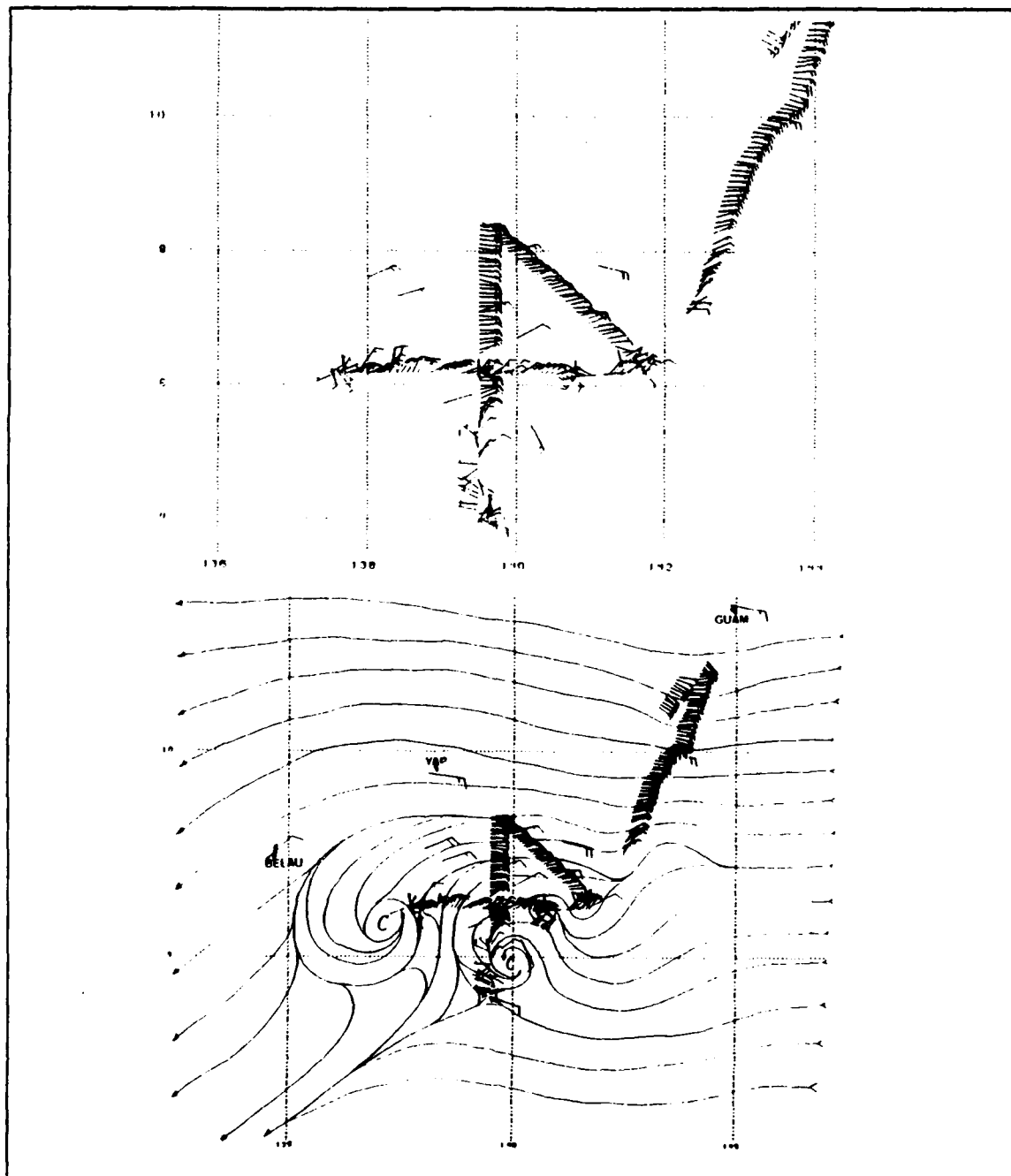


Figure 48. AOP 1 500 mb aircraft flight-level and dropwindsonde winds (kt) (top), and 0000 UTC 24 July Guam, Yap and Belau (Koror) rawinsonde winds (kt) with streamline analysis (bottom). Dropwindsonde winds are the large barbs.

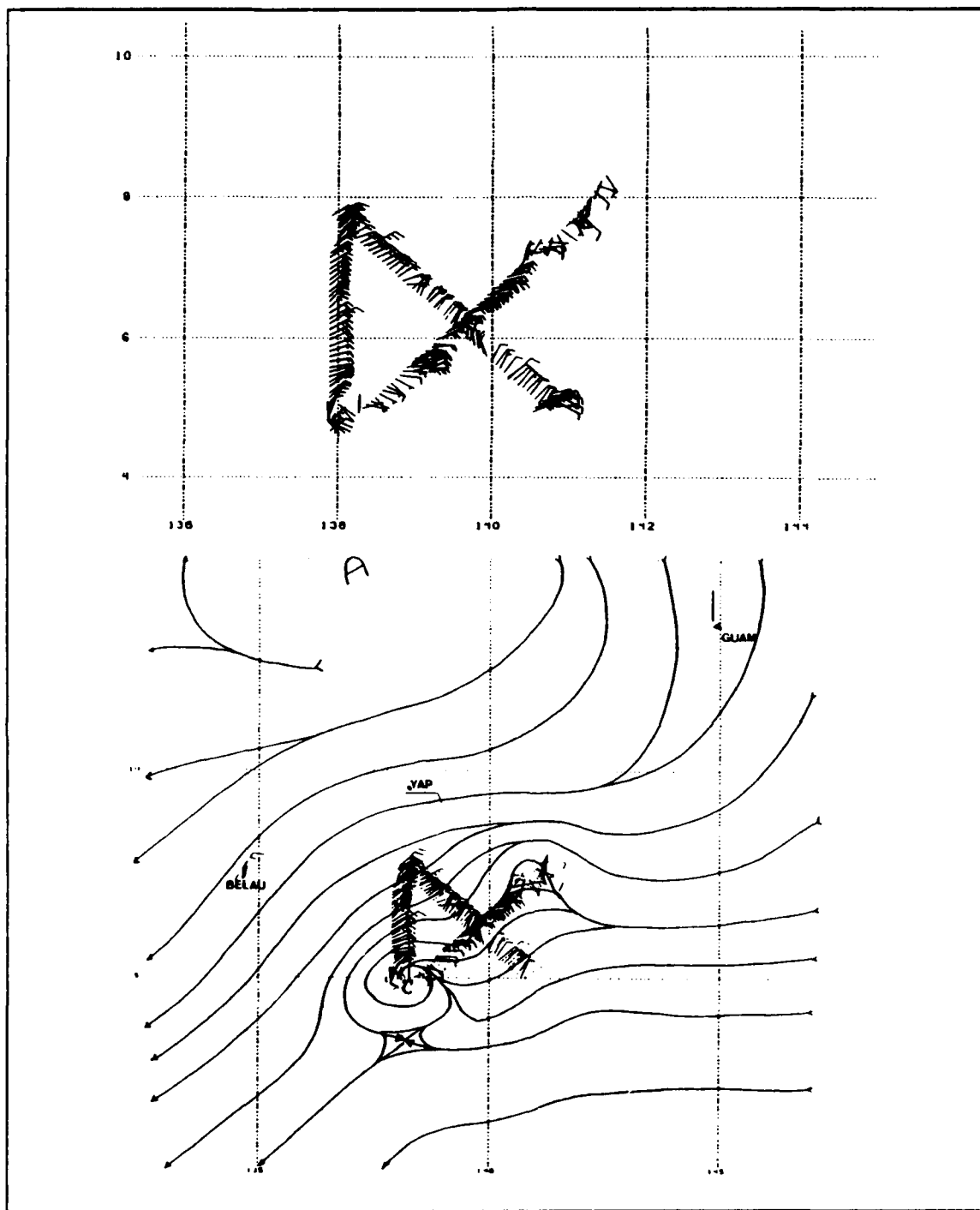


Figure 49. AOP 1 300 mb winds and analysis as in Fig. 48.

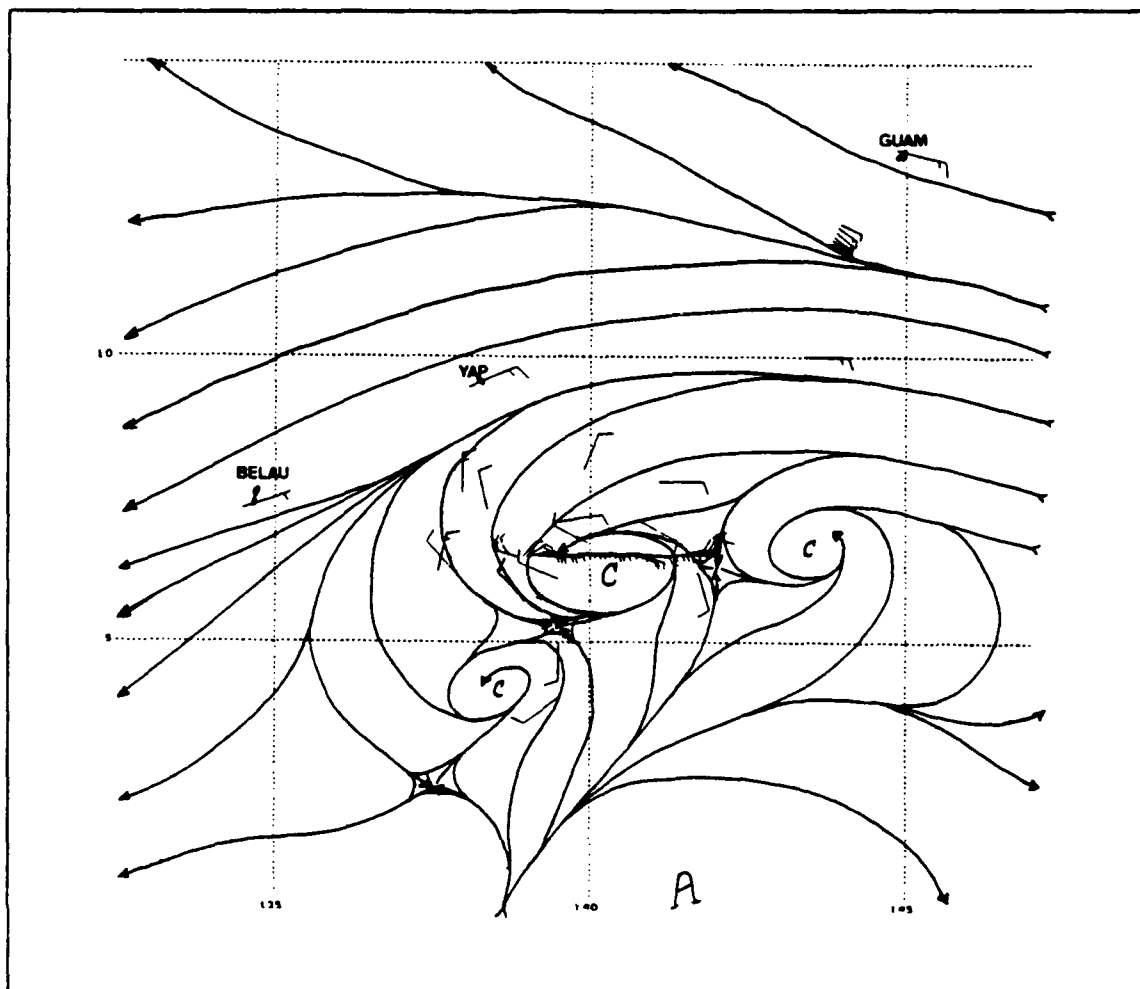
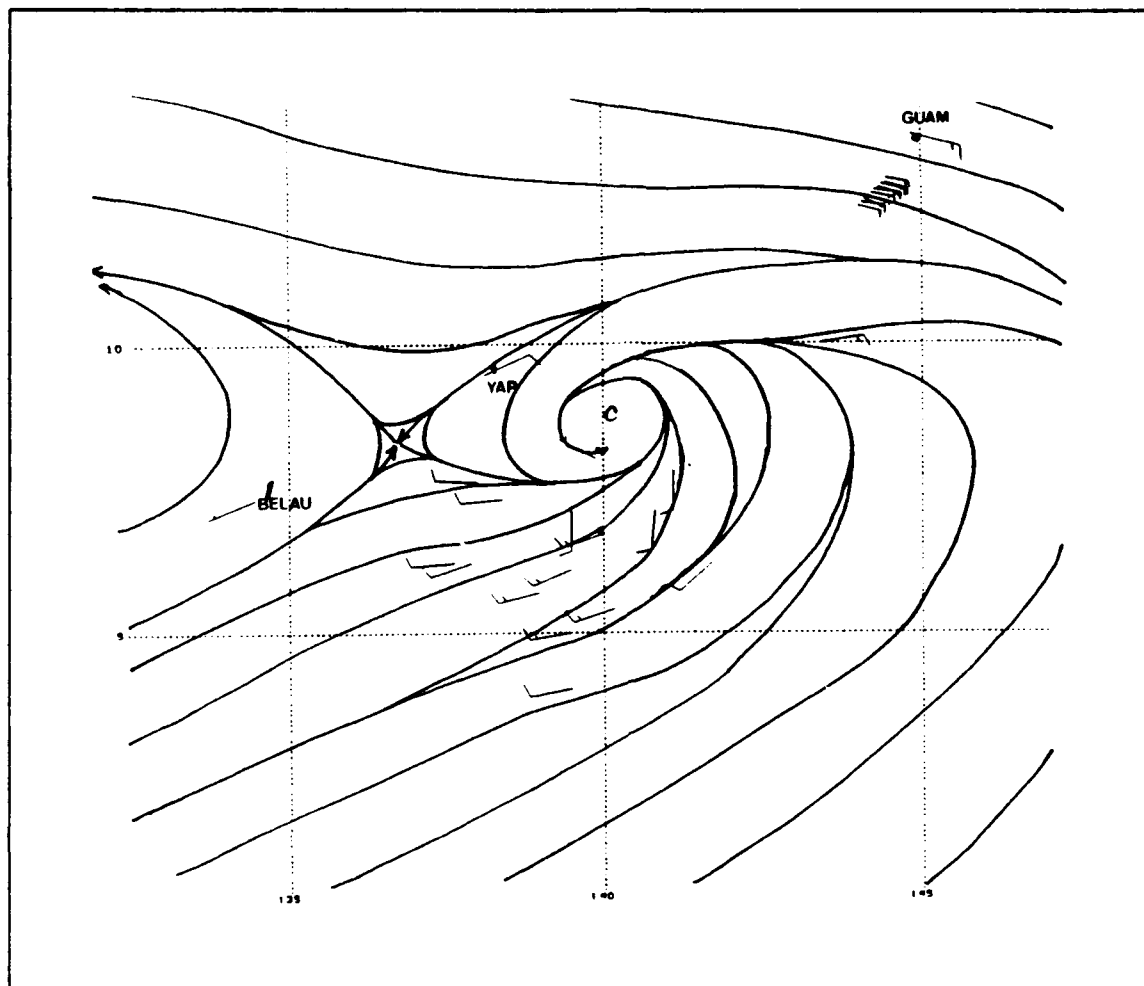


Figure 50. AOP 1 700 mb streamline analysis of aircraft flight-level, dropwindsonde and 0000 UTC 24 July Guam, Yap and Belau (Koror) rawindsonde winds (kt).

environment for the development of the MCS. Another possibility is that the low-level circulation was weak until the MCS developed. Once the convection became deep and persistent, the original circulation may have been enhanced until it eventually dominated the flow.

Temperature and dewpoint analyses from this AOP document several expected features, such as the presence of cold pools in the low levels (Table 1). The surface analysis in Fig. 53 depicts cold and moist pockets under the region of convection. These cold pockets may provide the lifting of the low-level air flowing into the MCS and thus





**Figure 51. AOP 1 850 mb streamline analysis of dropwindsonde and 0000 UTC 24 July Guam, Yap and Belau (Koror) rawinsonde winds (kt).**

serve to maintain the MCS. In addition, these cold and moist pockets exist in the lower levels up to 700 mb (Figs. 54 and 55), which would appear to provide the necessary environment for cyclone development. This aspect will also be addressed further in the vertical structure section. The mid- and upper-levels (Figs. 56 through 58) are both warmer and more moist than the surrounding environment as in the AOP 7 analyses, in agreement with the expectations in Table 1. In particular, the presence of significant moisture in the mid-levels is of primary importance in validating the assumptions of the Frank and Chen (1991) theory. However, there are some significant differences at the 400 mb and 300 mb levels. In the AOP 7 case, regions with high moisture content were

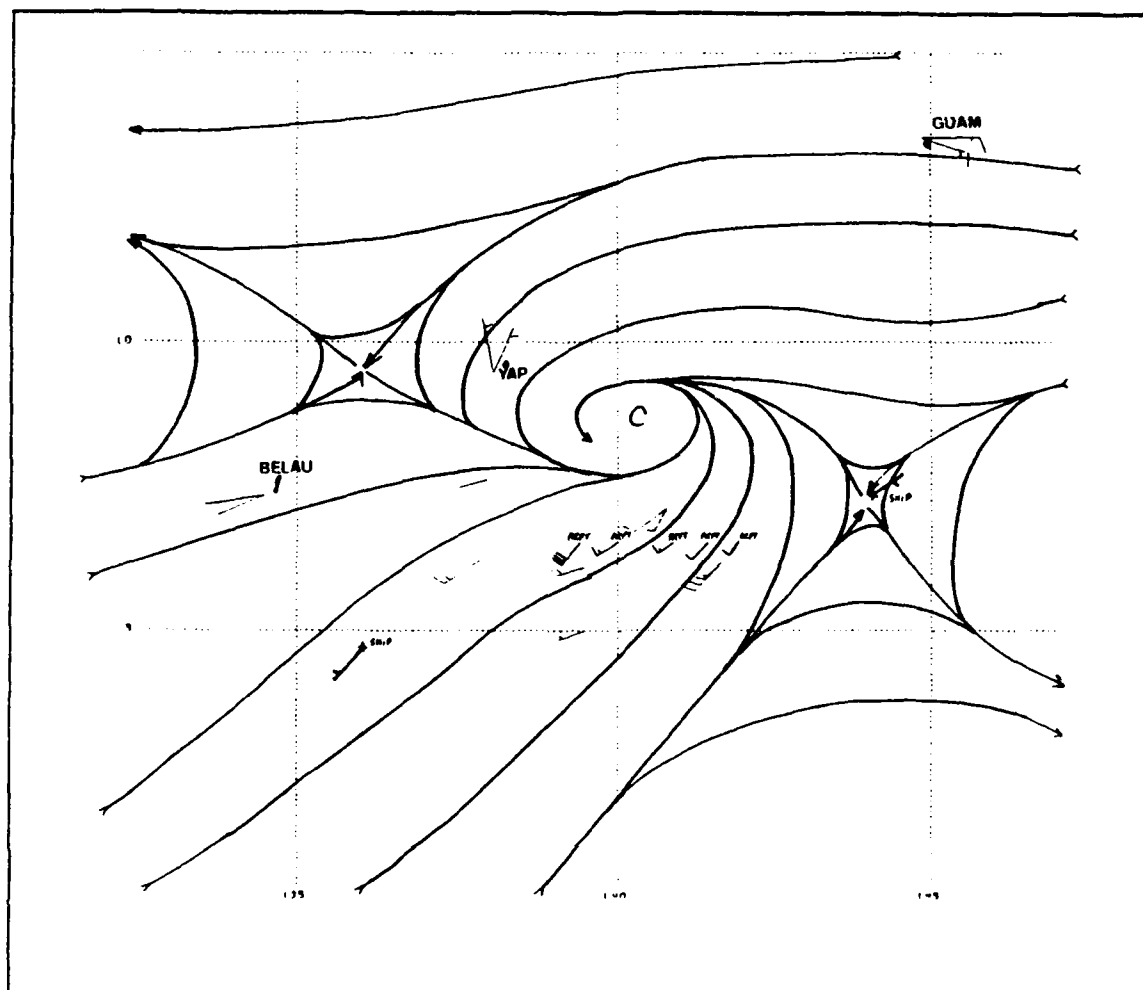


Figure 52. AOP 1 gradient level (960 mb-surface) streamline analysis of dropwindsonde and 0000 UTC 24 July Guam, Yap and Belau (Koror) rawindsonde. Also included are visually observed surface winds from aircraft (ACFT) and 0000 UTC 24 July ship reports (SHIP) winds (kt).

far more widespread and uniform. In AOP 1, the dewpoint depressions are generally larger than in the AOP 7 case by  $2^{\circ}$  to  $4^{\circ}$  C even though the temperatures were similar. This suggests a positive correlation may exist between size and intensity of the vortex and mid- and upper-level temperature and moisture fields.

## 2. Vertical structure

The vertical structure of this system is intriguing. As suggested above, the vortices appear to tilt from north to south with height. Winds in the low levels are

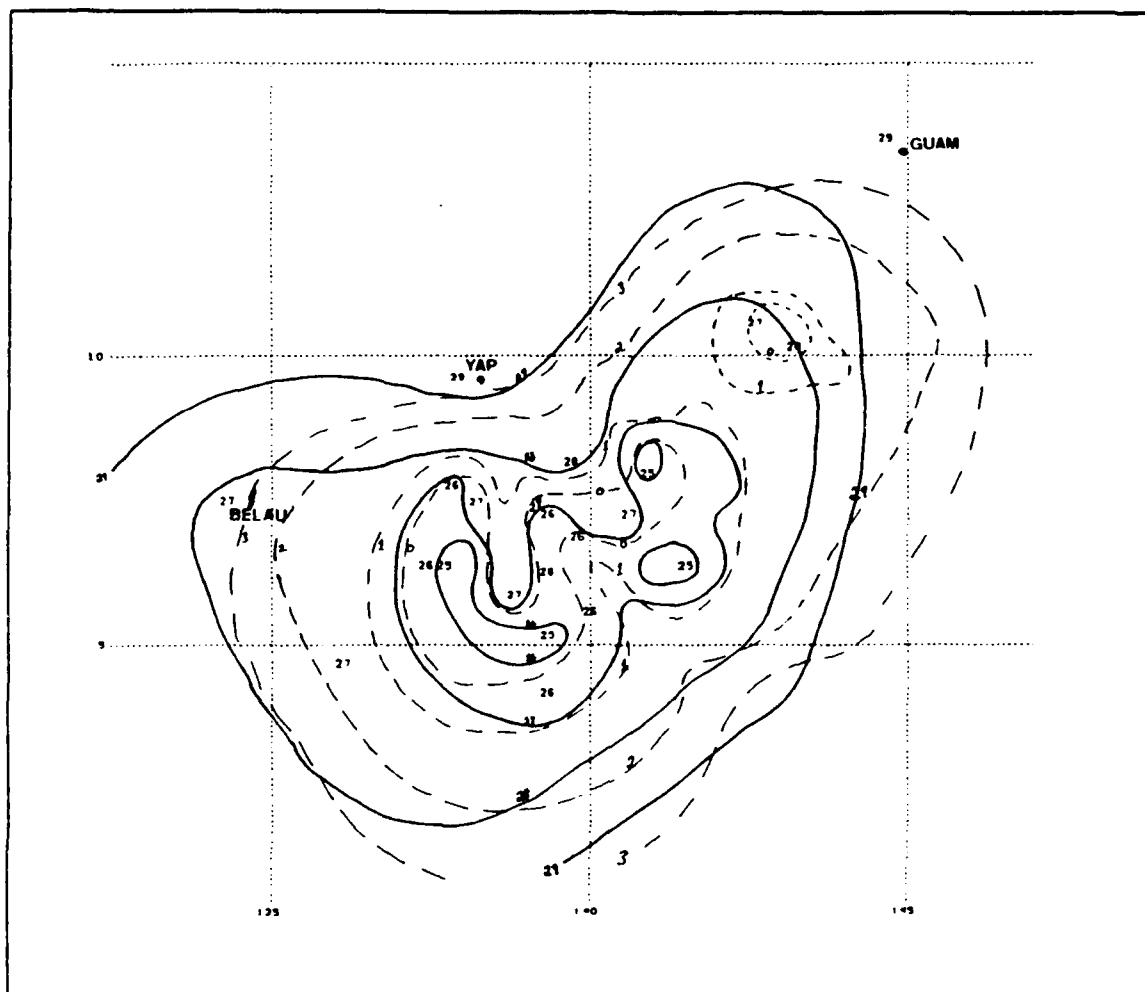
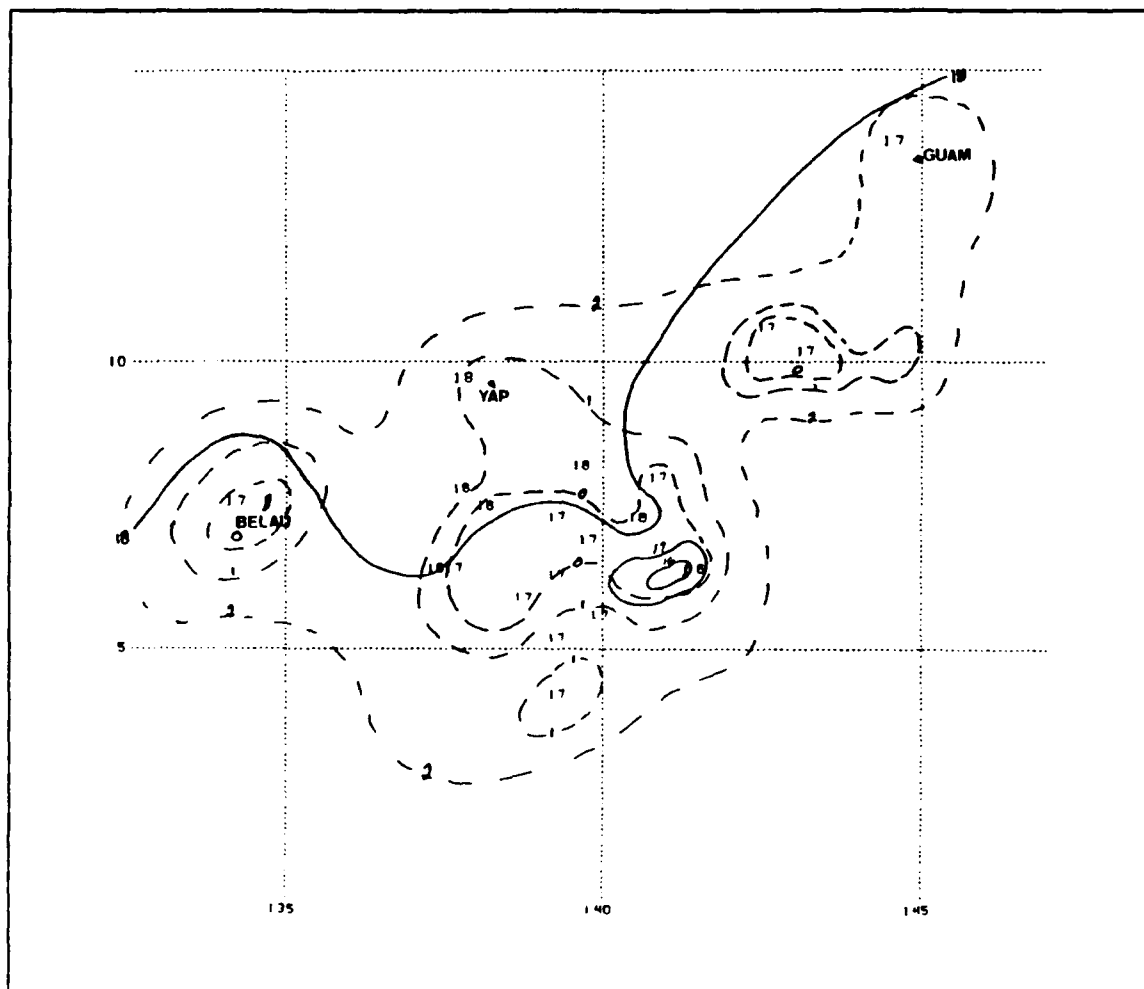


Figure 53. AOP 1 Surface temperature and dewpoint depression analysis. Solid lines are isotherms of 1 ° C increments, dashed lines are dewpoint depressions in 1 ° C increments. The 0000 UTC 24 July temperatures for Guam, Yap and Belau (Koror) are included in the analysis. Environmental temperatures for 0000 UTC 24 July are 28 ° to 29 ° C.

stronger on the equatorward side and the opposite is true at upper levels. Although the vortex at 300 mb appears to be displaced to the west relative to the 500 mb center, this is likely due, in part, to the relatively rapid movement of the MCS to the west during the two hours between the observations at these two levels. An analysis of the 700 mb vortex based on the dropwindsondes deployed from 300 mb appears to be farther west and north due to the time differential relative to the 700 mb flight-level data that also



**Figure 54. AOP 1 850 mb temperature and dewpoint depression analysis.** As in Fig. 53, except environmental temperatures for 0000 UTC 24 July are 18 ° to 19 ° C.

defines a circulation center (Fig. 50). The northward displacement may be as much as 80 n mi, which allows an analysis of centers with a fairly uniform north to south tilt of 250 n mi from the surface center to the 300 mb center. Such a tilt of roughly 40 n mi in the horizontal for every 1 n mi in the vertical may be realistic for the inactive monsoon trough environment. Winds associated with such a tilt should also shear the convection such that the low-level circulation would be exposed from under the deep convection. Although an exposed low-level circulation was not initially present, the cyclonic spiraling of low cloud in visual imagery at 0630 UTC (Fig A-11b, Appendix

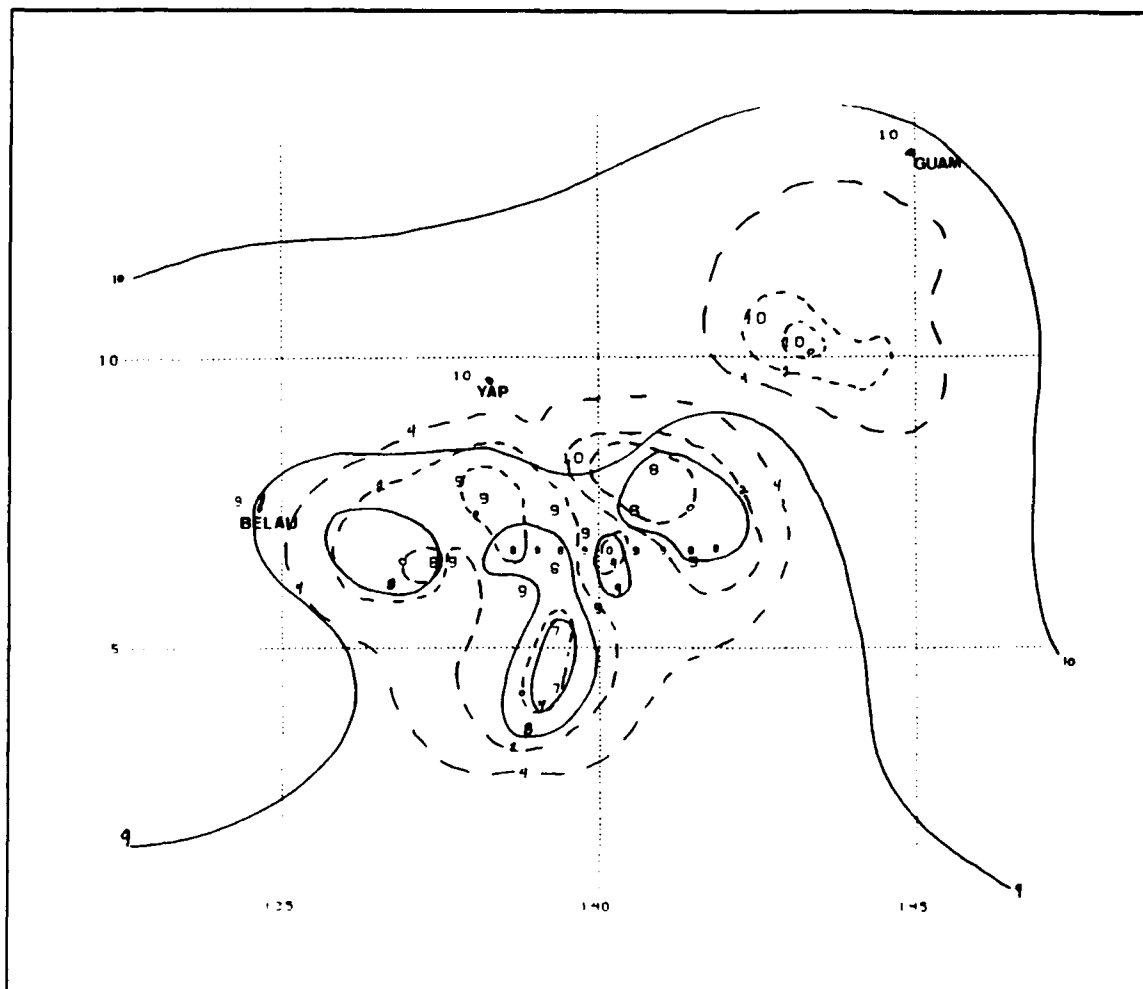


**Figure 55. AOP 1 700 mb temperature and dewpoint depression analysis.** Solid lines are isotherms of 1 ° C increments, dashed lines are dewpoint depressions in 2 ° C increments. The 0000 UTC 24 July Guam, Yap and Belau (Koror) rawindsondes are included in the analysis. Environmental temperatures for 0000 UTC 24 July are 9 ° to 10 ° C.

A) strongly suggested that one had developed, thus indicating a vertical tilt in the circulation.

The horizontal scales of the vortices at each level present a possible argument against the above reasoning. Whereas the lower level vortices are broader and clearly defined, the vortices in the mid- and upper-levels are about 33 percent smaller, and multiple vortices are found at these levels. Recall that the low-level circulation had

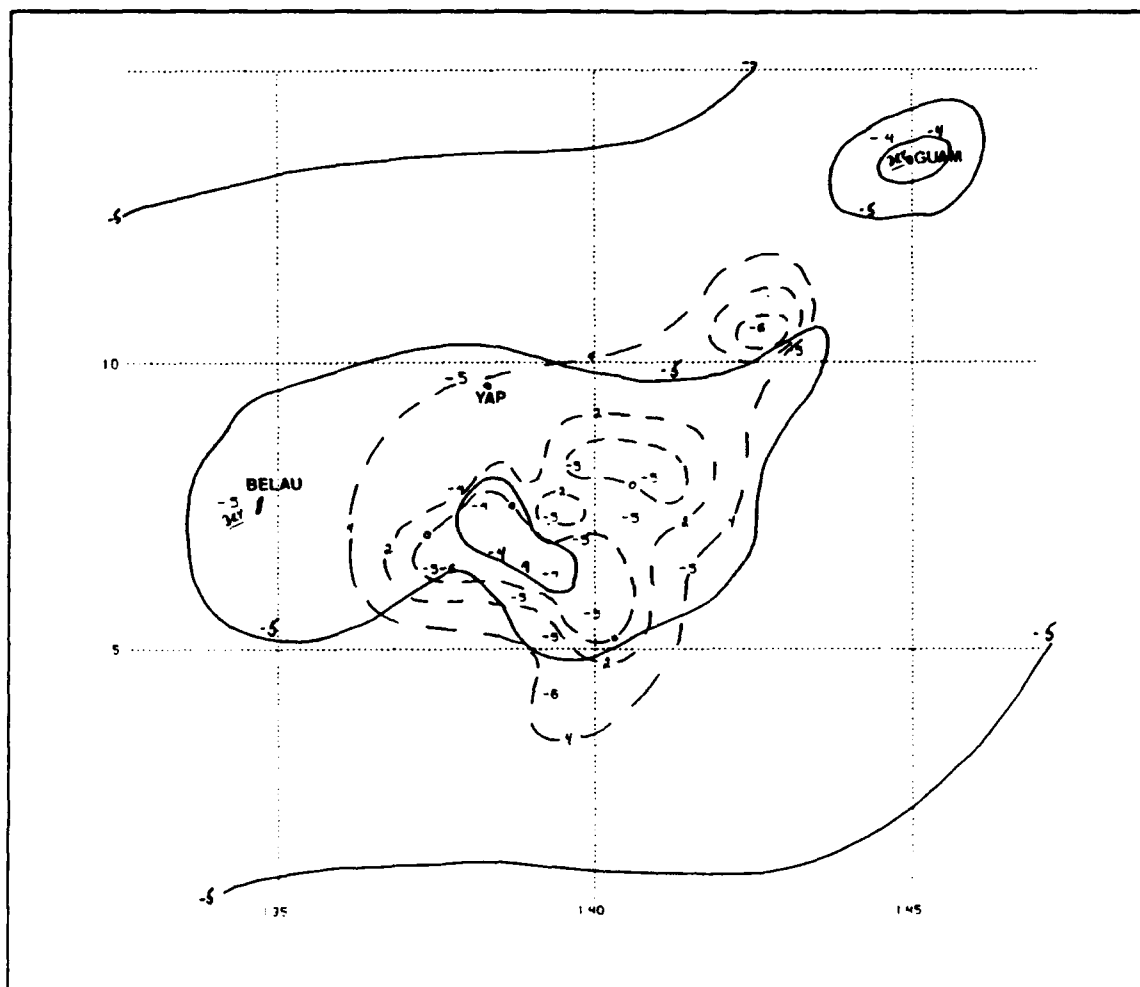


Figure 56. AOP 1 500 mb temperature and dewpoint depression analysis. As in Fig. 55, except environmental temperatures for 0000 UTC 24 July are  $-5^{\circ}\text{C}$ .

already existed for several days. The alternate explanation may be that the mid-level vortices developed independently within the stratiform rain region of the MCS. Thus, a completely separate circulation existed from that of the low-level circulation and its associated upper-level trough.

If the mid- and low-level circulations are indeed separate in this case, then the mid-level vortex circulation did not extend downward toward the surface as expected (Table 1). One reason why such a downward extension may not have occurred is the presence of the low-level circulation center to the northeast of the MCS region. As

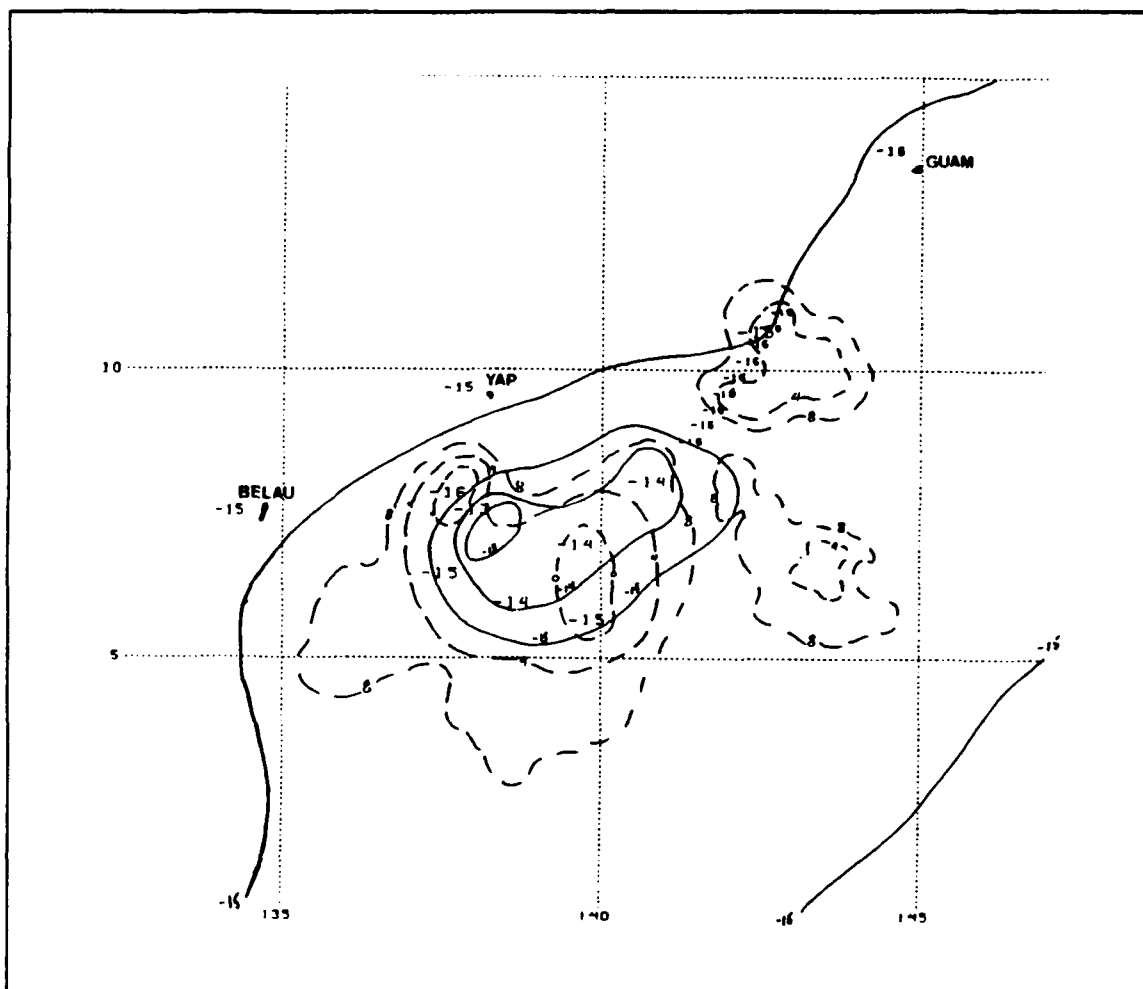


Figure 57. AOP 1 400 mb temperature and dewpoint depression analysis. Solid lines are isotherms of 1 ° C increments, dashed lines are dewpoint depressions in 4 ° C increments. The 0000 UTC 24 July Guam, Yap and Belau (Koror) rawinsondes are included in the analysis. Environmental temperatures for 0000 UTC 24 July are -15 ° C.

suggested above, the enhancement of this circulation by the second area of convection to the northeast of the MCS may have imposed sufficient shear on the vortex to disrupt the downward extension process.

Although the AOP 1 dropwindsonde profiles are generally similar to the AOP 7 soundings, evidence of strong low-level subsidence as in Fig. 44 is not present. Three separate categories could be discerned (Figs. 59 through 61): sondes that were moist

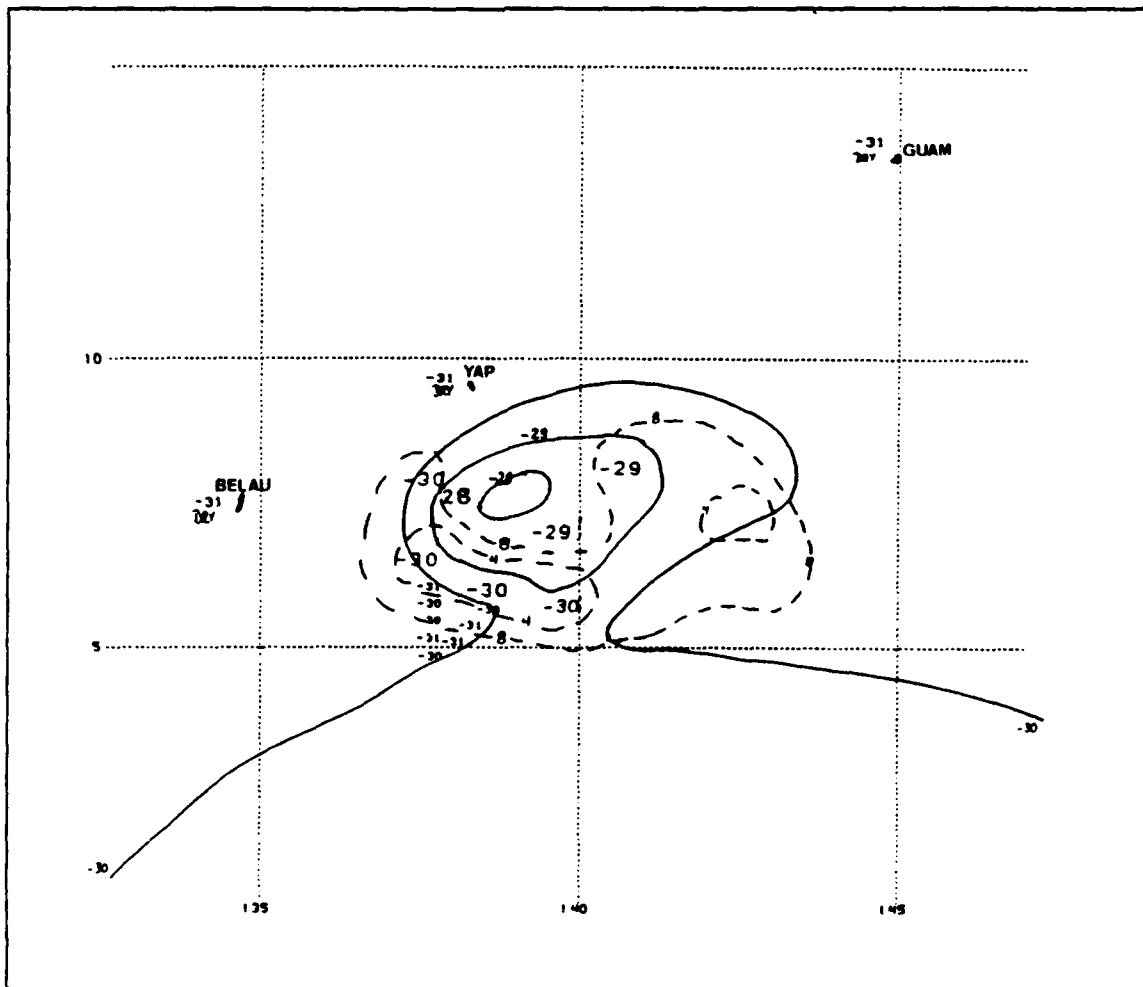
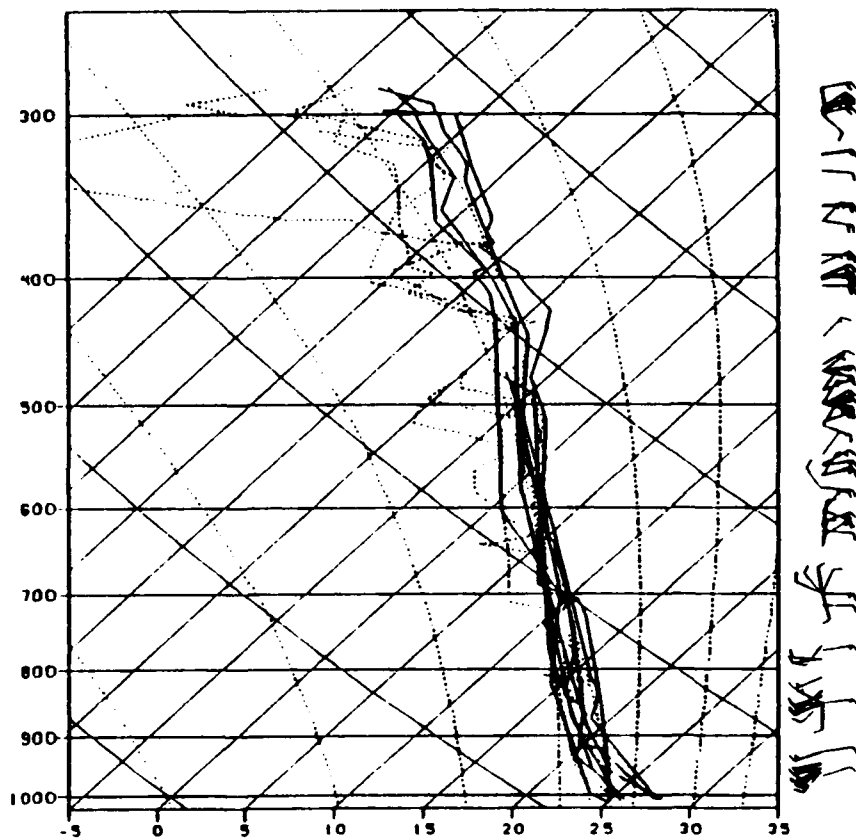


Figure 58. AOP 1 300 mb temperature and dewpoint depression analysis. As in Fig. 57, except environmental temperatures for 0000 UTC 24 July are  $-30^{\circ}$  to  $-31^{\circ}$  C.

throughout; those showing weak mid-level dry layers; and weak low-level dry layers. In this case, no consistent relationship between these three classes of profiles and the vortices could be established (Fig. 62). As mentioned above, horizontal analyses suggest higher moisture contents below 700 mb relative to AOP 7, which is confirmed by these soundings. Even though subsidence appears to be present, the degree of warming drying is significantly less than in the AOP 7 sondes. If this moist air was advected into the region of the low-level circulation center by its low-level flow through the MCS region, then the presence of this moist air may provide support to the hypotheses requiring



moist columns of low-level air in order to generate, or maintain, low-level circulation. The low-level circulation center in AOP 1 did develop into the dominant feature of the region with surface pressures 4 mb lower than the surrounding environment.



**Figure 59. Nine AOP 1 dropwindsonde temperature and dewpoint profiles representing moist and cool conditions through all levels.**

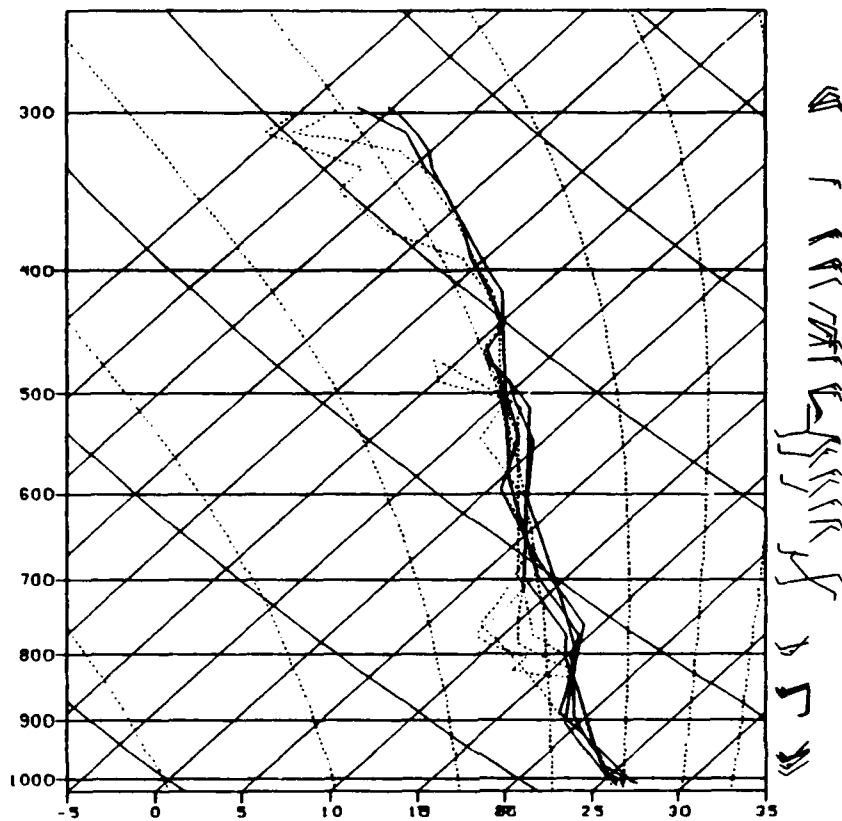


Figure 60. Four AOP 1 dropwindsonde temperature and dewpoint profiles that have weak mid-level warm and dry layers due to subsidence. The Yap rawindsonde is not included.

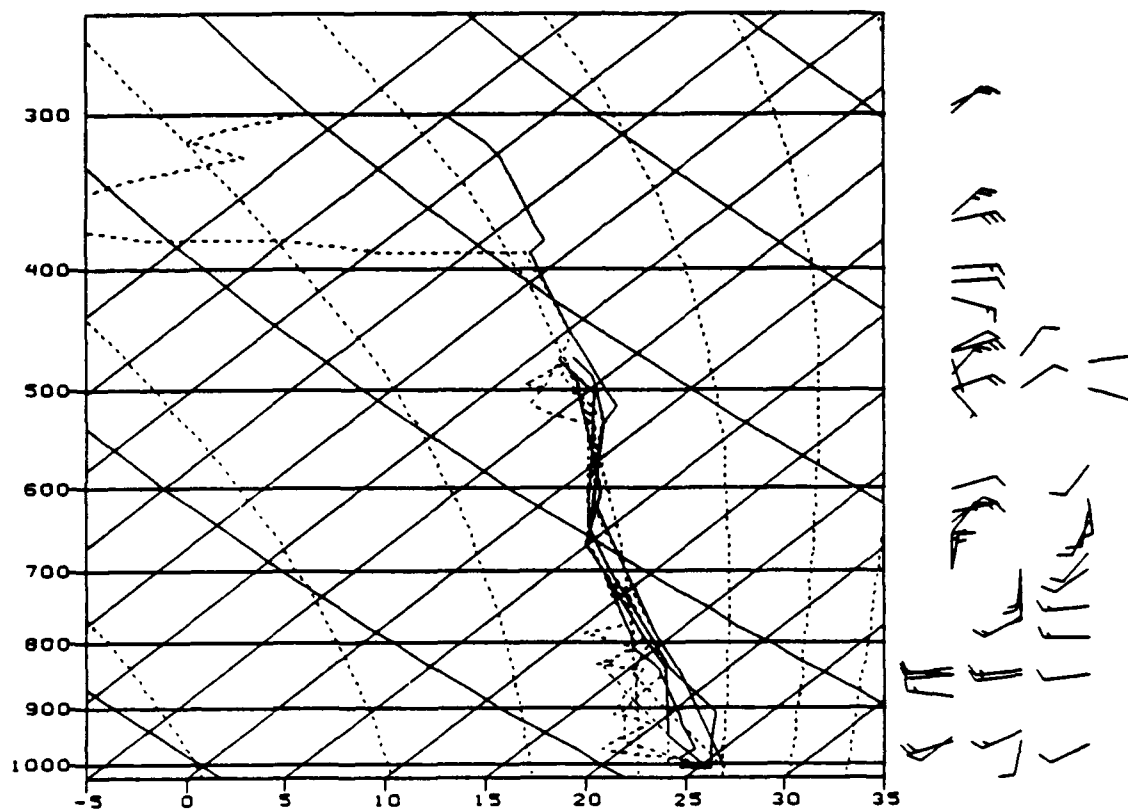
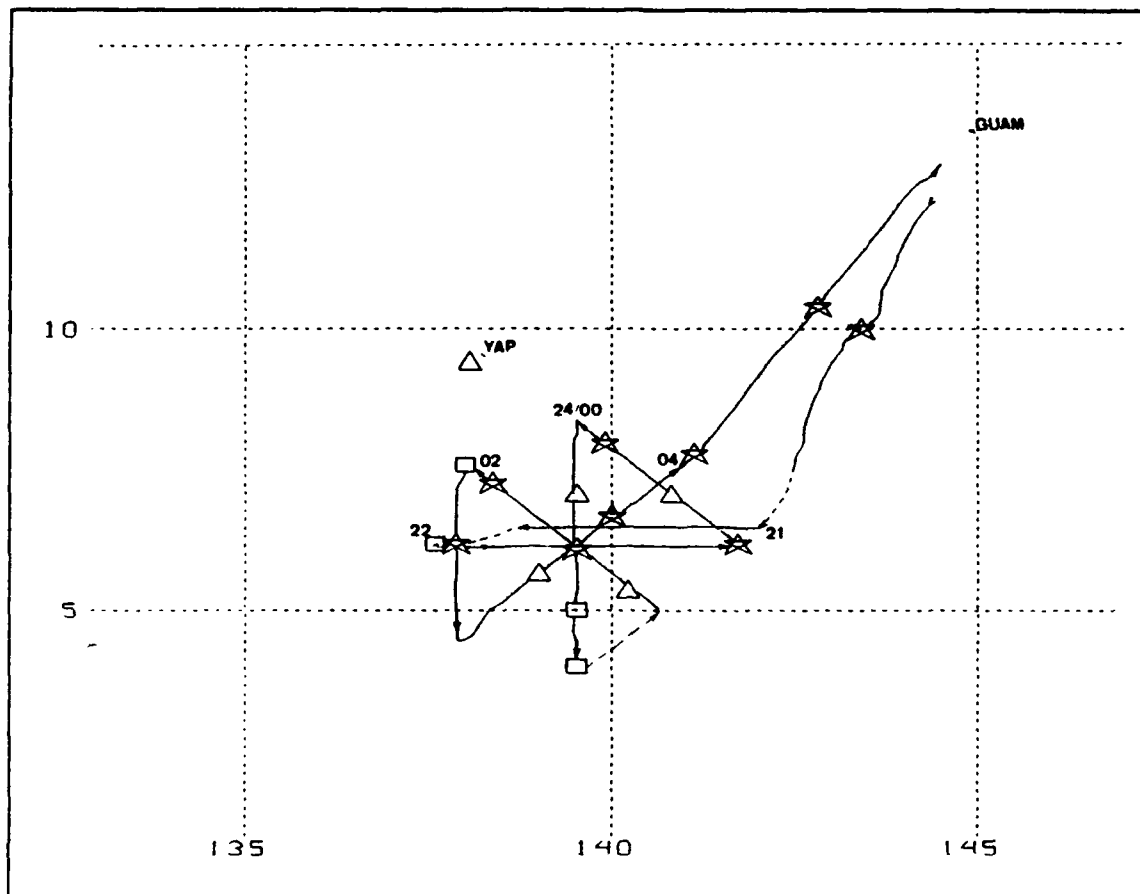


Figure 61. Four AOP 1 dropwindsonde temperature and dewpoint profiles that have weak low-level warm and dry layers due to subsidence.



**Figure 62.** Locations of AOP 1 dropwindsondes in relation to vertical profile: stars represent moist soundings; squares, dry low-levels; and triangles, dry mid-levels. Flight track is overlaid and numbers next to track indicate approximate time (UTC) when aircraft was at that position. The AOP 1 mission time was from 1920 UTC 23 July to 0600 UTC 24 July.

## V. SUMMARY

The above analyses document the presence of several significant features expected in both intense and moderate tropical MCS cases. Although other expected features could be said to be present, certain aspects departed from the expected structure and evolution. Table 2 provides yes/no responses as to whether the expected characteristics in Table 1 were present for AOP 7 and AOP 1. The following sub-sections contain interpretations of this table.

**Table 2. OBSERVED CHARACTERISTICS OF MCS STRUCTURE DURING AOP 7 AND AOP 1**

Feature	Position Relative to MCS	Convective Growth Stage	Horizontal Scale	AOP 7	AOP 1
<i>Mid-Level Vortex</i>	Stratiform Rain Region	Early Mature to Decaying	100 n mi to 125 n mi	Yes	Yes
<i>Low-Level Vortex</i>	Under Stratiform Rain Region	Late Mature to Decaying	200 n mi to 250 n mi	Yes	No
<i>Upper-Level Anticyclone</i>	Outflow Layer Above MCS	Mature and Decaying	175 n mi to 225 n mi	?	?
<i>Mid-Level Warming</i>	Stratiform Rain Region	Formation to Decaying	Minimum 100 n mi	Yes	Yes
<i>Low-Level Cold High</i>	Under Convective Rain Region	Formation to Mature	Order of 100 n mi	Yes	Yes
<i>Low-Level Warm, Moist Rear Inflow</i>	Into Rear of MCS (With Direction of Movement)	Formation to Mature	Of Similar Proportions to MCS	No	No
<i>TD Development</i>	Under Mid-Level Vortex	Mature to Decaying	Similar to Low-Level Vortex	No	No

### A. LOW- AND MID-LEVEL VORTICES

As suggested in the background, the development of a vortex within the stratiform rain region of the MCS is the feature of primary importance. The presence of a cyclonic circulation, or a vorticity center, is the basis of the suggested Fujiwhara-type interaction when a tropical cyclone (TC) and MCS are within some critical separation distance. The

analyses have shown that such a vortex did exist in both an intense and a weak MCS case. Horizontal development and the downward extension of the vortex are markedly different in the two cases. Although the visual imagery documents that the mid-level vortex during AOP 7 extended downward to the low levels, no such evidence exists for the AOP 1 case. The analysis of the dropwindsonde soundings from AOP 7 also implies a descent of the vortex toward the lower levels with time.

Several secondary vortices may be analyzed in the high-resolution aircraft flight-level observations at the 500 mb and 300 mb levels. In several cases, a cyclonic shift in the flight-level wind track could be closely correlated to stratiform cloud regions produced from intense convection. However, flight-level and dropwindsonde data and visual satellite imagery were inadequate to fully support the analysis of these secondary vortices. That is, the support for these vortices must be regarded as more tentative than for the primary vortices for which detailed observations are available. Nevertheless, it is the author's suggestion that these vortices can be realistically analyzed in association with similar convective signatures present with the primary vortices, especially that of the vortex near Guam (Fig. 32). These secondary vortices were generally smaller than those of the primary vortices and the vortex near Guam of the AOP 7 case. If these secondary vortices are forming within stratiform rain regions, then the intensity and size of the vortex may be proportional to the horizontal and vertical extent of these regions. For example, the primary MCS of AOP 7 exceeded by 50,000 to 100,000  $km^2$  the size definitions of the midlatitude MCC/MCS as posed by Maddox (1980), and the size of the associated vortex exceeded by almost 100 n mi (185 km) the simulated vortex in the Frank and Chen model. However, the secondary vortices were typically 60 to 80 n mi in diameter, and thus more difficult to detect.

## **B. UPPER-LEVEL ANTICYCLONE**

Although the existence of the mid- and low-level vortex is confirmed by the analyses, the presence of the upper-level outflow anticyclone is a more difficult feature to confirm. Because the highest altitude of the WC-130 is roughly 300 mb, it was impossible to use aircraft data to define any such feature above this level. Although the presence of anticyclonic turning is detected over the MCS regions in the synoptic analyses of the 200 mb wind field, it is difficult to state whether this was an effect of the MCS or simply a reflection of the synoptic-scale circulation in the region. It is for this reason that a question mark is entered for this item (Table 2) for both cases. In the AOP 7 case, the

existence of such a feature seems quite probable given the strength and size of the MCSs. However, it is still conjecture that an anticyclone existed.

### C. TEMPERATURE DISTRIBUTIONS

The magnitudes of mid-level warming and increased moisture appeared to be related to the strength and scale of these vortices (Table 2). In the most intense case (AOP 7), large areas of precipitation and stratiform cloud are observed surrounding the vortex regions. In the weaker MCS (AOP 1), similar temperature and moisture patterns are found, but they are not as well-defined in the horizontal or the vertical. For example, less moisture is found at the 300 mb and 400 mb levels in the AOP 1 case as compared to the AOP 7 case. In relation to the proposed hypotheses in which warm, moist air in the mid-levels provides the favorable environment for vortex development, the weaker patterns may be the primary reason for both the smaller horizontal scale of the AOP 1 vortex as well as its lack of downward propagation.

The location of the mid-level warm, moist air in relation to the vortices is of great interest. In the Frank and Chen model, it is suggested that the vortex develops between 600 mb and 400 mb. The analyses of these two cases suggest the vortices may have developed higher in the troposphere (between 400 mb and 300 mb). The presence of a relatively large and strong vortex at 300 mb in both cases suggests that either an upward propagation of the 500 mb vortex occurred, or the vortex formed closer to this level initially. Support for the latter interpretation is that although the temperature and moisture profiles are observed to be warmer and more moist than the surrounding environment at 500 mb, they are fairly weak (temperatures were about 1 ° C warmer, see Figs. 40 and 56). The temperature profiles of both cases suggest stronger warming in the 400 mb (3 ° C differences) and 300 mb (2 ° C differences) layers, which is expected in the Frank and Chen (1991) model in terms of warm air anomalies above the vortex and cool air below.

In both cases, the low-level analyses provide clear evidence of "cold pools" of air at the surface (2 ° to 3 ° C cooler). Such a significant departure from the environment lends support to the existence of a mechanism by which an inflow can be brought upward into the MCS over relatively long periods of time.

### D. TD DEVELOPMENT

Although the hypotheses related to TD development have been addressed in some detail, a firm conclusion is obviously difficult to support without more data within, and surrounding, the region. The suggestion by Fritsch (1992) and Emanuel (1992) is that

moist low-level conditions are required in the presence of a low-level vortex to provide the upward translation of surface energy in terms of rotation. Without such a moist layer, genesis of a TD can not occur even if a vortex exists at the surface. This scenario seems to apply for the AOP 7 low-level vortex. As shown in the soundings of Fig. 44, the air became dominated by mesoscale unsaturated downdrafts after the convection of the primary MCS had dissipated. In the case of AOP 1, the downward propagation of the mid-level vortex did not occur. Although a low-level, synoptic-scale circulation was present north and east of the AOP 1 observation region, the associated low-level temperature and moisture fields in that region do not appear relevant to the expected characteristics (Table 2).



## VI. CONCLUSIONS

From 21 July 1992 to 21 August 1992, a USAF Reserve weather reconnaissance aircraft accomplished several observational missions into tropical MCSs of varying size and intensity. The analysis of the data collected from two such missions successfully define several key characteristics in the tropical MCS. The two cases consisted of a strong tropical MCS and a weak tropical MCS. The strong case actually included two large and intense MCSs, although only one MCS was well observed during its mature and decaying stages with both aircraft data (flight-level and dropwindsonde) and hourly IR and visual satellite imagery. The second case contained a MCS of lesser organization and somewhat less intensity, though it was also well observed through its mature and decaying stages. The objective behind the selection of two such cases was to provide an ideal case in which expected characteristics should definitely be observed, and a weaker case for contrast.

The processes by which MCS structural characteristics are determined have been addressed by many researchers: Maddox (1980), Maddox et al. (1986), Menard and Fritsch (1989), Frank and Chen (1991), Hertenstein and Schubert (1991), Miller and Fritsch (1991), Raymond and Jiang (1991), Frank (1992) and Fritsch (1992). The majority of the above research applies primarily to the midlatitude MCS, and have been adapted here into the summary of expected tropical MCS characteristics (Tables 1 and 2) based upon the observed and modeled structures proposed by the various researchers.

Based on the analyses, it can be stated with confidence that a mid-level vortex does exist in tropical MCSs. These preliminary analyses indicate that the presence, and perhaps the intensity, of the vortices depends on the degree of intensity and centralization of convection within the MCS.

The failure of the observed low-level vortex in AOP 7 to develop into a TD is also an important aspect of this analysis. As suggested, presence of the low-level dry air apparently inhibited further vortex development, as suggested by Fritsch (1992) and Emanuel (1992). Although this data set is not adequate to fully test their hypotheses, it does lend support to the requirement of moisture in the low levels above such vortices for TD genesis.

The ultimate goal behind such an analysis is to use the observed characteristic structure of the tropical MCS in evaluating hypotheses that propose interactions

between TCs and MCSs as suggested by Holland and Lander (1991), Willoughby (1992) and Flatau (1991). Such MCS structures could be used as input to various numerical models to simulate TC/MCS interactions.

This analysis also highlights the need to complete the analyses on all TCM-92 MCS cases. An objective analysis scheme, such as the MultiQuadric Interpolation Scheme developed by Nuss and Titley (1992), should be applied to produce a gridded array of meteorological variables that can be used to calculate dynamical parameters such as vorticity, divergence, etc should be attempted. Such quantitative measures in the observed tropical MCSs are required to test the MCS/TC interaction hypotheses. Although the remainder of the cases consist of MCSs similar to the AOP 1 case, much can be gleaned from MCSs of a less intense nature. Perhaps a correlation between the MCS size and intensity and the vortex size and intensity could be accomplished. In addition, such analyses can provide a solid basis for another research experiment involving the use of weather reconnaissance aircraft. With a background of tropical MCS structure available, improved flight-plans within the TC and MCS interaction region or for the MCS structure missions could be created. Most of the TCM-92 cases observed the mid to later period of convective development. Efforts should be made in the future to observe the formation and growth stages of the tropical MCS. Obviously, this places a great burden on the forecaster who must predict the time and position of the MCS some 24 hours prior to its formation stage. Additional aircraft and crews could ease such a burden in that more complete temporal coverage of such long-lived MCSs could be accomplished.

## APPENDIX A. GEOSTATIONARY SATELLITE IMAGERY

This appendix contains both infrared (IR) and visual image sequences depicting the evolution of the MCSs observed during AOPs 7 and 1. Figs. A-1 through A-6 encompass the AOP 7 case and Figs. A-7 through A-11 are for the AOP 1 case. Regional coverage in AOP 7 imagery is 5 ° N to 20 ° N and 130 ° E to 150 ° E. Regional coverage in AOP 1 imagery is 0 ° to 15 ° N and 135 ° E to 150 ° E. Latitude and longitude lines are in 5 ° intervals. In both cases, an arrow (when visible) points to Guam.

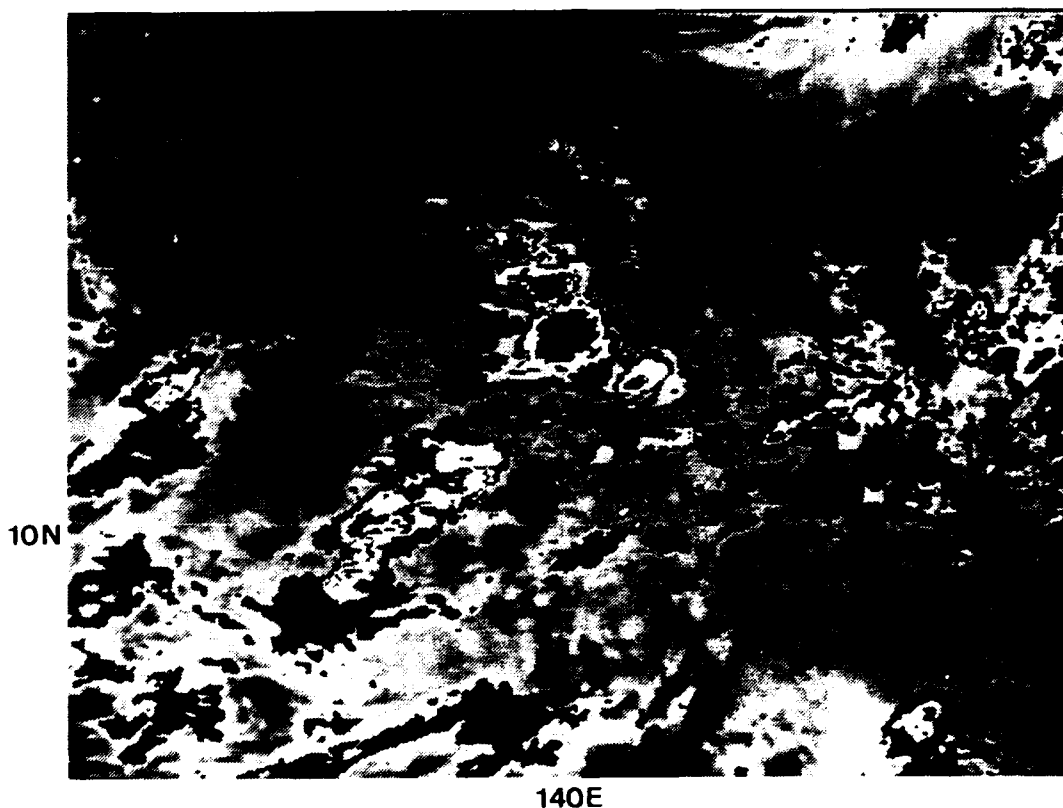


Figure A-1. 0930 UTC 14 August 1992 IR

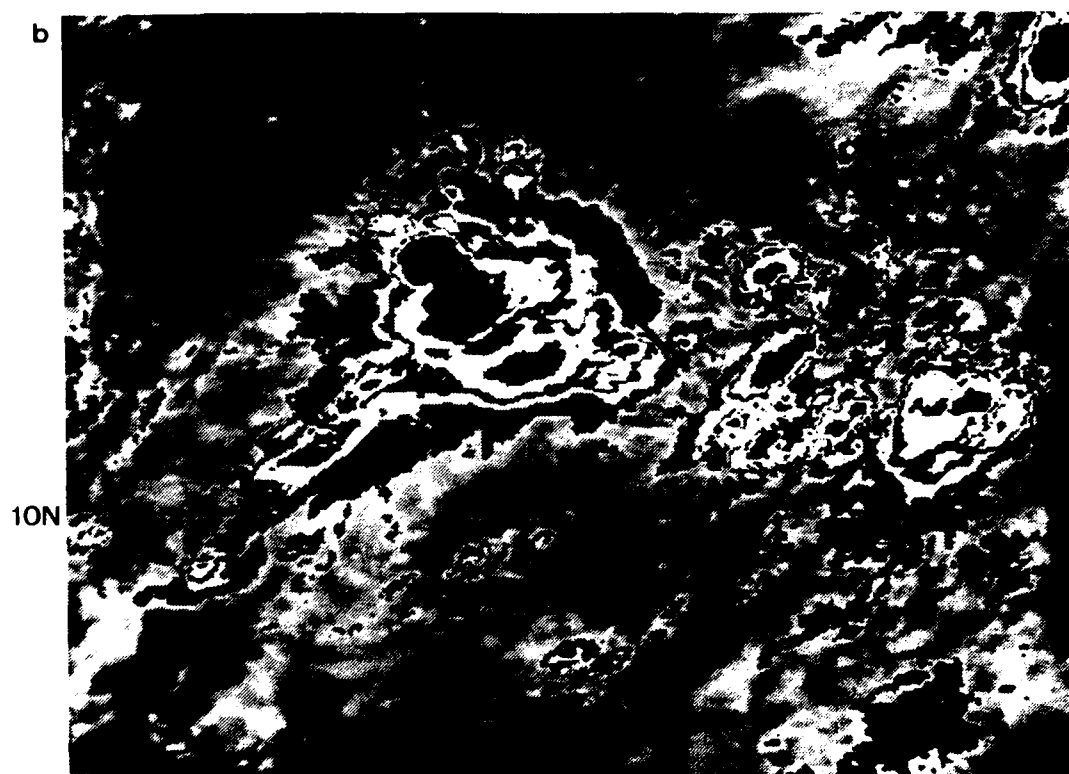
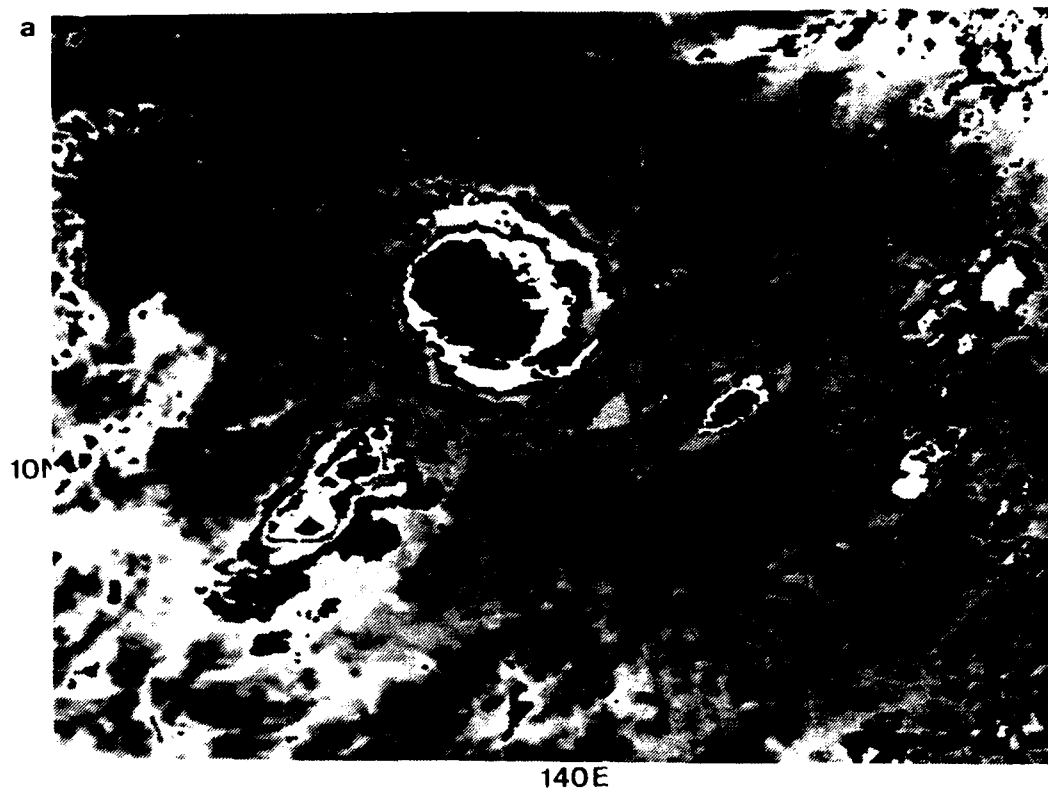


Figure A-2. (a) 1330 UTC IR and (b) 1730 UTC 14 August 1992 IR

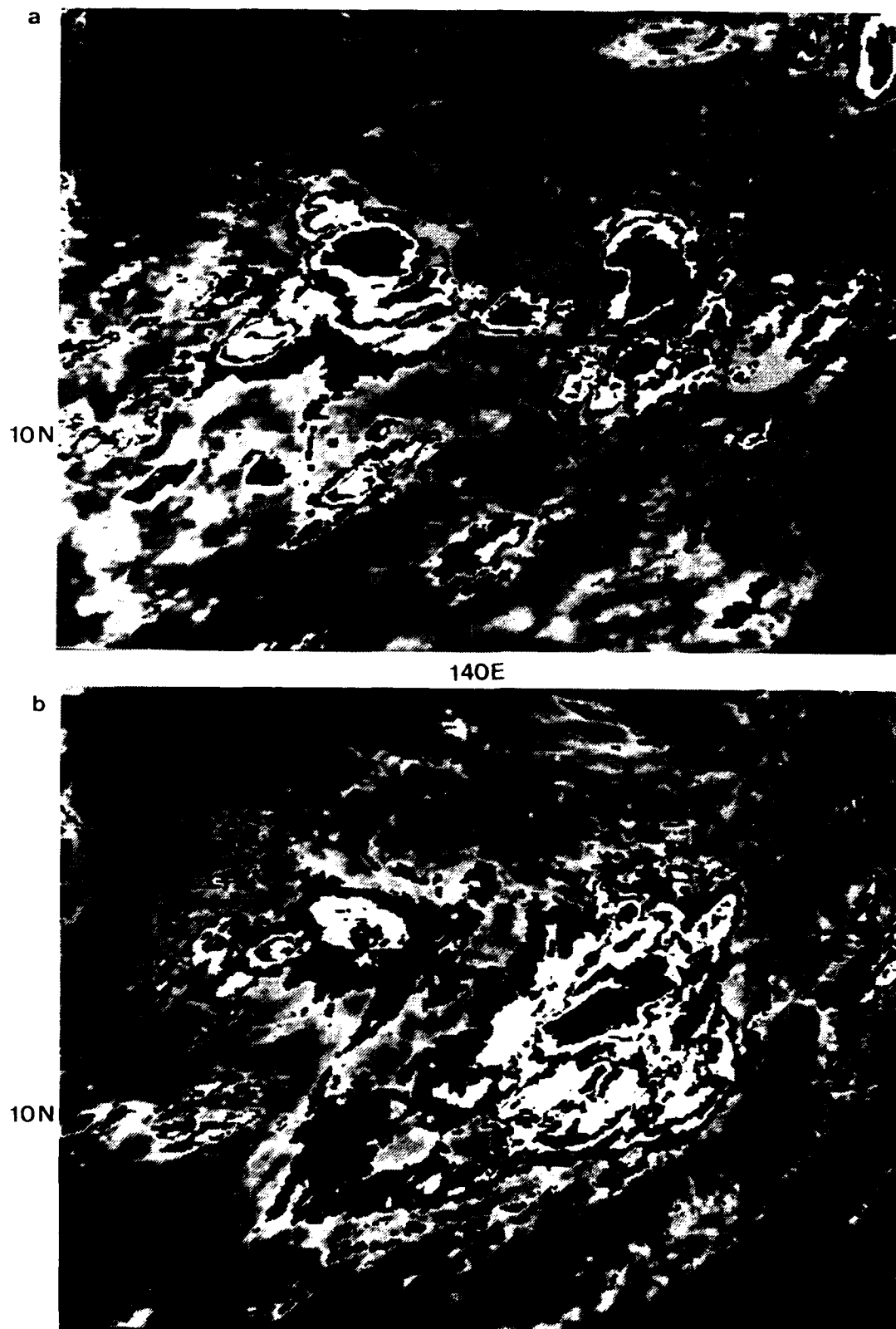


Figure A-3. (a) 1930 UTC IR and (b) 2330 UTC 14 August 1992 IR

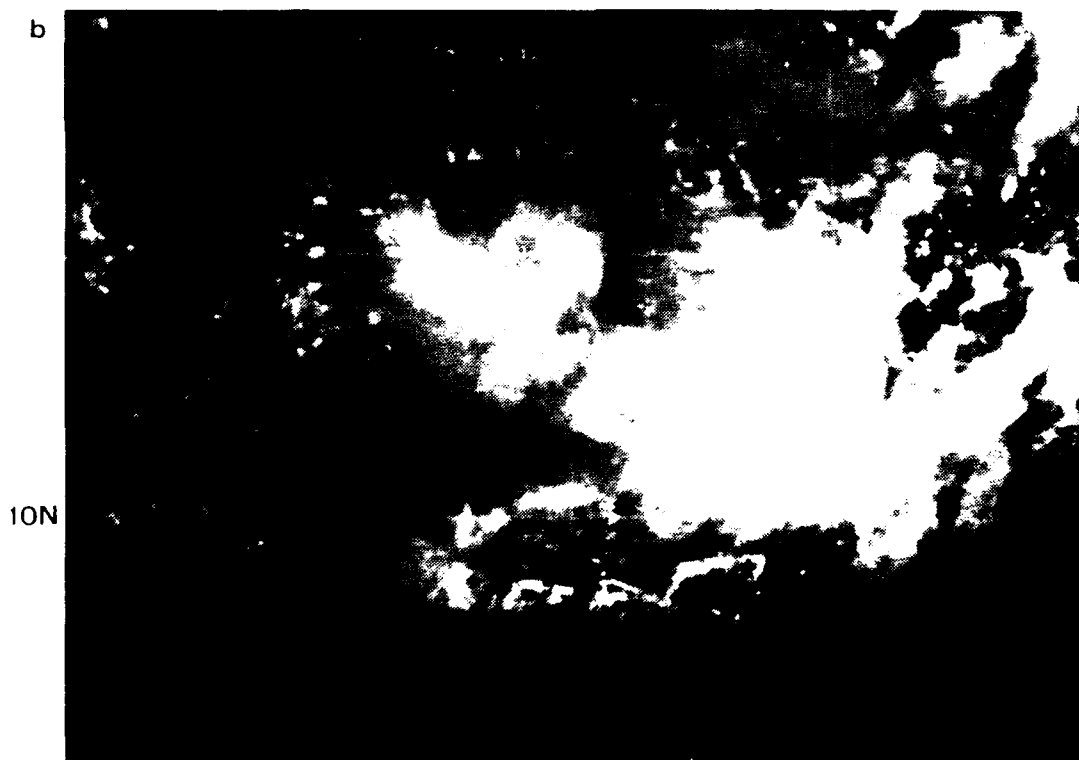
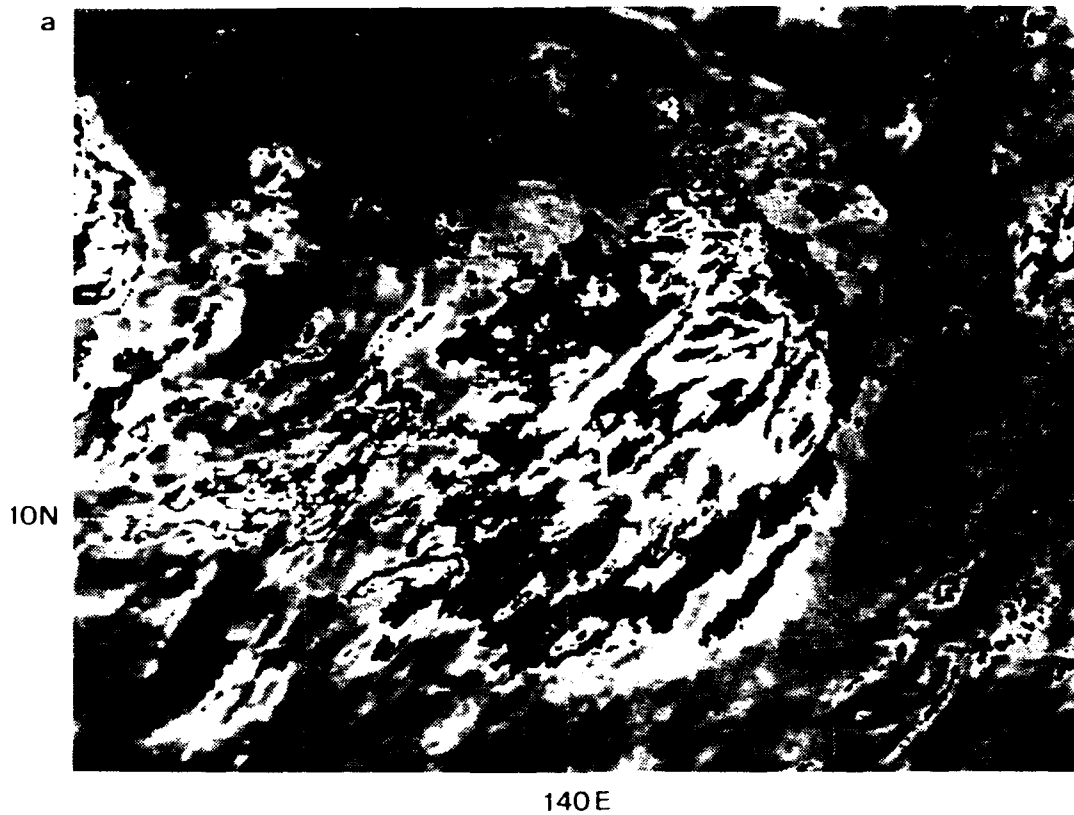


Figure A-4. (a) 0330 UTC 15 August IR and (b) 2130 UTC 14 August 1992 VIS

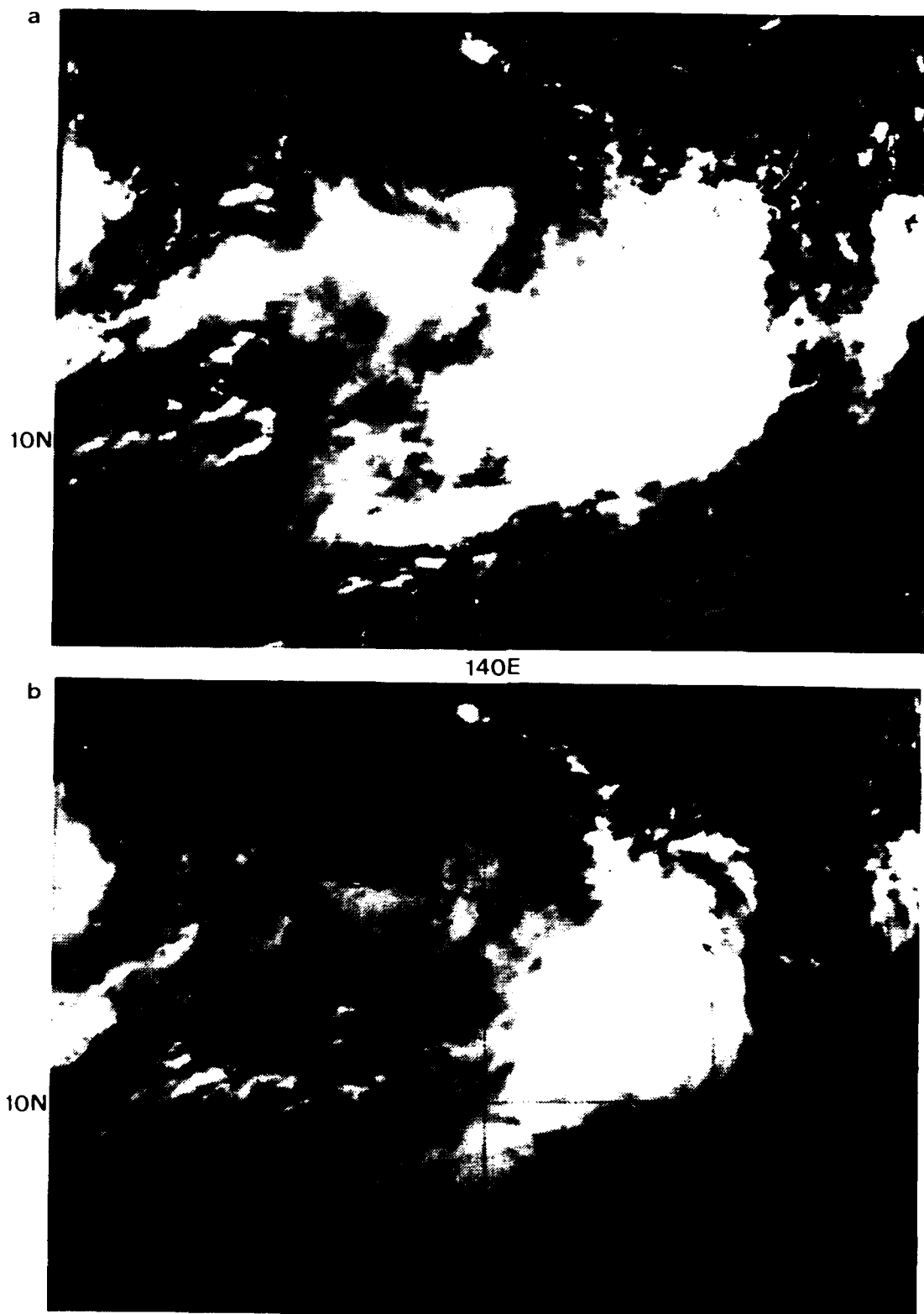


Figure A-5. (a) 2330 UTC 14 August VIS and (b) 0130 UTC 15 August 1992 VIS

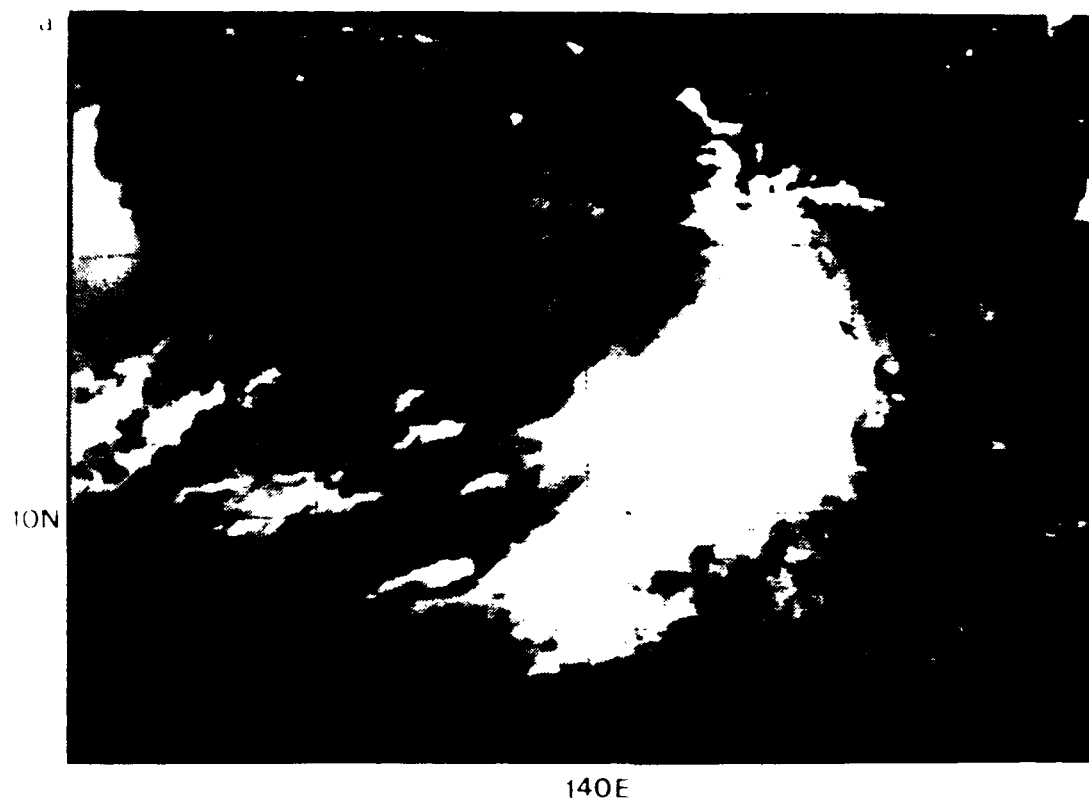


Figure A.6. (a) 0330 UTC VIS and (b) 0630 UTC 15 August 1992 VIS



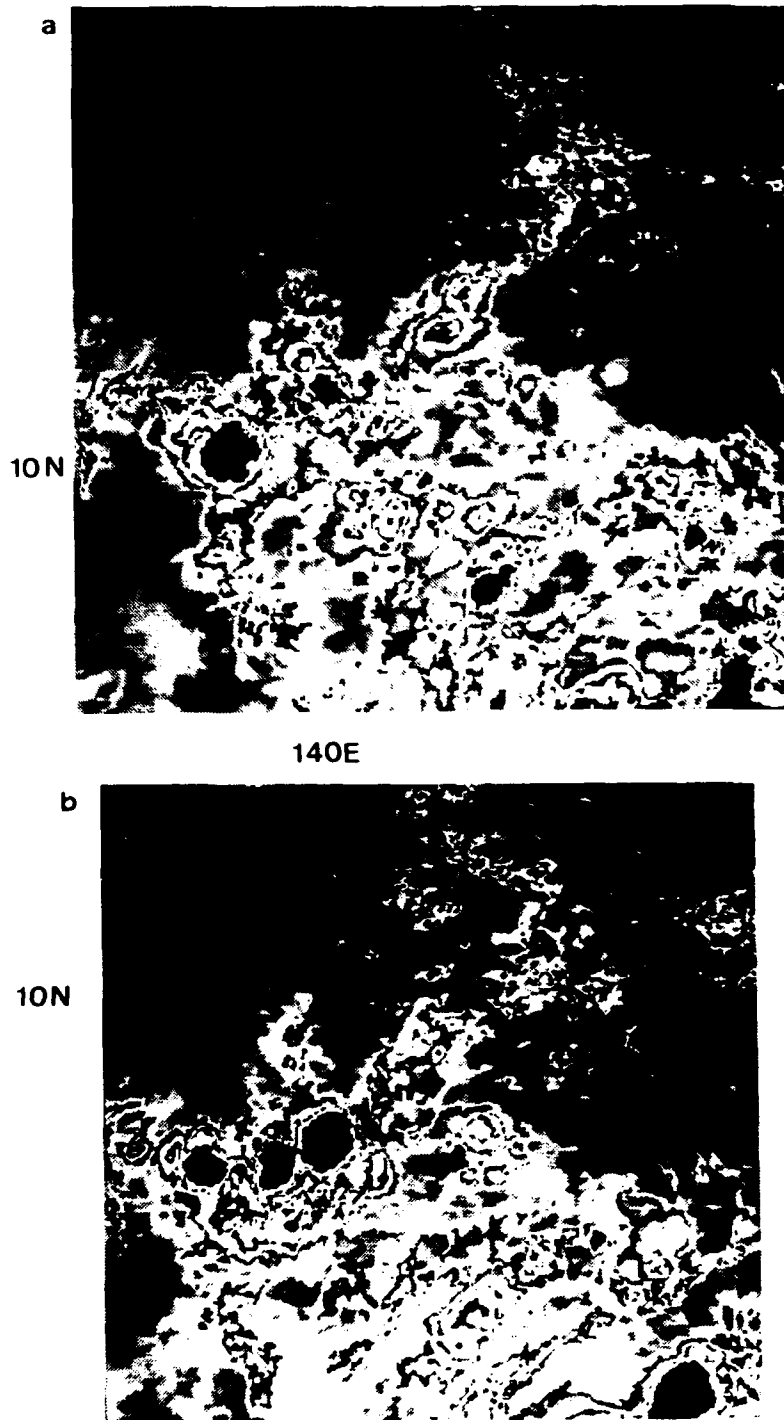


Figure A-7. (a) 1630 UTC IR and (b) 1830 UTC 23 July 1992 IR

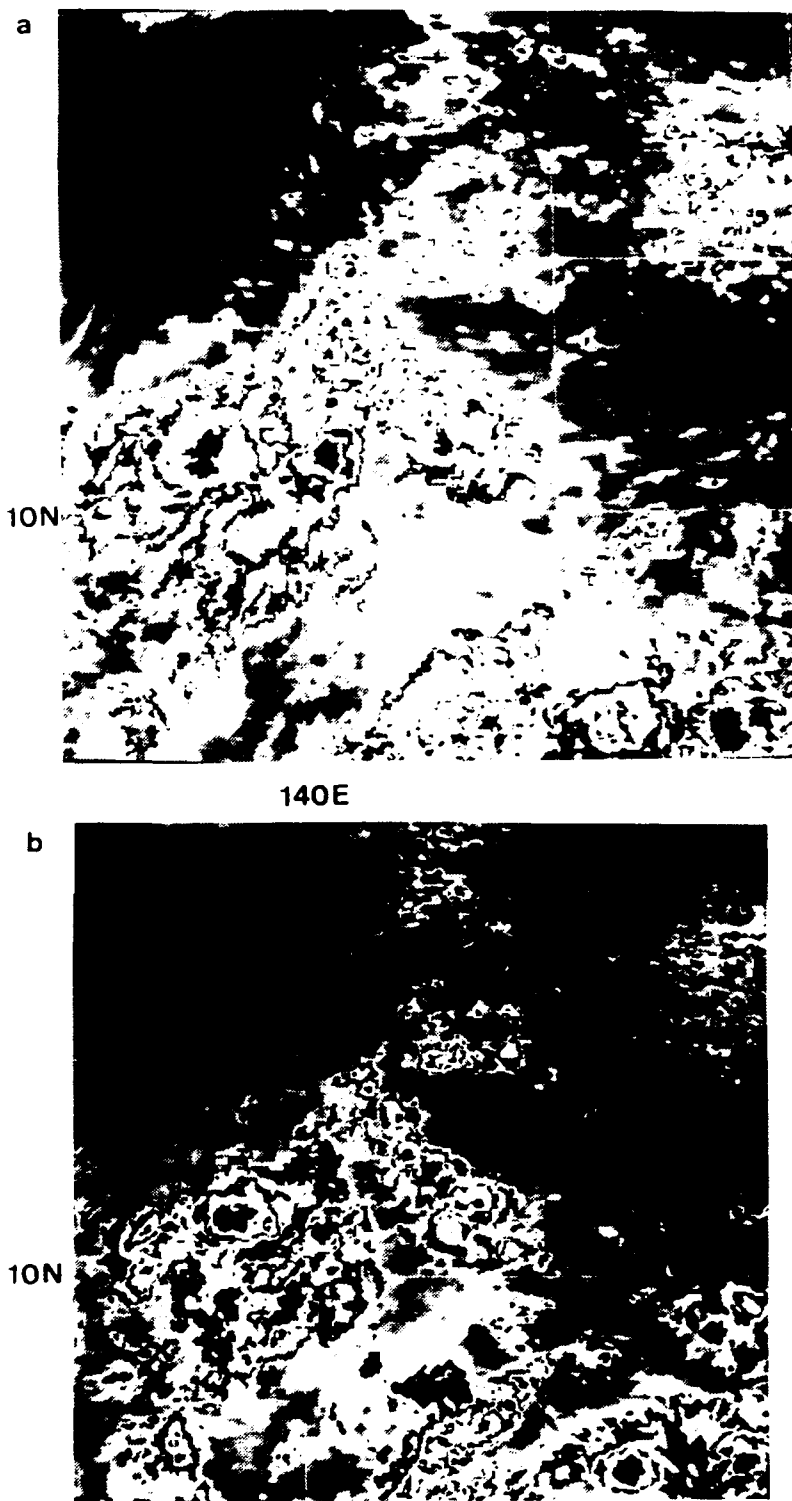
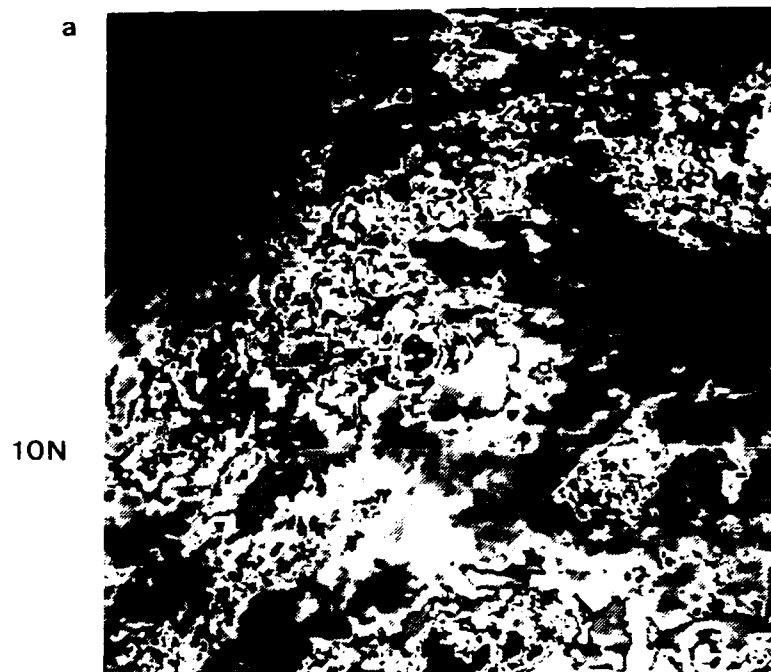


Figure A-8. (a) 2230 UTC 23 July 1992 IR and (b) 0030 UTC 24 July 1992 IR



140E

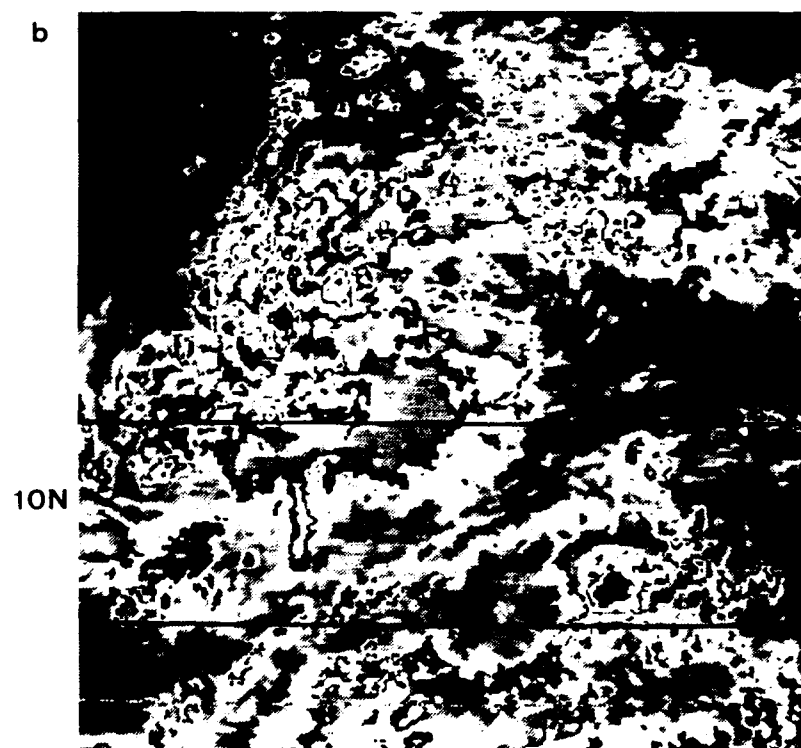


Figure A-9. (a) 0230 UTC IR and (b) 0630 UTC 24 July 1992 IR

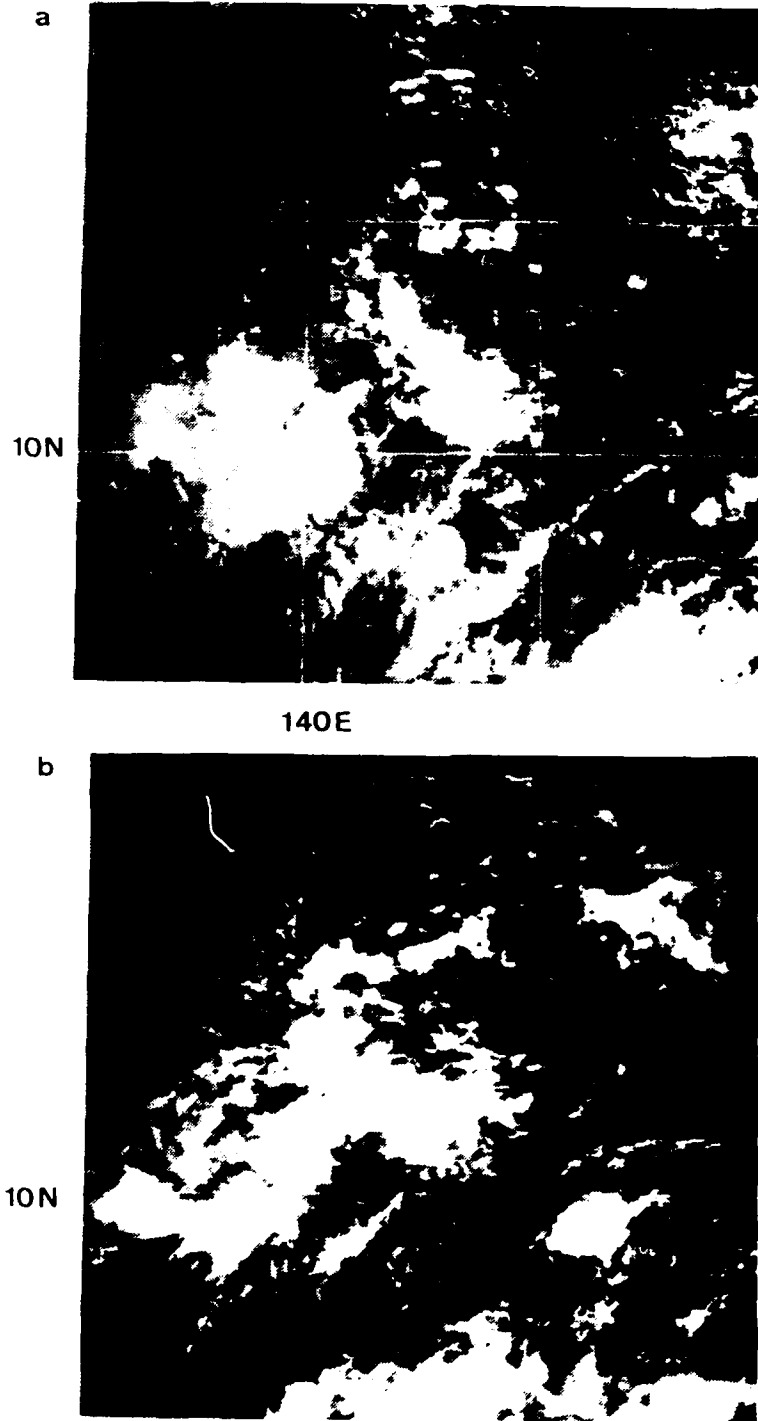


Figure A-10. (a) 2230 UTC 23 July 1992 VIS and (b) 0230 UTC 24 July 1992 VIS

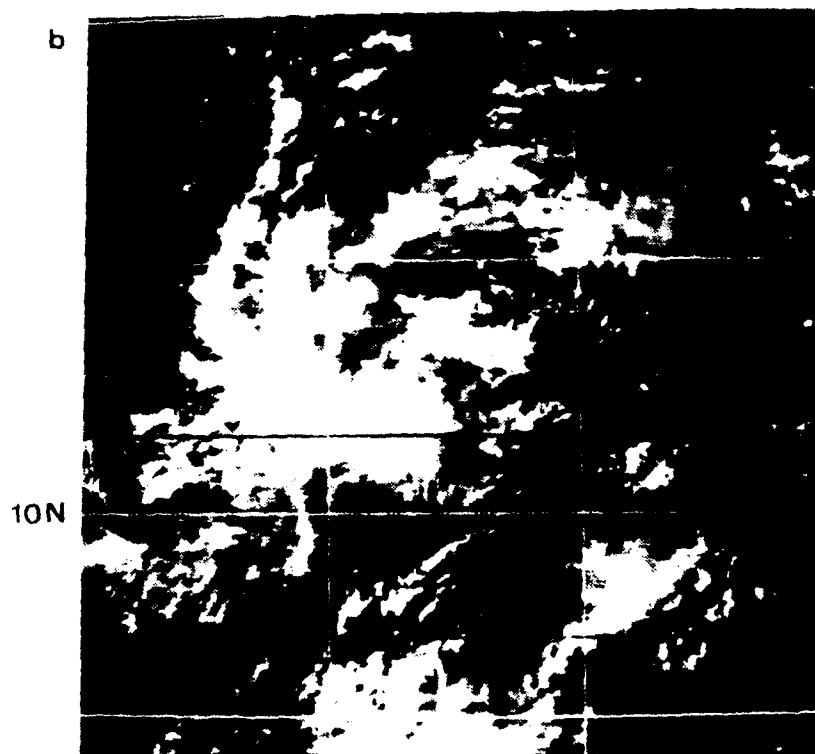
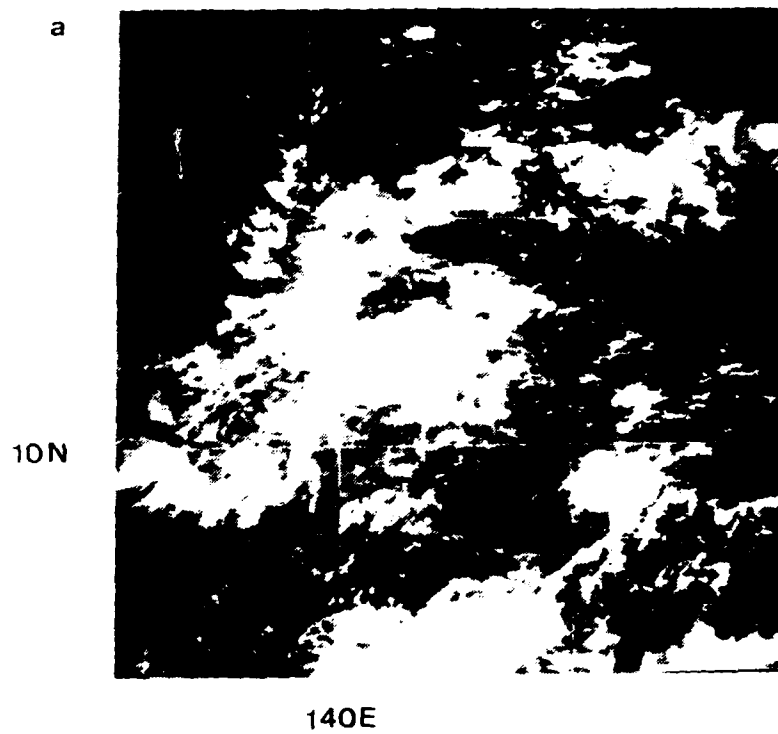


Figure A-11. (a) 0430 UTC VIS and (b) 0630 UTC 24 July 1992 VIS

## REFERENCES

Black, P.G., 1977: Some aspects of tropical storm structure revealed by hand-held camera photographs from space. *Skylab Explores the Earth*, NASA SP-380, Government Printing Office, Washington, DC, 417-462.

Dunnavan, G. M., E. J. McKinley, P. A. Harr, E. A. Ritchie, M. A. Boothe, M. Lander and R. L. Elsberry, 1992: Tropical Cyclone Motion (TCM-92) mini-field experiment summary. Tech. Report NPS-MR-93-001, Naval Postgraduate School, Monterey CA 93943.

Elsberry, R.L., 1987: Tropical cyclone motion. Chapter 4 in *A Global View of Tropical Cyclones*, Office of Naval Research, 91-131.

Elsberry, R. L., B. C. Diehl, J. C.-L. Chan, P. A. Harr, G. J. Holland, M. Lander, T. Neta and D. Thom, 1990: ONR tropical cyclone motion research initiative: Field experiment summary. Tech. Report NPS-MR- 91-001, Naval Postgraduate School, Monterey, CA 93943, 106 pp.

Elsberry, R. L., and R. F. Abbey, Jr., 1991: Recent advances in understanding tropical cyclone motion. Tech. Report NPS-MR-91-002, Naval Postgraduate School, Monterey, CA 93943, 124 pp.

Elsberry, R. L., G. M. Dunnavan and E. J. McKinley, 1992: Operations plan for the tropical cyclone motion (TCM-92) mini-field experiment. Tech. Report NPS-MR-92-002, Naval Postgraduate School, Monterey, CA 93943, 46 pp.

Emanuel, K., 1992: The physics of tropical cyclogenesis in the eastern Pacific. Presentation at International Symposium on Tropical Cyclone Disasters, Beijing, China.

Fett, R. W., and S. Brand, 1975: Tropical cyclone movement forecasts based on observations from satellites. *J. Appl. Meteor.*, 452-456.

Flatau, M., 1991: The role of baroclinic processes in tropical cyclone motion. *Preprints*, 19th Conference on Hurricanes and Tropical Meteorology, Miami, FL, American Meteorological Society, Boston, MA, 349-352.

Frank, W. M., 1992: Tropical cyclone formation. Presentation at Colorado State University Department of Atmospheric Sciences 30th Anniversary Symposium, 5-6 May.

Frank, W. M., and Shuyi Chen, 1991: Simulations of vortex formation in convective weather systems. *Preprints*, 19th Conference on Hurricanes and Tropical Cyclones, Miami, FL, American Meteorological Society, Boston, MA, 241-244.

Fritsch, J. M., 1992: Warm-core vortex amplification over land. Presentation at Colorado State University Department of Atmospheric Sciences 30th Anniversary Symposium, 5-6 May.

Hertenstein, R. F. A., and W. H. Schubert, 1991: Potential vorticity anomalies associated with squall lines. *Mon. Wea. Rev.*, **119**, 1663-1672.

Holland, G. J., and M. Lander, 1991: On the meandering nature of tropical cyclones. *J. Atmos. Sci.*, (submitted).

Kuo, H.-L., 1950: The motion of atmospheric vortices and the general circulation. *J. Met.*, **7**, 247-258.

Kuo, H.-L., 1969: Motions of vortices and circulating cylinder in shear flow with friction. *J. Atm. Sci.*, **26**, 390-398.

Lajoie, F. A., and N. Nicholas, 1974: A relationship between the direction of movement of tropical cyclones and the structure of their cloud systems. Tech. Report No. 11, Bureau of Meteorology, Melbourne, Australia, 22 pp.

Maddox, R. A., 1980: Mesoscale convective complexes. *Bull. Amer. Meteor. Soc.*, **61**, 1374-1387.

Maddox, R. A., K. W. Howard, D. L. Bartels and D. M. Rodgers, 1986: Mesoscale convective complexes in the middle latitudes. In *Mesoscale Meteorology and Forecasting*, P. S. Ray (Ed.), Amer. Meteor. Soc., Boston, MA, 390-413.

Menard, R. D., and J. M. Fritsch, 1989: A mesoscale convective complex-generated inertially stable warm core vortex. *Mon. Wea. Rev.*, **117**, 1237-1261.

Miller, D., and M. J. Fritsch, 1991: Mesoscale convective complexes in the western Pacific region. *Mon. Wea. Rev.*, **119**, 2978-2992.

Nuss, W. A., and D. W. Titley, 1992: Use of Multiquadric interpolation for meteorological objective analysis. (to be submitted).

Raymond, D. J., and H. Jiang, 1990: A theory for long-lived mesoscale convective systems. *J. Atmos. Sci.*, **47**, 3067-3077.

Ritchie, E. A., and G. J. Holland, 1992: On the interaction of tropical-cyclone scale vortices. II. Discrete vortex patches. *Quart. J. Roy. Meteor. Soc.*, (submitted).

Willoughby, H. E., 1992: Linear motion of a shallow-water barotropic vortex as an initial value problem. *J. Atmos. Sci.*, **49**, 2015-2031.

Yeh, T. C., 1950: The motion of tropical storms under the influence of a superimposed southerly current. *J. Met.*, **7**, 108-113.



## INITIAL DISTRIBUTION LIST

		No. Copies
1.	Defense Technical Information Center Cameron Station Alexandria, VA 22304-6145	2
2.	Library, Code 52 Naval Postgraduate School Monterey, CA 93943-5002	2
3.	Chairman (Code MR/Hy) Department of Meteorology Naval Postgraduate School Monterey CA 93943-5000	1
4.	Professor R. L. Elsberry (Code MR/Es) Department of Meteorology Naval Postgraduate School Monterey, CA 93943-5000	1
5.	Capt Eric J. McKinley HQ ACC/DOWR Langley AFB, VA 23665	1
6.	Commanding Officer Naval Oceanography Command Center COMNAVMARIANAS Box 12 FPO San Francisco CA 99630	1
7.	Commanding Officer Fleet Numerical Oceanography Center Monterey, CA 93943-5005	1
8.	Chief of Naval Research 800 N. Quincy Street Arlington, VA 22217	1
9.	Air Weather Service Technical Library Scott AFB, IL 62225-5008	1
10.	Maj. M. Smith Air Force Institute of Technology Wright-Patterson AFB, OH 45433	1
11.	Commanding Officer Air Force Global Weather Central Offutt AFB, NE 68113	1

- |     |  |   |
|-----|--|---|
| 12. | 815th WS ARWO<br>Keesler AFB, MS 39534   | 1 |
| 13. | E. A. Ritchie<br>Bureau of Meteorology Research Centre<br>GPO Box 1289K<br>Melbourne, Victoria 3001<br>Australia | 1 |